REPORT DOCUMENTATION PAGE

Form Approved
OMB No. 0704-0188

1. AGENCY USE ONLY (Leave blank)	2. REPORT DATE	3. REPORT TYPE AND DATES COVERED
	10 Sep 95	

4. TITLE AND SUBTITLE
Exploratory Study of an Icing Index From Satellite Remote Sensing of Cloud Liquid Water Over Land

5. FUNDING NUMBERS

6. AUTHOR(S)
David T. Lawyer

7. PERFORMING ORGANIZATION NAME(S) AND ADDRESS(ES)
AFIT Students Attending:

Colorado State University

8. PERFORMING ORGANIZATION REPORT NUMBER
95-111

9. SPONSORING/MONITORING AGENCY NAME(S) AND ADDRESS(ES)
DEPARTMENT OF THE AIR FORCE
AFIT/CI
2950 P STREET, BLDG 125
WRIGHT-PATTERSON AFB OH 45433-7765

10. SPONSORING/MONITORING AGENCY REPORT NUMBER

11. SUPPLEMENTARY NOTES

12a. DISTRIBUTION/AVAILABILITY STATEMENT
Approved for Public Release IAW AFR 190-1
Distribution Unlimited
BRIAN D. GAUTHIER, MSgt, USAF
Chief of Administration

12b. DISTRIBUTION CODE

13. ABSTRACT *(Maximum 200 words)*

14. SUBJECT TERMS	15. NUMBER OF PAGES 111
	16. PRICE CODE

17. SECURITY CLASSIFICATION OF REPORT	18. SECURITY CLASSIFICATION OF THIS PAGE	19. SECURITY CLASSIFICATION OF ABSTRACT	20. LIMITATION OF ABSTRACT

THESIS

EXPLORATORY STUDY OF AN ICING INDEX FROM SATELLITE REMOTE SENSING OF CLOUD LIQUID WATER OVER LAND

Submitted by

David T. Lawyer

Department of Atmospheric Science

In partial fulfillment of the requirements

for the Master of Science

Colorado State University

Fort Collins, CO 80523

Summer 1995

COLORADO STATE UNIVERSITY

May 17, 1995

WE HEREBY RECOMMEND THAT THE THESIS PREPARED UNDER OUR SUPERVISION BY DAVID T. LAWYER ENTITLED EXPLORATORY STUDY OF AN ICING INDEX FROM SATELLITE REMOTE SENSING OF CLOUD LIQUID WATER OVER LAND BE ACCEPTED AS FULFILLING IN PART REQUIREMENTS FOR THE DEGREE OF MASTER OF SCIENCE.

Committee on Graduate Work

Adviser

Department Head

ABSTRACT OF THESIS

EXPLORATORY STUDY OF AN ICING INDEX FROM SATELLITE REMOTE SENSING OF CLOUD LIQUID WATER OVER LAND

Applications of satellite microwave measurements to aircraft icing have been restricted to areas over the ocean. In this study, data from the DMSP SSM/I polar orbiter high frequency channels (85.5 GHz) and GOES 7 infrared (IR) and visible data are used to retrieve cloud liquid water (CLW) over land areas and determine if it is feasible to develop an icing index from this information. The area selected for the study was over the northern plains during the first weeks of February and March 1992 when icing conditions were known to exist.

In order to retrieve CLW, surface emittance calculations were made using co-located SSM/I and GOES IR data for clear sky conditions over land ignoring lakes and reservoirs. Due to periodic cloud contamination, clear sky surface emittances were composited over several days for the cases in this study. Higher variability of surface emittance was found in the horizontal polarized channel (Channel 7) of the SSM/I due to the effects of surface roughness and soil moisture. Snow cover produced the lowest emissivity values (near 0.6).

Integrated CLW results were consistent with previous research aircraft data (under similar meteorological conditions) with values ranging from 0.07 kgm^{-2} to 5 kgm^{-2}. By incorporating CLW measurements, estimated cloud top temperatures (CTTs), cloud depths (CD), and cloud texture (CT), an icing index nomogram is proposed for possible use as an operational icing forecast tool. PIREPS reported over the areas of interest were used to "fine-tune" the icing index nomogram. 66% of the PIREPS fell within the predetermined guidelines of the nomogram. This result is encouraging and indicates that developing an icing index may indeed be possible from satellite remote sensing techniques. However, additional regions and meteorological situations need to be assessed in order to further refine the satellite-based icing index. Our first tests show that the Index, at this stage of development, is a better positive aircraft icing indicator than a failsafe negative indicator.

David T. Lawyer
Department of Atmospheric Science
Colorado State University
Fort Collins, Colorado 80523
Summer 1995

ACKNOWLEDGEMENTS

I wish to express my sincere thanks to my advisor, Dr. Thomas H. Vonder Haar for his support, guidance, and excellent suggestions for this study. Without his expertise in the field of satellite remote sensing, the results from this project would have been much more difficult to achieve. I also want to extend my thanks to my other committee members, Drs. Mahmood Azimi-Sadjadi and Steven Rutledge for their input and suggestions for this research.

A special thanks goes to Andy Jones and Cindy Combs for their continued support throughout this last year and a half. Andy's expert help with microwave remote sensing, and FORTRAN programming along with his PORTAL data fusion, made difficult tasks manageable. Cindy Combs provided unlimited and unselfish support in both FORTRAN programming and cloud liquid water retrieval. Without their help, this study could not have been completed in this short period of time.

Thanks also go to Ben Berstein and Dr. Marcia Politovich for their help in data acquisition and thought provoking discussions of the aircraft icing forecast problem. Their expert advice proved invaluable. Thanks to Linda Wharton and Matt Kelsch from FSL who on numerous occasions provided PIREP data and expert views on the PIREP verification problem.

I would like to thank all of the folks in the climatology branch of CIRA who provided suggestions and comments for this research. Their expertise helped in understanding all aspects of satellite remote sensing and its applications pertinent to my work. A special thanks goes to the NESDIS RAMM branch at CIRA for providing the satellite data for this study and to Loretta Wilson for her help in drafting this thesis.

Finally, I must thank my wife and children for their support during the often harrowing times of putting together this research. They were always there when I needed them the most.

TABLE OF CONTENTS

1 Introduction 1
1.1 Previous Aircraft Icing Research 4
1.2 Research Objective 7

2 Passive Microwave Remote Sensing 8
2.1 The Microwave Radiative Transfer Equation 9
2.1.1 Non-Scattering Atmosphere 10
2.1.2 Plane-Parallel Atmosphere 11
2.1.3 Non-Blackbody Surface Boundary Condition 12
2.2 Ocean vs Land Cloud Liquid Water Retrieval 13

3 Data 17
3.1 Special Sensor Microwave Imager Instrument Description 17
3.2 GOES VISSR Instrument Description 18
3.3 Polar Orbiter Remapping and Transformation Application Library (PORTAL) 19
3.4 General Description of data base 23
3.4.1 Satellite data 25
3.4.2 Sounding and PIREP data sets 27
3.5 Synoptic Analysis 34

4 Icing Index 40
4.1 General Description 40
4.2 Measurement of Surface Emittance 41
4.2.1 Surface Emittance Retrieval Method 42
4.2.2 Results 44
4.3 Cloud Liquid Water Retrieval 50
4.3 1 Theoretical Brightness Temperature Calculations 50
4.3.2 Cloud Top and Base Determination 51
4.3.3 Precipitation Threshold 52
4.3.4 Procedure for Determining Cloud Liquid Water 53
4.3.5 Results 53
4.4 Infrared Cloud-Top Temperature Measurement 77
4.4.1 Cloud Top Temperature Procedure 77
4.4.2 Results 79
4.5 Cloud Texture Method from Visible and Infrared 93
4.5.1 Gray Level Co-Occurrent Matrix(GLCM) 93
4.5.2 Neural Network Based Texture Method 95
4.5.3 Subjective Cloud Texture Analysis 96
4.6 Operational Icing Index Nomogram 97

5 Summary and Conclusions 102
5.1 Plan for a Forecasting Test of the Icing Index 104
5.2 Future Work and Applications of the Satellite-derived Icing Index 104

6 References 107

LIST OF FIGURES

1.1 Sample NAWAU icing forecast 3
1.2 Sample AFGWC icing forecast 3

2.1 Microwave transmittance as a function of frequency (from Liou 1980) 9
2.2 Plane-Parallel Geometry 12
2.3 Brightness temperature/rain rate relationships at 18, 37, and 85.6 GHz 15
2.4 Real and imaginary parts of the dielectric constant for soils (from Schmugge and Choudhury 1981) 16
2.5 Calculated values of emissivity at 1.4 GHz using the dielectric constants from Figure 2.4 (from Schmugge and Choudhury 1981) 16

3.1 Conceptual diagram of PORTAL 20
3.2 GOES 7 IR (Channel 8) image collected at CIRA during the STORM-FEST project 21
3.3 Channel 6 (85.5GHz) SSM/I image 21
3.4 Remapped GOES IR image from Fig 3.2 to the SSM/I projection in Figure 3.3. 22
3.5 Surface airways observation (SAO) sites for STORM-FEST region 24
3.6 NWS upper air, CLASS, and wind profile sites for STORM-FEST region 24
3.7 SSM/I 85.5 GHz horizontal polarized (Channel 7) brightness temperature for 5 Mar 1992 at 11Z. 26
3.8 GOES IR (Channel 8) for 5 Mar 1992 11Z. 26
3.9a PIREP icing intensities for 11 Feb 1992. 29
3.9b PIREP icing altitudes for 11 Feb 1992. 29
3.10a PIREP icing intensities for 12 Feb 1992 30
3.10b PIREP icing altitudes for 12 Feb 1992. 30
3.11a PIREP icing intensities for 5 Mar 1992 31
3.11b PIREP icing altitudes for 5 Mar 1992. 31
3.12a PIREP icing intensities for 8 Mar 1992 32
3.12b PIREP icing altitudes for 8 Mar 1992. 32
3.13a PIREP icing intensities for 9 Mar 1992 33
3.13b PIREP icing altitudes for 9 Mar 1992. 33
3.14a Surface map for 12Z 11 Feb 1992. 35
3.14b 500mb heights for 12Z 11 Feb 1992 35
3.15a Surface map for 12 Feb 1992. 36
3.15b 500mb heights for 12 Feb 1992 36
3.16a Surface map for 12Z 5 Mar 1992. 37
3.16b 500 mb heights for 12Z 5 Mar 1992 37
3.17a Surface map for 12Z 8 Mar 1992. 38
3.17b 500mb heights for 12Z 8 Mar 1992 38
3.18a Surface map for 12Z 9 Mar 1992. 39
3.18b 500mb Heights for 12Z 9 Mar 1992 39

4.1 Channel 6 composite surface emittance for 5-12 Feb 1992. 45
4.2 Channel 7 composite surface emittance for 5-12 Feb 1992. 46
4.3 Channel 6 composite surface emittance for 5-9 Mar 1992. 48
4.4 Channel 7 composite surface emittance for 5-9 Mar 1992. 49
4.5 24 Hour observed precipitation ending 12Z 5 Mar 1992 49
4.6 Skewt of Huron (HON), SD for 03Z 12 Feb 1992 55
4.7 Channel 6 (85.5GHz Vertical Polarization) CLW for 03Z 12 Feb 1992 58
4.8 Channel 7 (85.5GHz Horizontal Polarization) CLW for 03Z 12 Feb 1992 58

4.9 Schematic depiction of likely cloud situation over South Dakota for 03Z 12 Feb 1992. 59
4.10 Remapped GOES IR image for 03Z 12 Feb 1992. 59
4.11 Skewt of Rapid City, SD for 03Z 5 Mar 1992. 62
4.12 Channel 6 CLW for 03Z 5 Mar 1992. 63
4.13 Channel 7 CLW for 03Z 5 Mar 1992. 63
4.14 Schematic depiction of likely cloud situation over eastern Wyoming for 03Z 5 Mar 1992. 64
4.15 Remapped GOES IR image for 03Z 5 Mar 1992. 64
4.16 Skewtof Rapid City, SD for 00Z 8 Mar 1992. 66
4.17 Channel 6 CLW for 03Z 8 Mar 1992.. 67
4.18 Channel 7 CLW for 03Z 8 Mar 1992.. 67
4.19 Schematic depiction of likely cloud situation over eastern Wyoming for 03Z 8 Mar 1992. 68
4.20 Remapped GOES IR image for 03Z 8 Mar 1992. 68
4.21 Skewt of Rapid City, SD for 00Z 9 Mar 1992. 70
4.22 Channel 6 CLW for 03Z 9 Mar 1992. 71
4.23 Channel 7 CLW for 03Z 9 Mar 1992. 71
4.24 Schematic depiction of likely cloud situation over South Dakota for 03Z 9 Mar 1992. 72
4.25 GOES IR image for 03Z 9 Mar 1992. 72
4.26 Skewt of Rapid City, SD for 210Z 9 Mar 1992. 74
4.27 Channel 6 CLW for 00Z 10 Mar 1992. 75
4.28 Channel 7 CLW for 00Z 10 Mar 1992. 75
4.29 Schematic depiction of likely cloud situation over South Dakota for 00Z 10 Mar 1992. 76
4.30 Remapped GOES IR image for 00Z 10 Mar 1992. 76
4.31 Scatterplot of Channel 6 cloud liquid water versus cloud top temperature for 03Z 12 Feb 1992. 80
4.32 Scatterplot of Channel 7 cloud liquid water versus cloud top temperature for 03Z 12 Feb 1992. 81
4.33 Scatterplot of Channel 6 cloud liquid water versus cloud depth for 03Z 12 Feb 1992. 83
4.34 Scatterplot of Channel 7 cloud liquid water versus cloud depth for 03Z 12 Feb 1992. 84

4.35 Scatterplot of Channel 6 cloud liquid water versus cloud top temperature for 03Z 5 Mar 1992. 86
4.36 Scatterplot of Channel 7 cloud liquid water versus cloud top temperature for 03Z 8 Mar 1992. 87
4.37 Scatterplot of Channel 6 cloud liquid water versus cloud depth for ..... 03Z 5 Mar 1992. 88
4.38 Scatterplot of Channel 7 cloud liquid water versus cloud depth for 03Z 5 Mar 1992. 89
4.39 Combined scatterplot of Channel 6 cloud liquid water versus cloud top temperature for 12 Feb, 5, 8, 9, and 10 Mar 1992. 91
4.40 Combined scatterplot of Channel 6 cloud liquid water versus cloud depth for 12 Feb, 5, 8, 9, and 10 Mar 1992. 92
4.42 Prototype icing nomogram. 99
4.43 PIREP icing intensities from 12 Feb, 5 Mar, 8 Mar and 9 Mar 1992. 101
4.44 PIREP icing altitudes from 12 Feb 5 Mar, 8 Mar, 9 Mar 1992. 101

LIST OF TABLES

3.1 SSM/I instrument characteristics 18

4.1 Composite surface emittance statistics for 5-12 Feb 1992 44

4.2 Composite surface emittance statistics for 5-9 Feb 1992 47

4.3 CLW Statistics of South Dakota region for 03Z 12 Feb 1992 55

4.4 CLW Statistics for 03Z 5 Mar 1992 62

4.5 CLW Statistics for 03Z 8 Mar 1992 66

4.6 CLW Statistics for 03Z 9 Mar 1992 70

4.7 CLW Statistics for 00Z 10 Mar 1992 74

4.8 GOES 7 Channel 8 calibration table 78

4.9 Icing index classification 99

1 Introduction

Aircraft icing has long been recognized as a major hazard to both fixed-wing and rotary aircraft. In the past 20 years, icing was a major cause or factor in over 800 aviation accidents in the continental United States (Cole and Sand 1991). More recently (November 1994), the National Transportation Safety Board (NTSB) recommended to the Federal Aviation Administration (FAA) to prohibit some commuter aircraft from flying into known or forecast of any icing conditions. This recommendation came on the heals of a deadly crash of a commuter aircraft in northwest Indiana where icing on the airframe was determined as the cause of the accident.

The accretion of ice can occur on wings or fuselage of a fixed-wing aircraft or on the blades or rotor of a helicopter. Two distinct processes occur during icing. First, supercooled cloud droplets impact on the airframe or rotor and secondly, these supercooled cloud droplets freeze onto the aircraft. If small droplets (< 30 μm) freeze upon impact with the leading edge of the wing, fuselage, or rotor, the ice buildup is rough and opaque. This type of icing is known as rime and is usually not dangerous except in large amounts on small aircraft. If the droplets are large enough (> 30 μm), smear upon impact, and subsequently freeze, the ice forms a glaze on the aircraft. This condition is clear icing and can be extremely hazardous since the aerodynamic shape of the airfoil can be altered significantly (AWS 1980). Sand et al. (1984), found that icing affects aircraft performance through increased drag, decreased lift, additional weight (affecting fuel consumption), decreased engine performance, and decreased propeller efficiency.

At present, the National Aviation Weather Advisory Unit (NAWAU) in Kansas City, MO. is the sole provider of commercial aircraft icing forecasts for the continental United States while Air Force Global Weather Central (AFGWC) is the sole provider of military aircraft icing forecasts. These forecasts are issued as 12-hour outlooks that can be updated every 8 hours and often cover expansive areas (often times up to 2000 km^2) of the country (See Figure 1.1 and 1.2 for sample forecasts). There are currently a variety of methods used by forecasters at NAWAU and AFGWC, but generally speaking, these forecasts focus on synoptic scale events. In reality, icing conditions often occur on much smaller scales, and are quite variable in time and space. Meteorologists infer icing conditions from information such as model output of temperature, humidity, and vertical velocities (Schultz and Politovich 1992; AWS 1980). There is no explicit model forecast of an icing hazard or cloud liquid water although the latest numerical model (ETA) from the National Meteorological Center (NMC) is expected to eventually provide a cloud liquid water product.

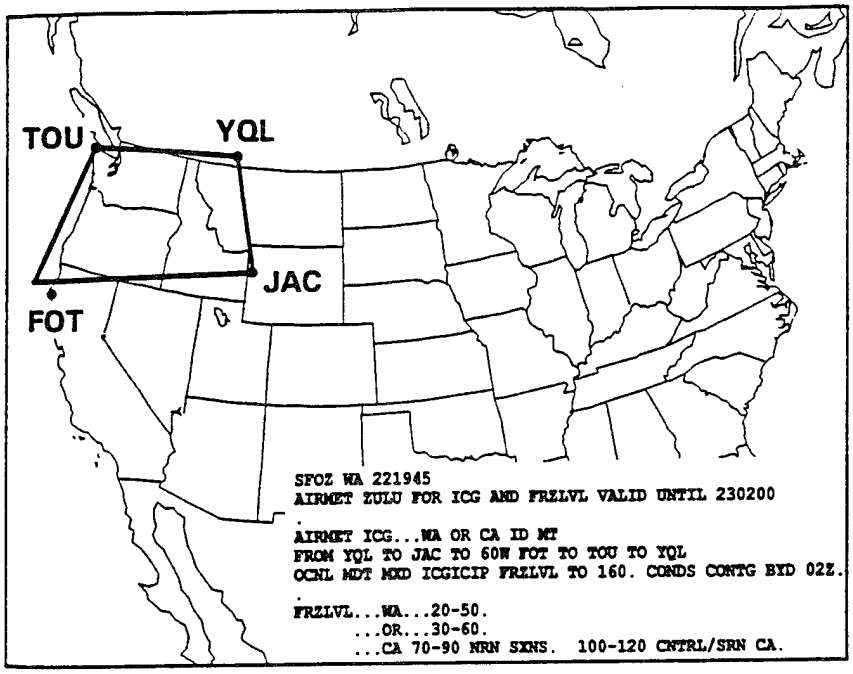

Figure 1.1. Sample NAWAU icing forecast. Forecast is actually disseminated as text (AIRMET) from which a graphical representation can be displayed/drawn on an appropriate map.

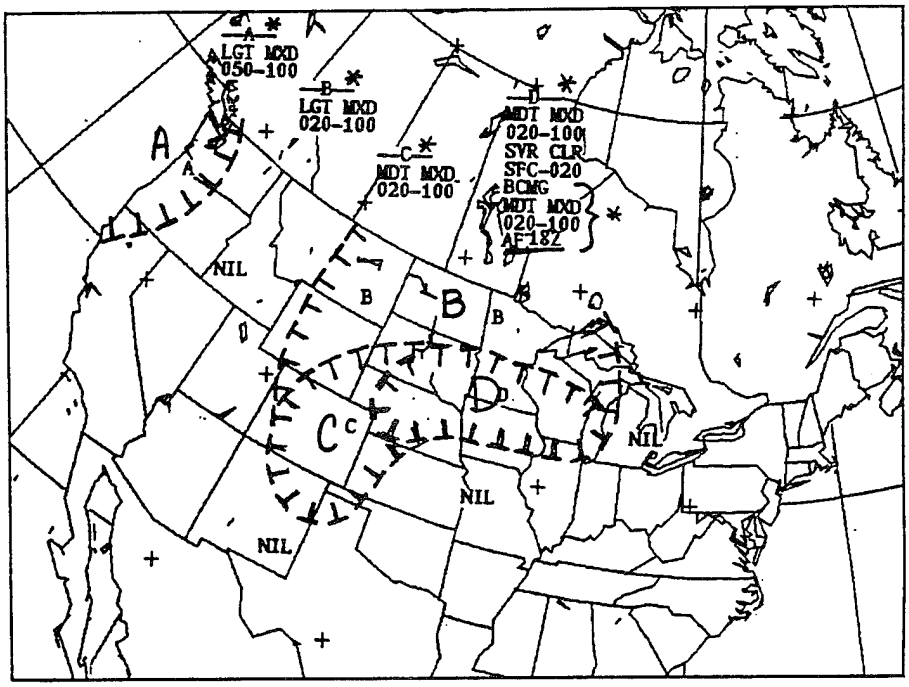

Figure 1.2. AFGWC sample icing forecast.

1.1 Previous Aircraft Icing Research

In the mid 1980's, the FAA Icing Forecasting Improvement Program was developed in response to a NTSB recommendation to improve icing forecasts. As a result, the Winter Icing and Storms Project (WISP) was initiated and later conducted in the Colorado area during the winter months (late January to late March) from 1990-1994. One of the main goals of this project (in addition to improving icing forecasts) was to study the processes leading to the formation and depletion of supercooled liquid water in winter storms.

Aircraft icing conditions were encountered on several research flights during WISP90 and WISP91. Large supercooled droplets (> 50 μm) were found near cloud top (CTTs averaged ≥ -10°C but were occasionally as low as -16°C) in the presence of strong wind shear (both directional and speed). This can be explained through the process of inhomogeneous mixing (Cooper 1989). Droplet evaporation is occurring on a shorter time scale compared to that of turbulent mixing. Entrainment of dry air at cloud top mixes with the cloud, evaporating some of the droplets. As a result, other droplets form into larger droplets through condensation and coalescence. This reduces the droplet concentration but broadens the droplet size distribution (Telford et al. 1984). Thus large supercooled droplets exist near cloud top providing the necessary environment for aircraft icing (clear icing). The WISP field project provided an extremely detailed database from which researchers could study various aspects of aircraft icing. Rasmussen et al. (1992) provides a detailed description of the project.

Shultz and Politovich (1992) approached the icing forecast problem from a model perspective. Their study developed automated forecasting schemes based on synoptic-scale model output of temperatures and relative humidity to predict aircraft icing potential. They found their method to only slightly improve manually-derived forecasts produced by the National Aviation Weather Advisory Unit (NAWAU). Smart (1992) took this approach a step further and included vertical winds to derive an experimental technique for forecasting supercooled liquid water (SLW) over eastern Colorado during WISP 1991. His results also indicated just slight improvement in forecasting of aircraft icing.

Several attempts have been made in recent years to remotely measure various meteorological parameters and relate these parameters to aircraft icing potential. Popa Fotino et al (1986) used ground-based remote sensors to detect atmospheric conditions conducive to aircraft icing. Zenith measurements of liquid water and atmospheric temperature were made by microwave radiometers near Denver, Colorado over a two year period. In addition, several other variables including pilot reports (PIREPS) were incorporated into a PIREP-based icing index. This study, through statistical analysis, found that the cloud liquid measurements were vitally important in the detection of icing conditions. Furthermore, the ground-based radiometers provided a continuous measure of this cloud liquid, therefore potential icing conditions could be detected on a continuous basis. Similar results were found by Stankov et al. (1992) and Stankov and Bedard (1994). They included other ground-based detectors in addition to the microwave radiometer. Profiling radars, radio-acoustic sounding systems, and lidar ceilometers were used to enhance detection and prediction (both spatially and temporally) of aircraft icing.

Researchers continue to expand the use of satellite remote sensing for potential applications to aircraft icing. Satellites, as opposed to ground-based instruments, have the capability to measure various meteorological parameters on a large, yet regional scale. This would lead to a much more useful tool for areal coverage of hazardous icing conditions. Curry and Liu (1992) explored the potential use of satellite data for the development of a climatology of aircraft icing probability over ocean regions. The Nimbus-7 Scanning Multichannel Microwave Radiometer (SMMR) was one of several satellite-based tools used in this study. Cloud temperature, horizontal extent, depth, and liquid water along with precipitation characteristics were obtained from their research over the North Atlantic region. These parameters were found to be important in developing aircraft icing probabilities over the ocean. An interesting result from this study was that 99% of mid-level clouds (2.5 to 3.5 km) observed fell into the temperature range of -2° to -36°C (temperature range where aircraft icing threat was high, although Sand et al. (1984), found 0° to -20°C was the temperature regime for supercooled water over land) while only 14% of the low-level clouds (< 2.5 km) fell into this range.

Lee et al. (1994) investigated possible applications of CLW for estimating marine aircraft icing. Integrated CLW was derived over the North Pacific Ocean (Gulf of Alaska and Bering Sea) from SSM/I 85.5 GHz channels aboard the DMSP polar-orbiting satellite. The CLW was combined with infrared cloud top temperature (CTT) and numerical model output to develop a prototype system for forecasting icing potential. Icing watch regions were specified when the CLW exceeded 0.2 kg m^{-2} and CTTs were between 0° and -20°C. Results of this method indicated that the inclusion of satellite data

refined the icing threat areas (from forecasting scheme developed by Schultz and Politovich, 1992) considerably.

1.2 Research Objective

Unlike the previous research described above, the main purpose of this research is to provide the forecaster with a measurement of cloud liquid water sensed remotely from a satellite platform over land. The DMSP SSM/I 85.5GHz channels will be used in conjunction with GOES 7 IR and visible data to compute vertically integrated cloud liquid water (CLW) over specific land areas in winter-time situations. In addition to CLW, cloud-top temperature (CTT), cloud depth (CD), and cloud texture (CT) information will be incorporated into an empirically-based icing index. This Index, while developed from a rather coarse temporal resolution, will capture semi-permanent features of typical wintertime clouds in the mid-latitudes with a spatial resolution of approximately 13 km. It is hoped that the index will not only provide additional information not currently available to icing forecasters, but provide a more regionalized, small-scale (30-50 km^2) forecast of icing potential over land areas.

2 Passive Microwave Remote Sensing

The microwave region of the electromagnetic spectrum extends from roughly 0.3 to 300 GHz (1 mm to 1m in wavelength). Figure 2.1 (from Liou 1980) illustrates the clear sky transmittance through the atmosphere for the microwave spectrum. Atmospheric windows are apparent near 35, 90, and 135 GHz while strong O_2 absorption bands occur near 60 and 120 GHz. A strong H_2O vapor absorption band is located near 180 GHz with a much weaker absorption band around 20 GHz.

The O_2 absorption band in the neighborhood of 50-60 GHz has been used by multifrequency radiometers for retrieving atmospheric temperature profiles (similar to the 15 μm CO_2 absorption band temperature retrieval in the infrared portion of the spectrum). Of more common use is the relatively transparent frequencies < 40 GHz. There have been many applications of these frequencies especially for retrieval of water vapor profiles and vertically integrated cloud liquid water. More recently, research has begun to exploit the frequencies around 90-100 GHz (Spencer et al. 1989; Jones and Vonder Haar 1990; Lee et al., 1994) for cloud liquid water retrieval. As will be discussed in further detail in future chapters, this study will incorporate the higher frequency (85.5GHz) channels for cloud liquid water retrieval.

The remaining portions of this chapter will provide details on the microwave radiative transfer equation (Section 2.1) along with the important assumptions made for the calculation of the upwelling radiance (Sections 2.1.1, 2.1.2, 2.1.3). In section 2.2, a contrast of ocean and land cloud liquid water retrieval methods will be discussed to further describe the various aspects of microwave remote sensing applicable to this work.

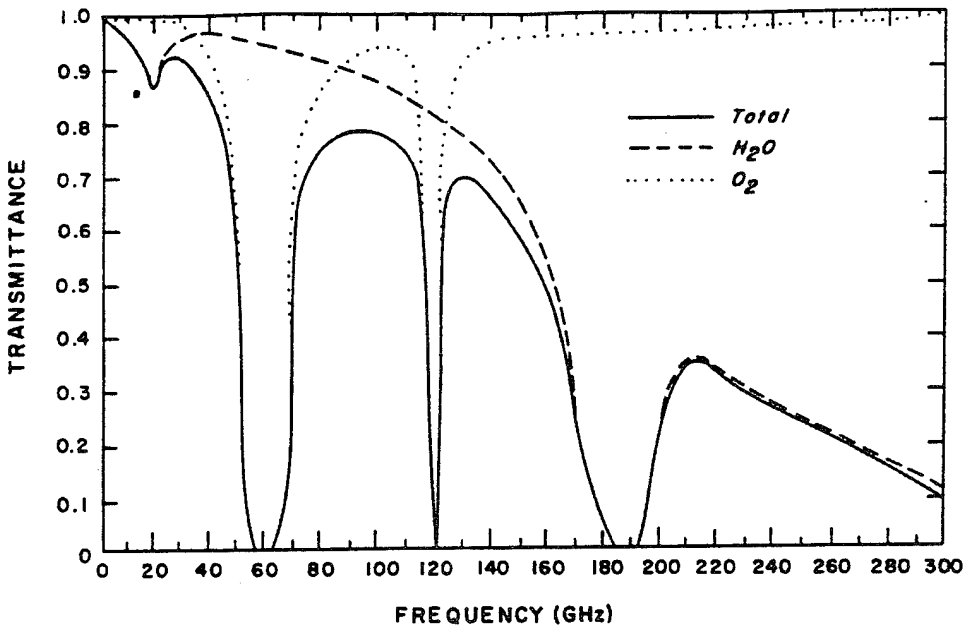

Figure 2.1. Microwave Transmittance as a function of frequency(from Liou 1980).

2.1 The Microwave Radiative Transfer Equation

The integrated radiate transfer equation used in this study is expressed by Liou (1980) as

$$L_\nu(0) = \varepsilon_\nu B_\nu(T_s)\tau_\nu(p_s,0) + \int_{p_s}^{0} B_\nu[T(p)]\frac{\partial \tau_\nu(p,0)}{\partial p}dp$$

$$+(1-\varepsilon_\nu)[\tau_\nu(p_s,0)]^2 \int_{p_s}^{0} \frac{B_\nu[T(p)]}{[\tau_\nu(p,0)]^2}\frac{\partial \tau_\nu(p,0)}{\partial p}dp \qquad (2.1)$$

where $L_\nu(0)$ is the upward radiance observed by the satellite at pressure $p = 0$, ν is the frequency, ε_ν is the surface emittance, $B_\nu(T)$ is the Planck function at a given temperature and $\tau_\nu(p,0)$ is the atmospheric transmittance for a layer between p and the satellite. The subscript s indicates values at the surface. The first term on the right hand side (RHS) of

equation 2.1 is the surface contribution to upwelling radiance, which is a function of both surface temperature and emittance. The second term on the RHS is the direct atmospheric contribution to emission and the third term is the reflected atmospheric contribution to emission from the surface, both of which are functions of the temperature and moisture profile of the atmosphere. In equation 2.1, we assume the atmosphere is a non-scattering, plane-parallel atmosphere with a non-blackbody surface boundary condition.

2.1.1 Non-Scattering Atmosphere

In the microwave region of the electromagnetic spectrum in a clear atmosphere, the absorption and emission of radiation is much more dominant than scattering (Ulaby et al. 1981) therefore scattering can be neglected. At high microwave frequencies (> 37 GHz) liquid water is a much stronger absorber than scatterer of radiation, while ice , if large enough (> 150 μm), is more efficient at scattering than absorbing (Spencer 1989). Due to the different scattering and extinction efficiencies of liquid water (usually spherical particles) and ice, it is important to differentiate between precipitating and non-precipitating clouds. In precipitating clouds, the Rayleigh approximation is not valid since particle sizes are often greater than the incident wave and scattering of the microwave energy dominates. In the microwave region of the spectrum, the size parameter,

$$\chi = \frac{2\pi r}{\lambda} \qquad (2.2)$$

where r is the droplet radius and λ is the wavelength of incident radiation, determines the radiative properties of the particles (spherical droplets or ice). Mie theory determines the scattering and absorbing characteristics of the precipitation-sized particles where χ is near 1. However, for non-precipitating clouds, χ is $<< 1$ for cloud droplets and the Rayleigh approximation is valid where the atmospheric absorption is directly related to liquid water content and not a function of the cloud droplet size distribution (Ulaby et al. 1981). Hence, the Rayleigh limit approximation of negligible scattering compared to absorption is valid for clouds which in fact may be partially composed of both ice ($r <$ 150 μm) and liquid water ($r < 85$ μm). Since the absorption by ice is much smaller than the absorption by CLW in non-precipitating clouds, the microwave frequencies can penetrate high level cirrus clouds with very little attenuation. This allows for microwaves to "see" middle to low level clouds which contain valuable information unavailable to other sensors at shorter wavelengths.

2.1.2 Plane-Parallel Atmosphere

The plane-parallel assumption is commonly employed in satellite meteorology. The distance along the atmosphere path ds is related to the vertical depth dz by

$$ds = \sec\theta \; dz \qquad (2.3)$$

where θ is the satellite zenith angle or the angle of incidence at the surface as measured from the vertical. Figure 2.2 is a diagram of the plane-parallel atmosphere. By making

this assumption, the temperature and absorption coefficients are functions of height (vertical coordinate z) only.

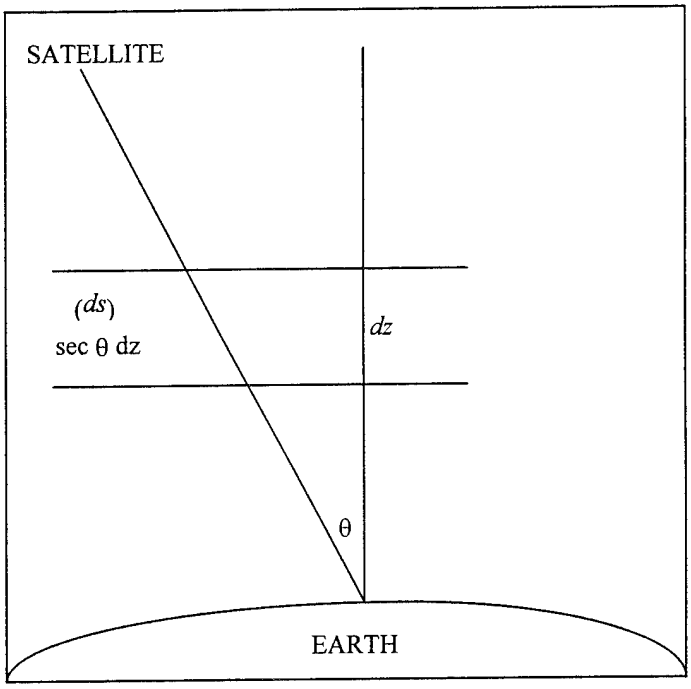

Figure 2.2. *Plane-Parallel Geometry*

2.1.3 Non-Blackbody Surface Boundary Condition

In the microwave region of the spectrum, the surface does not emit as a blackbody but rather as a grey body, the surface in this case emits less than a blackbody and does not necessarily absorb all the energy incident upon it. An electromagnetic wave incident upon a surface boundary can be described by the reflectance, absorptance and transmittance. These quantities must sum to one to assure conservation of energy. Surface emittance, ε_ν is a quantity related to the reflectance and is described as the ratio

of the observed brightness temperature to the brightness temperature of an ideal blackbody in thermodynamic equilibrium,

$$\varepsilon_v = \frac{T_{MW}}{T_{BB}} \qquad (2.4)$$

In addition, if the surface is considered opaque, then the surface emittance is directly related to absorption. The other components of the radiance at the surface is due to reflected radiation from above the surface. The deep space emission due to the cosmic background radiation, another component of surface radiance, is neglected because of its small relative contribution to the total upwelling radiance.

2.2 Ocean Vs Land Cloud Liquid Water Retrieval

In the microwave region of the spectrum, ocean surfaces (down to 1 cm depth) appear radiatively cold due to water's low surface emittance (approximately 0.5). When CLW is retrieved over an ocean surface, the microwave sensor detects higher brightness temperatures for clouds due to absorption and emission of radiation by the liquid water; thus, clouds appear radiatively warmer over the ocean surface. However, as the CLW amount increases, the brightness temperature in fact decreases when the microwave energy originates at higher levels of the clouds. Remote sensing of CLW over the ocean has been studied extensively (Greenwald, et al. 1992; Petty and Katsaros 1990; among others) and has generally been accepted throughout the meteorological community. Additionally, Spencer et al. (1989) used the SSM/I frequencies to retrieve precipitation information over the ocean as well as the land. Microwave remote sensing of hydrometeors can be divided into two categories, emission-based and scattering-based

methods for precipitation retrieval. In emission-based retrieval, liquid precipitation causes brightness temperature increases over a radiometrically cold (ocean) background. Scattering-based retrieval on the other hand, causes brightness temperature decreases (especially above the freezing level over a radiometrically warm (land) background). Figure 2.3 shows an example of rain rate vs brightness temperature for three different microwave frequencies of the SSM/I over land and ocean. Note how the precipitation over land causes brightness temperature decreases while over the ocean, the brightness temperature increases up to a point, then decreases. This change in brightness temperature is due to high emission from the water droplets up to a point, then the colder ambient temperature of the precipitation causes brightness temperature decreases.

Retrieval of CLW over land is made much more difficult because of the higher emittance (highly variable as well) of the land surface. This causes the microwave radiometer to be insensitive to CLW content variations. It has been shown by Yeh and Liou (1983) that an over-estimation of the surface emittance directly affects the vertically integrated CLW.

Several properties of the surface influence the radiation emitted. One of the most important properties is the soil moisture which influences or changes the dielectric constant of land. An increase in soil moisture increases the dielectric constant of the soil (See Figure 2.4). Schmugge and Choudhury (1981) in turn found a marked increase in surface emittance for increasing levels of soil moisture (See Figure 2.5). These emittance values usually come from the top 1 cm of the soil and are generally not influenced by sub-surface moisture. Surface roughness and non-homogeneity such as vegetation and terrain also affect surface emittance. By accurately measuring the microwave surface

emittance, the surface boundary conditions can be properly determined for calculations of the total upwelling radiance. This upwelling radiance can then be used to accurately retrieve CLW over land. The method of calculating surface emittance by Jones and Vonder Haar (1990) showed absolute accuracies ranging from 0.008 to 0.012 for a summer situation (August time frame) in an area of eastern Colorado and western Nebraska. This method will be used in this study and will be discussed in more detail in chapter 4.2.

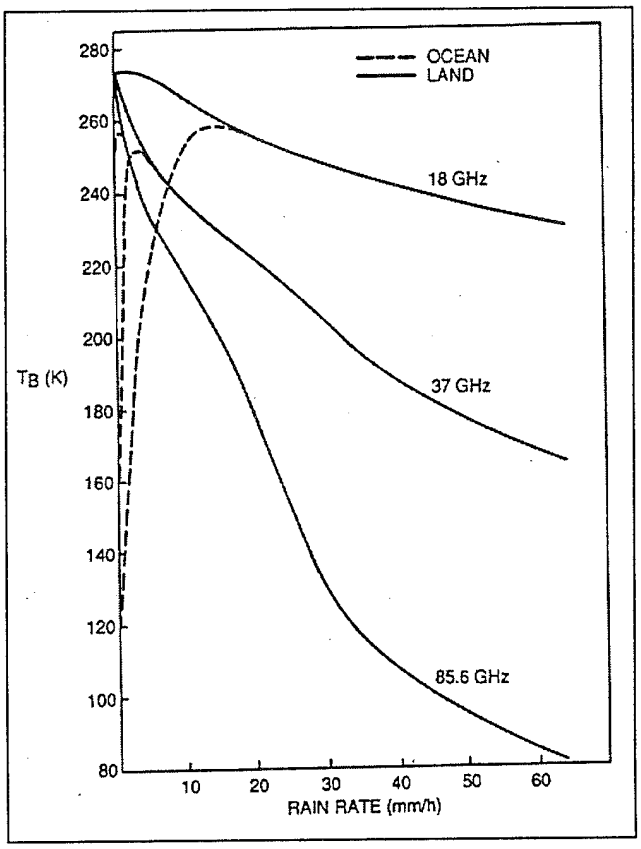

Figure 2.3. *Brightness temperature/rain rate relationships at 18, 37, and 85.6 GHz. The vertical distribution of hydrometeors was based upon averaged radar results and assumed ice precipitation above and liquid precipitation below the freezing level.*

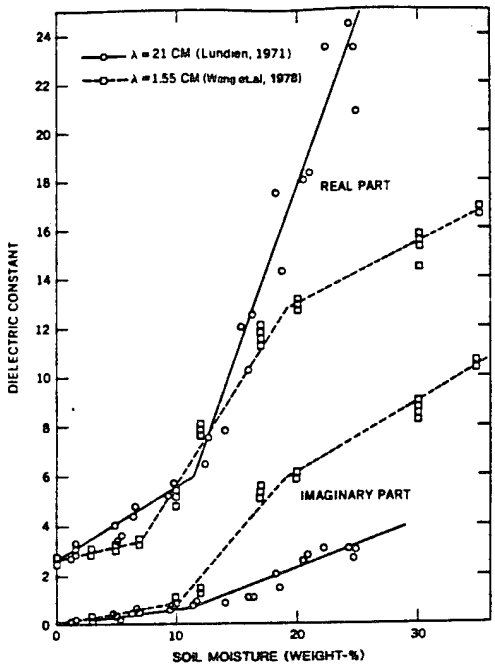

Figure 2.3. *Real and imaginary parts of the dielectric constant. The data are from laboratory measurements at frequencies of 1.4 (λ = 21 cm) and 19.4 (λ = 1.55 cm) GHz (from Schmugge and Choudhury 1981).*

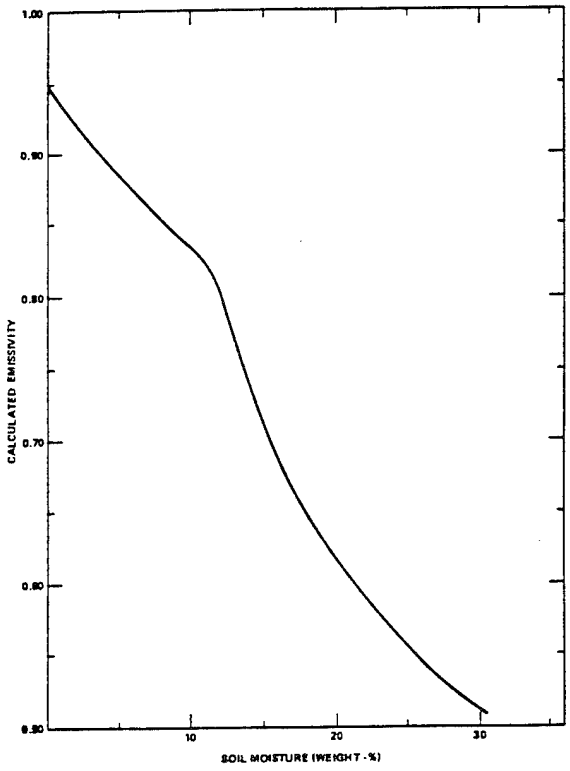

Figure 2.4. *Calculated values of emissivity at 1.4 GHz based on the dielectric constants in Figure 2.4 (from Schmugge and Choudhury 1981).*

3 Data

3.1 Special Sensor Microwave Imager Instrument Description

The Special Sensor Microwave Imager (SSM/I) on the Defense Meteorological Satellite Program (DMSP) F10 and F11 Satellites were launched on 1 December 1990 and 28 November 1991 respectively. Both satellites orbit the earth in a near circular, sun synchronous near-polar orbit at an altitude of approximately 830 km ± 50-70 km. The variation in altitude is due to the eccentricity of the orbit and oblateness of the earth. The DMSP orbital period is approximately 102 minutes at an inclination of 98.8° which allows for twice daily coverage poleward of 50° latitude. The data are collected to the fore (F10) and aft (F11) of the spacecraft in a 102° arc which results in a 1394 km wide swath. The conical scanning pattern has a zenith angle of 53.1° eliminating changing limb effects due to varying zenith angle. The swath and orbital inclination provide complete coverage of the Earth in two to three days, except for two small sectors at the North and South poles. The SSM/I is a passive microwave radiometer operating at four frequencies (19.35, 22.235, 37.0, and 85.5 GHz) and dual polarization capabilities on all except the 22.235 GHz frequency which only records the vertical polarization (see Table 3.1, adapted from Hollinger 1990). Each radiometric channel has a sensitivity denoted by the maximum Noise Equivalent Delta Temperature (NEdT in Table 3.1) in Kelvin, defined as the minimum detectable change in signal. Since the instrument uses the same antenna for the different channels, the effective-field-of-view (EFOV) of the sensor varies with frequency, with the highest frequency (85.5GHz) having the highest resolution. The

85.5 GHz channel samples 128 times over the 102° arc. As a result, the 85.5 GHz channel has an effective ground resolution of 13 km x 15 km. The effective ground resolution of all four channels is shown in Table 3.1. Since two DMSP satellites were orbiting during the period used in this study, there were potentially from 3 to 5 passes a day. The SSM/I data for this study was collected by the National Environmental Satellite Data and Information Service (NESDIS) Regional and Mesoscale Meteorology (RAMM) branch at CIRA and was in final, calibrated form of sensor brightness temperatures.

Table 3.1. *SSM/I instrument characteristics.*

Channel Number	Frequency (GHz)	Polarization (H or V)	Effective-field of-View(EFOV) (km)	Sensitivity (NEdT) (K)
1	19.35	V	69 X 43	0.45
2	19.35	H	69 X 43	0.42
3	22.235	V	60 X 40	0.74
4	37.0	V	37 X 28	0.37
5	37.0	H	38 X 29	0.38
6	85.5	V	15 X 13	0.69
7	85.5	H	15 X 13	0.73

3.2 GOES VISSR Instrument Description

The Geostationary Operational Environmental Satellite (GOES-7) is operated by the National Oceanic and Atmospheric Administration (NOAA). GOES-7 maintains a geosynchronous orbit above the equator at an altitude of 35,800 km and was positioned at 108°W longitude. The primary instrumentation on GOES-7 used in this study is the Visible and Infrared Spin-Scan Radiometer (VISSR) and when operated in dwell sounding mode is known as the VISSR Atmospheric Sounder (VAS). This sensor is

capable of measuring the upwelling radiance in the visible (0.5 to 0.7 μm wavelength) and Infrared (10.5 to 12.5 μm). In addition, VAS had four IR detectors and 12 narrow band filters that produced multi-spectral data (from 3.95 to 14.73μm). In normal VISSR mode, the visible (Channel 13) and surface Infrared (Channel 8) are transmitted each half hour for the whole hemisphere. The STORM-FEST GOES-7 data used in this study were transmitted in VISSR mode with occasional Rapid Interval Scan Operations Plan (RISOP) mode or "Rapid Scan". During RISOP, up to 12 visible and IR scans per hour were obtained depending on the location of interest. The visible (Channel 13) resolution at nadir is 1 km and Channel 8 (IR) has a nadir resolution of 8 km. The VISSR data was collected by the NESDIS RAMM branch of NOAA located at CIRA. The VISSR data was navigated using the CSU Interactive Research Imaging System (IRIS) based on the automatic navigation parameters of the satellite transmitting to the ground station.

3.3 Polar Orbiter Remapping and Transformation Library(PORTAL)

Jones et al. (1995) recently developed a remapping technique which combines satellite data from multiple sensors. Specifically, PORTAL reformats the original satellite data into a generalized data format (JDF). Once in the JDF format, the constraints posed on the original data format are bypassed in all other software considerations, thus simplifying the research application software design without sacrificing data integrity. The original data resolution and associated earth-location information are therefore retained. Once in JDF format, the data file can then be used for

intermediate analysis undergoing several iterations until the final analysis of the data is complete (see Figure 3.1). Furthermore, PORTAL can remap multisensor data into a specified projection space tailored to the needs of the user. The final output is then a combination of multiple sensor data on a specifically defined common projection space. This technique allows for a tremendous amount of flexibility in that information from several sensors can be presented in a single map projection chosen from one of many different map projections. For this study, the PORTAL software system was used to reformat GOES-7 IR (Channel 8) data as well as DMSP SSM/I microwave data (specifically Channels 6 & 7), then remap the GOES IR into SSM/I projection space. Figures 3.2-3.4 show an IR image which underwent the PORTAL technique along with the corresponding SSM/I image. Once remapped, the satellite data (both remapped IR and SSM/I) were then used to calculate surface emissivity and cloud liquid water, a topic which will be discussed in further detail in Chapter 4.

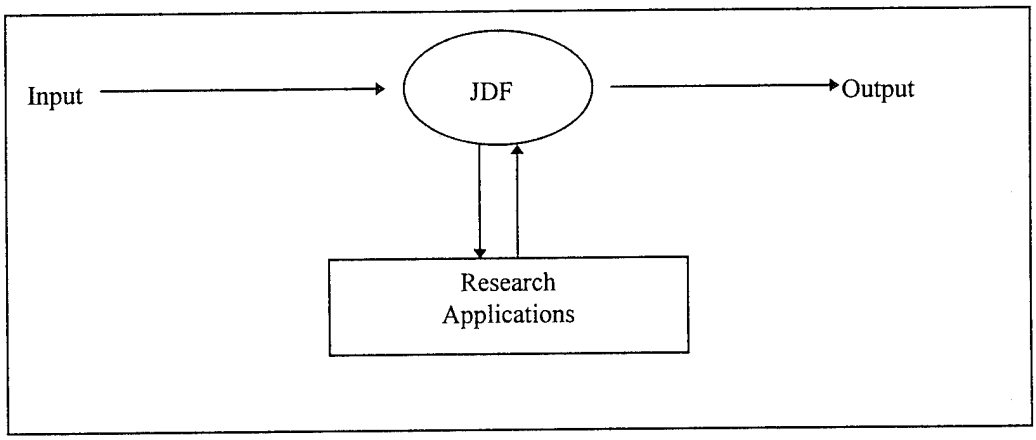

Figure 3.1. *Conceptual Diagram of PORTAL method.*

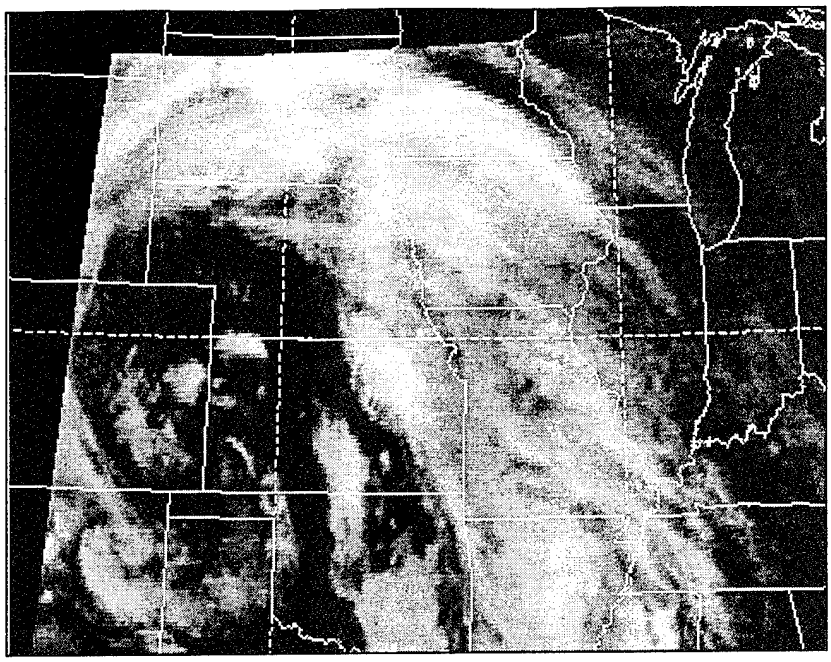

Figure 3.2 *GOES-7 IR(Channel 8) image collected at CIRA during the STORM-FEST project. The black area in the left and upper portions of the image indicates no data was collected by the CIRA groundstation for those regions.*

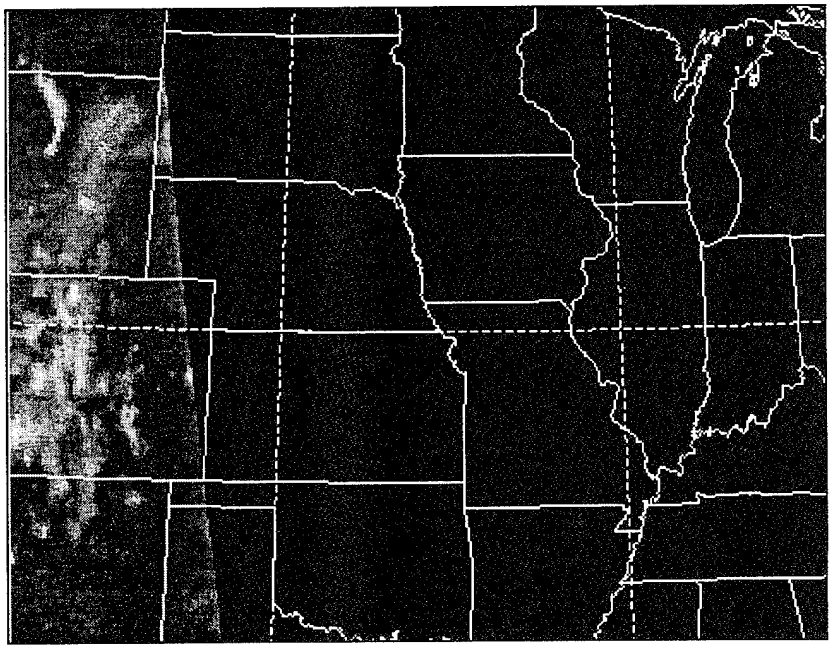

Figure 3.3 *Channel 6(85.5GHz) SSM/I image.*

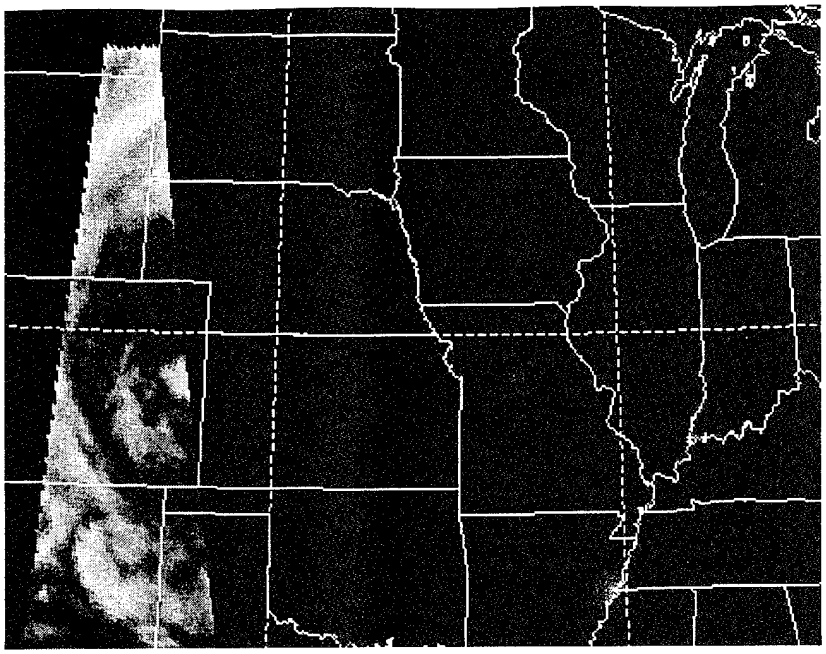

Figure 3.4 *Remapped GOES IR image from Figure 3.2 to the SSM/I Projection in Figure 3.3.*

3.4 General Description of Data Base

The cases for this study were chosen from the Stormscale Operational and Research Meteorology-Fronts Experiment Systems Test (STORM-FEST) Project. The field phase of STORM-FEST was conducted from 1 February - 15 March 1992. This project was designed to investigate the structure and evolution of fronts, embedded precipitation, and associated mesoscale phenomena in winter storms over the central United States. An extremely large database was established in and near the STORM-FEST project domain. From this database, two periods were chosen for this study, 11-12 February and 5-9 March 1992. These cases were chosen on the basis that icing conditions were known to exist both from commercial and research aircraft observations. Another important factor for selecting these periods was the availability of both SSM/I 85.5 GHz and GOES data. The area of interest for the February case is an area approximately 580 x 580 km (40° - 46° N latitude and 96° - 102° W longitude) and approximately 580 x 580 km (37° - 43° N latitude and 101° - 107° W longitude) for the March case. Figures 3.5 and 3.6 shows the high density of the surface and upper air meteorological network available from the STORM-FEST database, both inside and outside of the project domain.

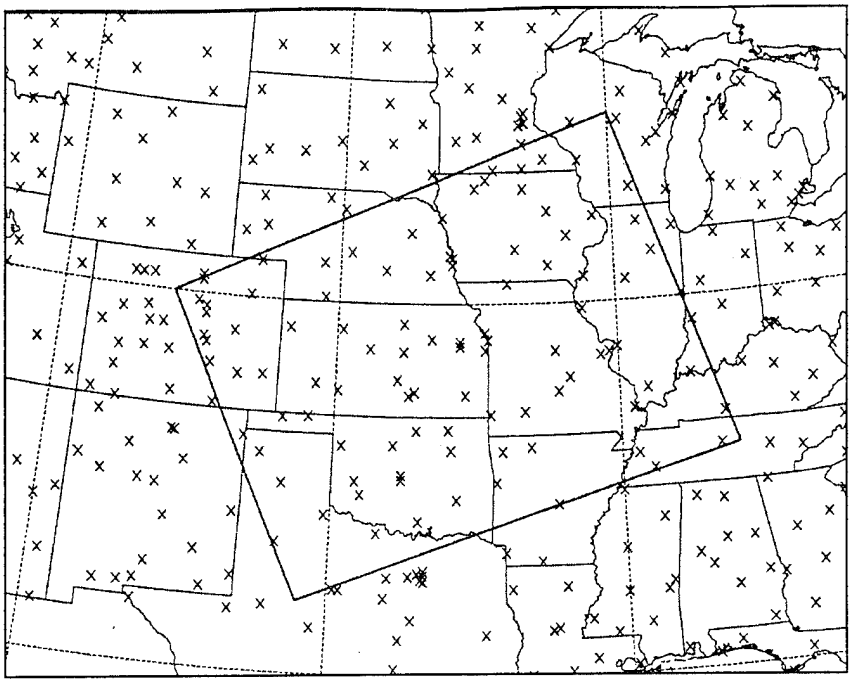

Figure 3.5. *Surface Airways Observation(SAO) sites. STORM-FEST project area is shown by the rectangular area in the Figure.*

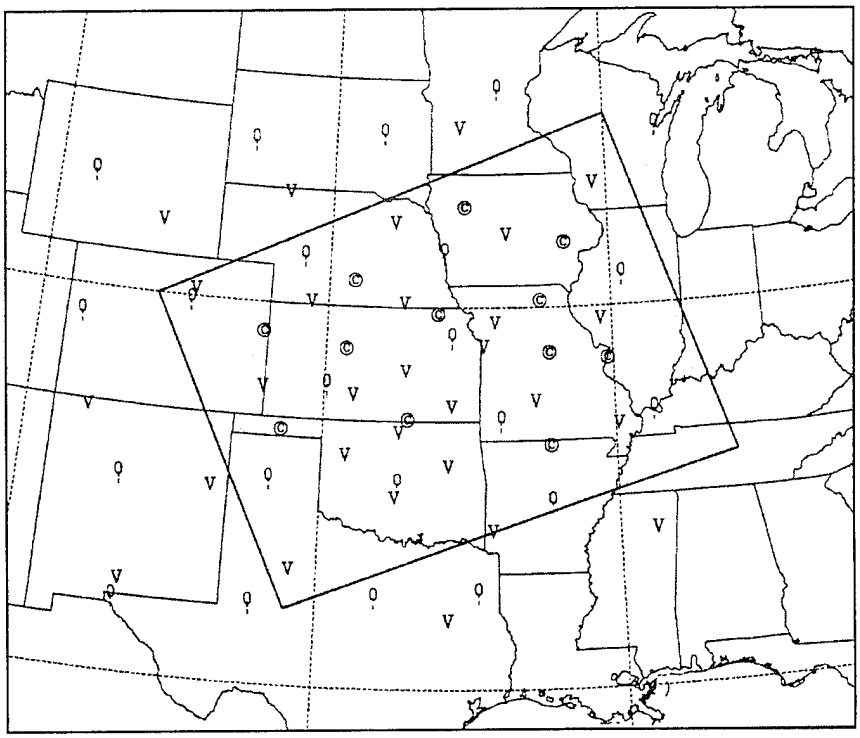

Figure 3.6. *NWS upper air sites(0), CLASS sounding sites(©), and wind profile sites(v) over the STORM-FEST region.*

3.4.1 Satellite Data

Satellite data from both GOES and SSM/I were chosen concurrently for an eight day period from 5 - 12 February 1992 and a five day period from 5 - 9 March 1992. The SSM/I and GOES data sets were selected within ±15 minutes of each other to ensure that both data sets were nearly similar in time in order to make future, time-dependent calculations. An example of an SSM/I image is shown in Figure 3.7. This image is similar in appearance to the GOES IR image (Figure 3.8) in that clouds appear radiatively cold (white). However, water surfaces in the SSM/I image such as the Great Lakes appear noticeably colder than in the IR image. This feature in the microwave brightness temperature field is due to the low surface emittance of water (appears cold in the microwave frequency). In addition, it is evident by comparing Figure 3.7 with Figure 3.8 that many of the cloud features on the IR image are thin in nature and are most likely cirrus. The microwave frequencies can penetrate these thin ice clouds and measure radiation coming from deeper in the atmosphere. This feature of the microwave frequencies allows for deeper penetration into cloud systems such as thunderstorms which in turn provides a more detailed look at the structure of the storm.

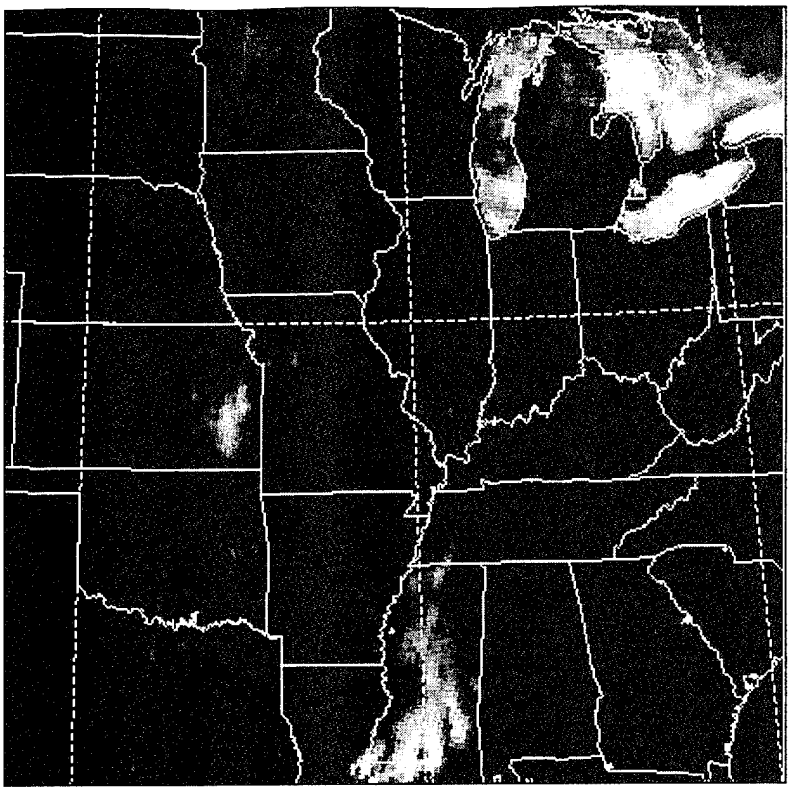

Figure 3.7*. SSM/I 85.5 GHz horizontal polarized (Channel 7) brightness temperature for 11Z 5 Mar 1992.*

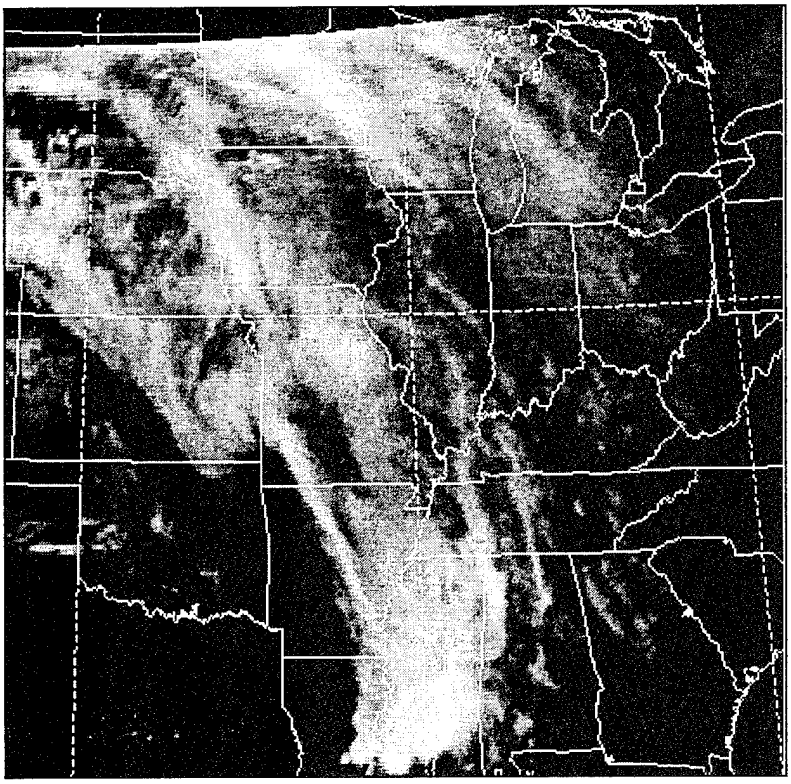

Figure 3.8. *GOES IR(Channel 8) for 5 Mar 1992 11Z*

3.4.2 Sounding and PIREP data sets

Upper air soundings from STORM-FEST were available from conventional (National Weather Service (NWS), Military and Canadian Atmospheric Environment Service (AES)) and research (Cross-chain Loran Atmospheric Sounding System (CLASS), dropwindsonde and Profiler systems) observations. The CLASS soundings were deployed to supplement the existing rawinsonde stations. The STORM-FEST Data Management Center (SFDMC) created a composite upper air data set from all surface-based rawinsonde and aircraft-based dropwindsonde data sets. All individual data sets were converted to National Center for Atmospheric Research (NCAR) CLASS format and interpolated to standard 10 mb pressure levels. A final quality assurance was performed by the SFDMC. Only NWS and CLASS composite soundings were used in this study. The data was collected by a VAX system at CIRA via internet through the Cooperative Distributed Interactive Atmospheric Catalog System (CODIAC). Both the CLASS and NWS soundings provided profiles of atmospheric temperature and water vapor mixing ratio necessary for the calculation of atmospheric transmittance used in this study.

Commercial and private pilot reports (PIREPS) were obtained from the Federal Aviation Administration (FAA) through the NOAA Forecast Systems Laboratory (FSL) at Boulder, CO as well as the data management people at NCAR, also located in Boulder, CO. The PIREP database contained information on aircraft type, location (both altitude and lat/lon) of the icing occurrence, icing intensity, and icing type. At this time, PIREPS provide the only means of icing verification (other than an occasional research aircraft), however, their spatial and temporal coverage is quite often intermittent. In fact, icing

usually varies from one aircraft type to another and is often subject to the pilot's experience, making PIREPS of icing very subjective. In addition, no-icing reports are extremely rare and may be the result of no aircraft in a particular area, or perhaps the aircraft did encounter icing but did not report. Figures 3.9 - 3.13 show a geographical distribution of PIREP icing intensities and altitudes for the three cases in this study. These PIREPS will be used in part to compare with the CLW measurements. The majority of PIREPs of icing commonly occur during the ascent or descent into an airfield (note the clusters of reports near major cities in Figures 3.9-3.13). Also note the variability of the height of the icing occurrences, and in many cases, the pilots failed to even report an altitude. For the most part, however, the icing was reported at heights generally under 15,000ft. Politovich et al. (1992) also found that more frequent PIREPS of icing occurred during daylight hours as opposed to nighttime. This was an indication of more flights during the day, not more icing. It is very difficult to report icing conditions during darkness.

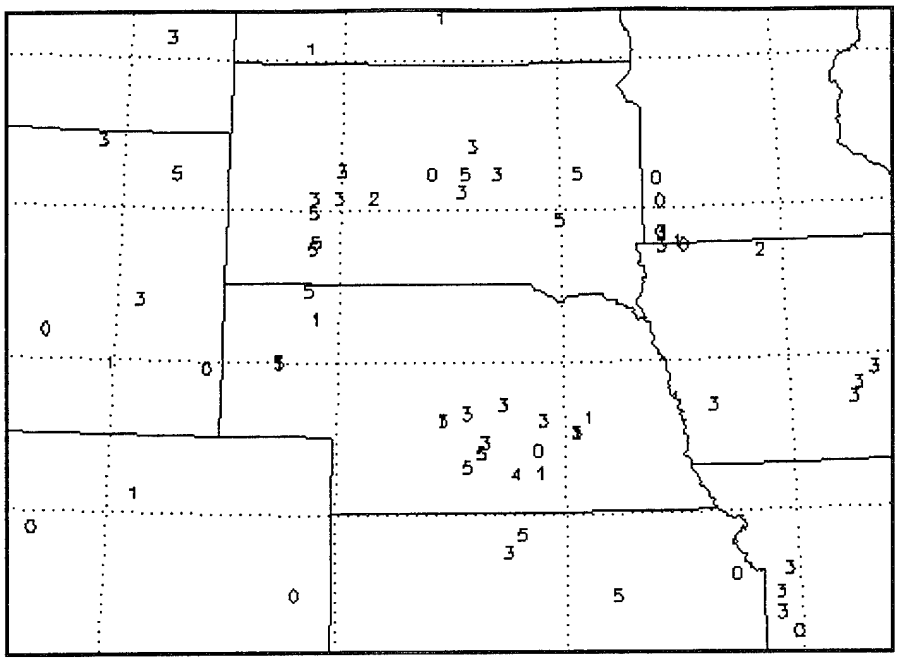

***Figure 3.9a**. PIREP Icing Intensities for 11 Feb 1992. 0=None, 1=Trace, 3=Light, 4=Light/moderate, 5=Moderate, 6=Moderate/Severe, 7=Heavy or Moderate/Severe, 8=Severe.(Category 6 is rarely reported for Moderate/Severe Icing, Category 7 is usually reported by pilots). Each number represents a specific latitude and longitude where icing was reported.*

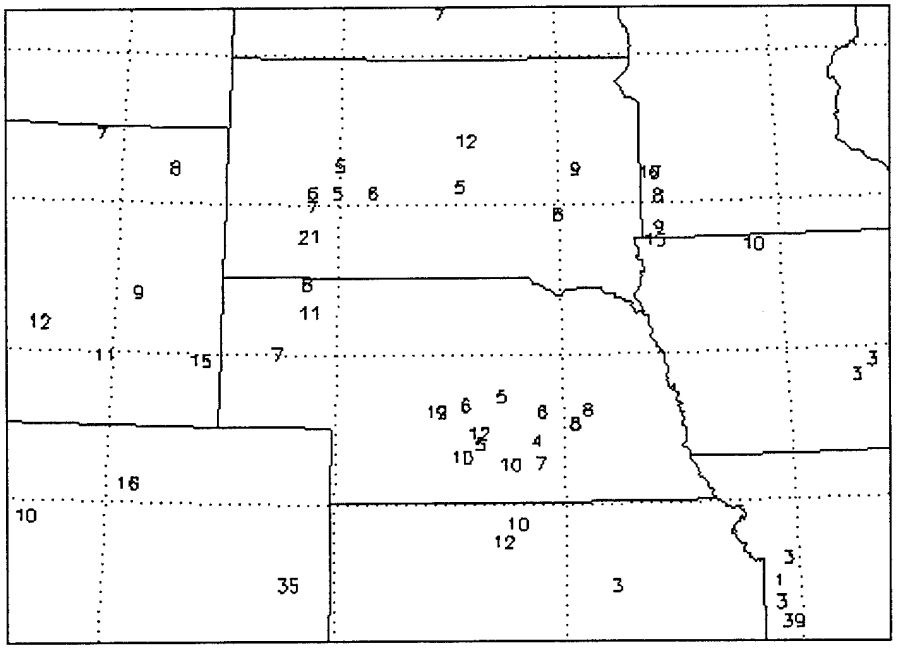

***Figure 3.9b**. PIREP icing altitudes in thousands of feet for 11 Feb 1992.*

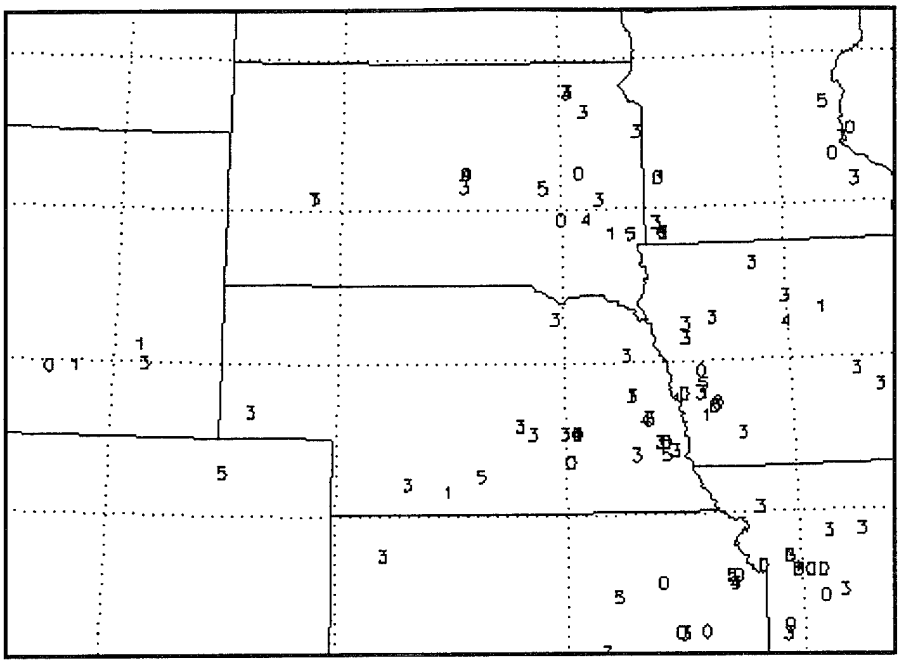

***Figure 3.10a**. PIREP icing intensities for 12 Feb 1992*

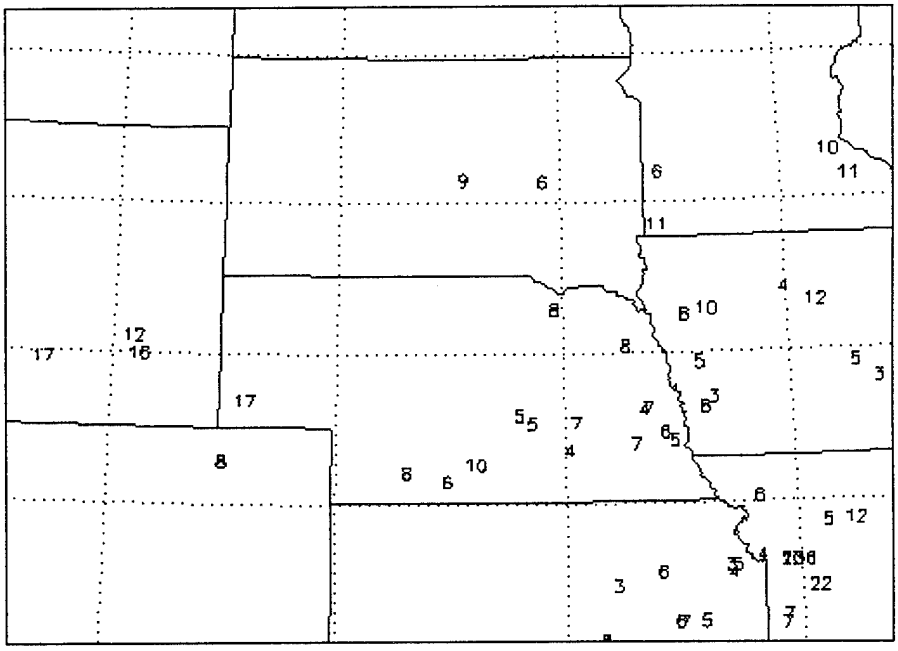

***Figure 3.10b** PIREP icing altitudes in thousands of feet for 12 Feb 1992.*

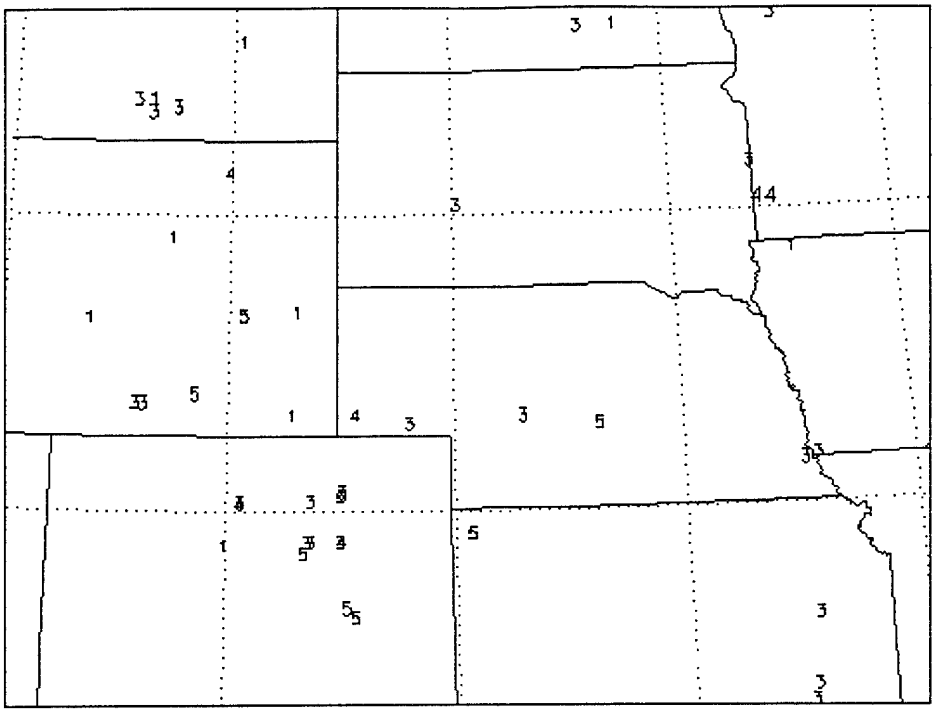

***Figure 3.11a**. PIREP icing intensities for 5 Mar 1992.*

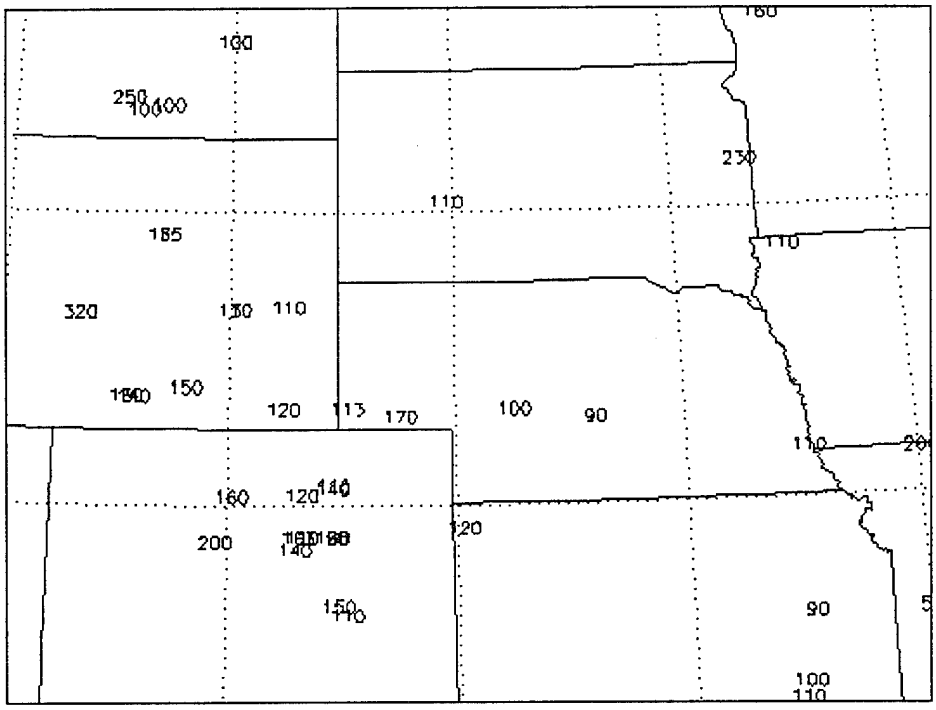

***Figure 3.11b**. PIREP icing intensities in hundreds of feet for 5 Mar 1992.*

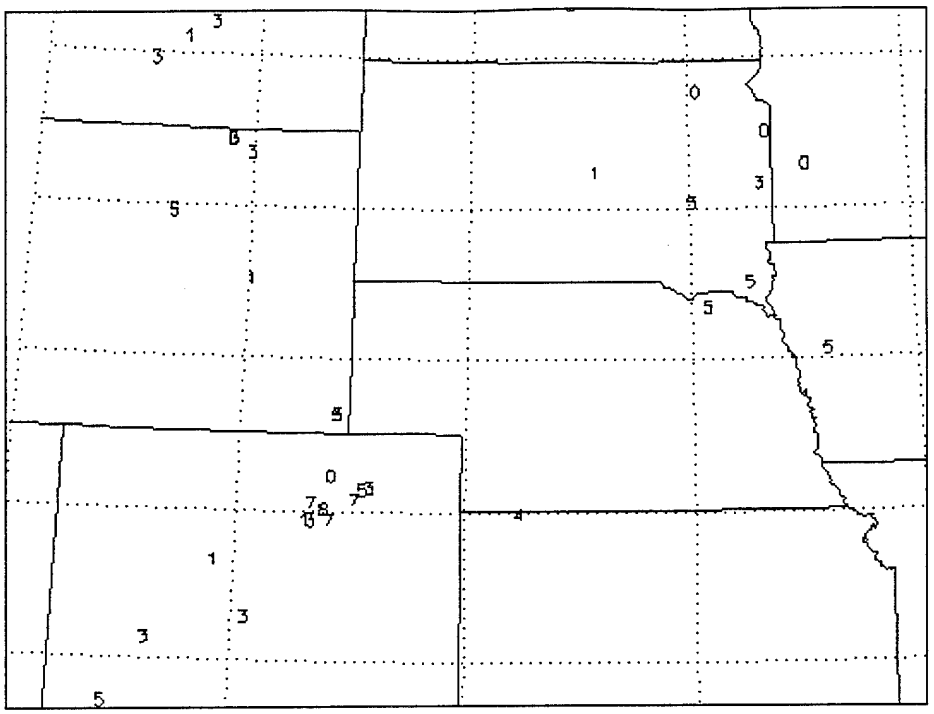

***Figure 3.12a**. PIREP icing intensities for 8 Mar 1992.*

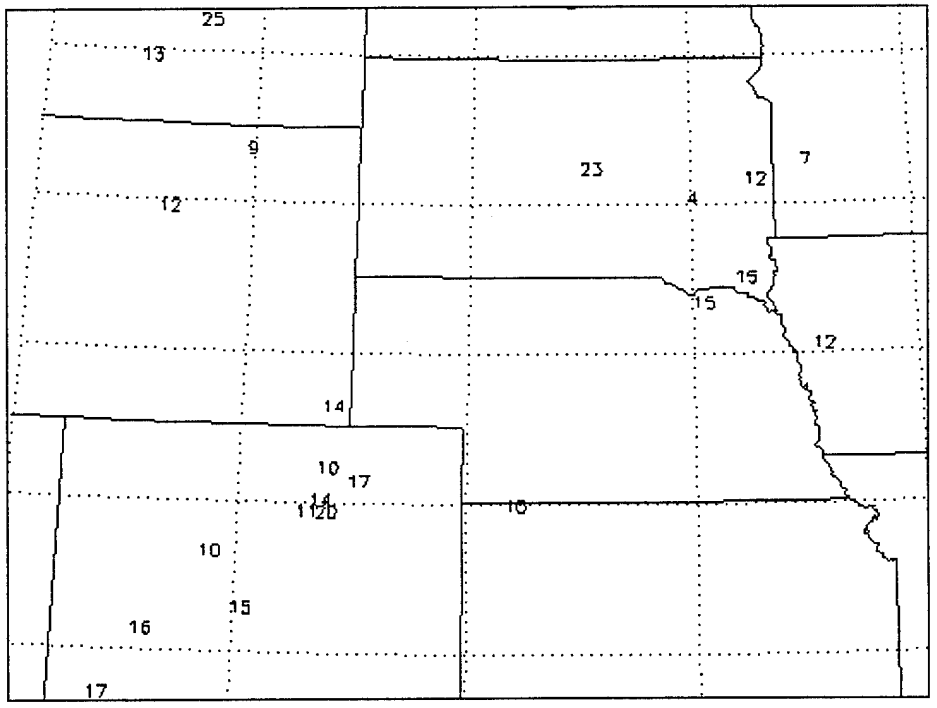

***Figure 3.12b**. PIREP icing altitudes in thousands of feet for 8 Mar 1992.*

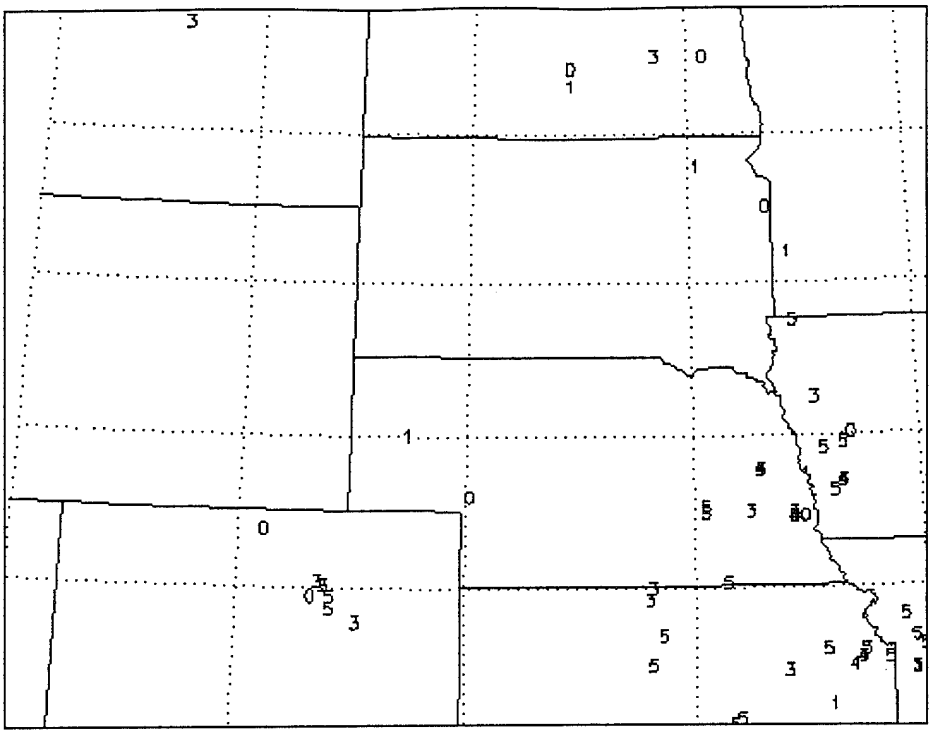

***Figure 3.13a**. PIREP icing intensities for 9 Mar 1992.*

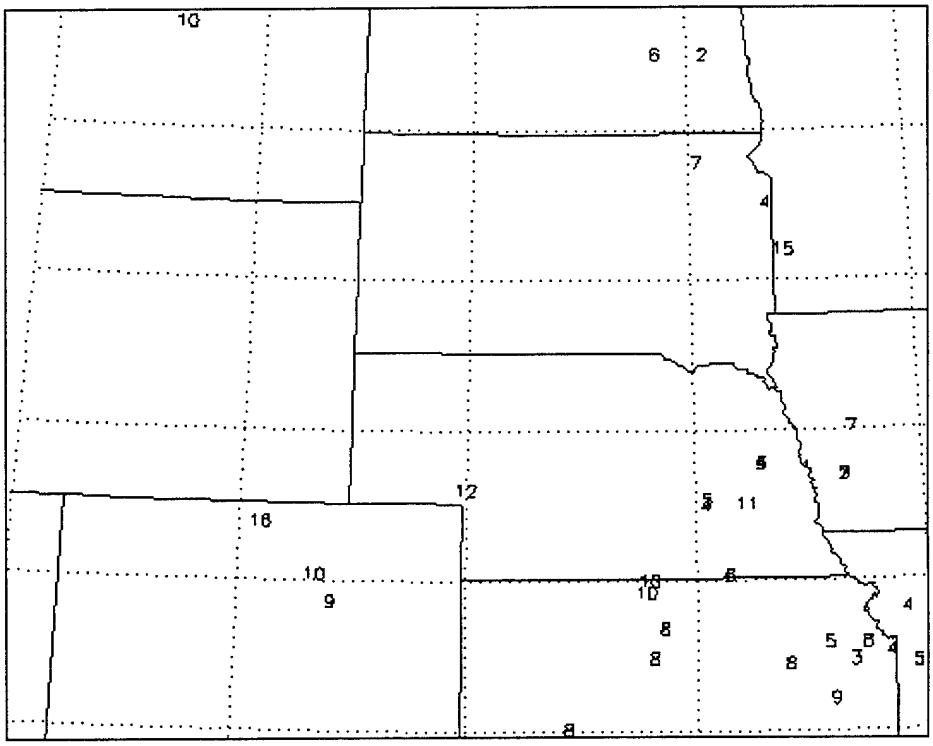

***Figure 3.13b**. PIREP icing altitudes in thousands of feet for 9 Mar 1992.*

3.5 Synoptic Analysis

For the first case, a strong arctic high pressure system centered in southern Canada brought much colder air into the northern and central Plains (Figure 3.14a). A rather strong, north-northeast flow of cold, arctic air set the stage for low clouds, fog and even occasional freezing drizzle behind a shallow cold front in the central plains. At 500mb (Figure 3.14b), a broad but weak shortwave was located over the Great Basin. By the 12th (Figures 3.15a,b), the shortwave had moved out into the southern plains as a low pressure system developed along the cold frontal boundary in eastern Oklahoma. Warm, moist air streamed northward from the Gulf of Mexico overrunning the shallow arctic air mass to the north. Light precipitation in the form of snow and freezing rain/drizzle developed from the Tennessee Valley into the central and northern plains.

The synoptic situation was entirely different in the second case period. On the 5th of March, a deep cyclonic storm system was located over the central United States with the low pressure nearly stacked from the surface to 500mb (See Figures 3.16a and 3.16b). A deep, strong fetch of moisture was prevalent across much of the central portion of the nation with backwash clouds and precipitation as far north and west as Utah and Wyoming. An arctic boundary was entering the northern plains; however, it would not play a role in the weather situation for the area of interest in this study. On 8 Mar 1992 a strong upper-level trough and closed low formed over the southwest, while at the surface, an arctic front had moved southward into Wyoming and South Dakota (Figure 3.15). Warm, moist air flowed freely from the Gulf into the plains ahead of both features. On the 9th (Figure 3.16), a deep surface low developed in Southeast Colorado as the upper level system moved toward the high plains. As the cold front plunged through Northern

Colorado, deep, cyclonically induced upslope conditions developed behind the front causing heavy snow (up to two feet in some locations) to fall from Boulder to Ft. Collins.

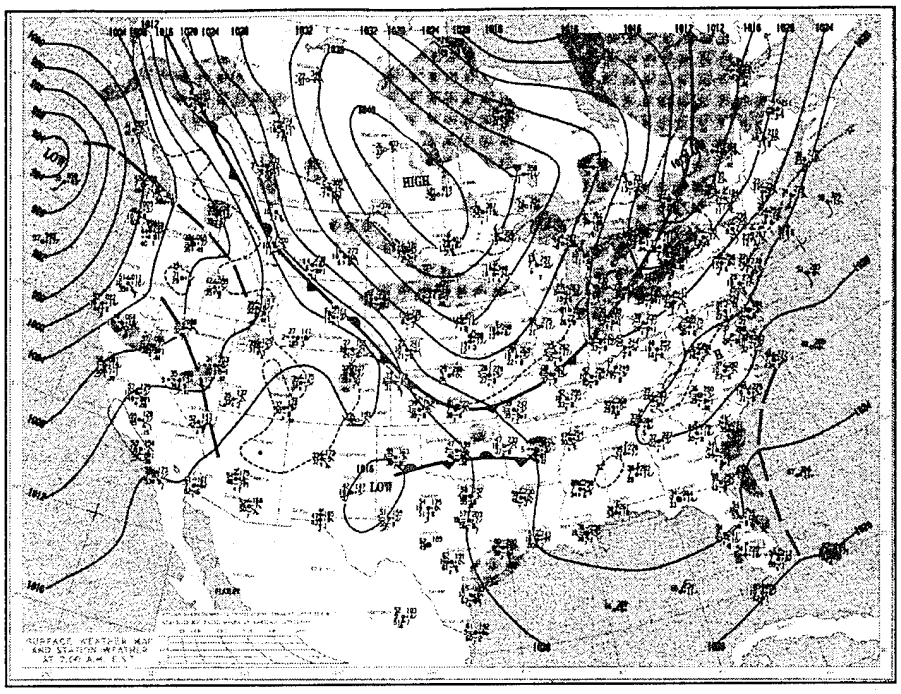

Figure 3.14a. *Surface map for 12Z 11 Feb 1992. Precipitation areas are shaded in gray.*

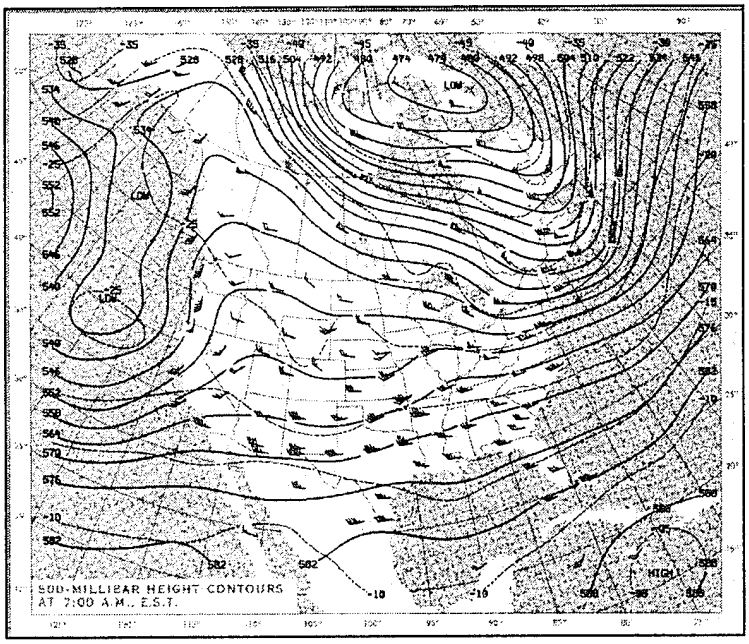

Figure 3.14b. 500mb Heights for 12Z 11 Feb 1992

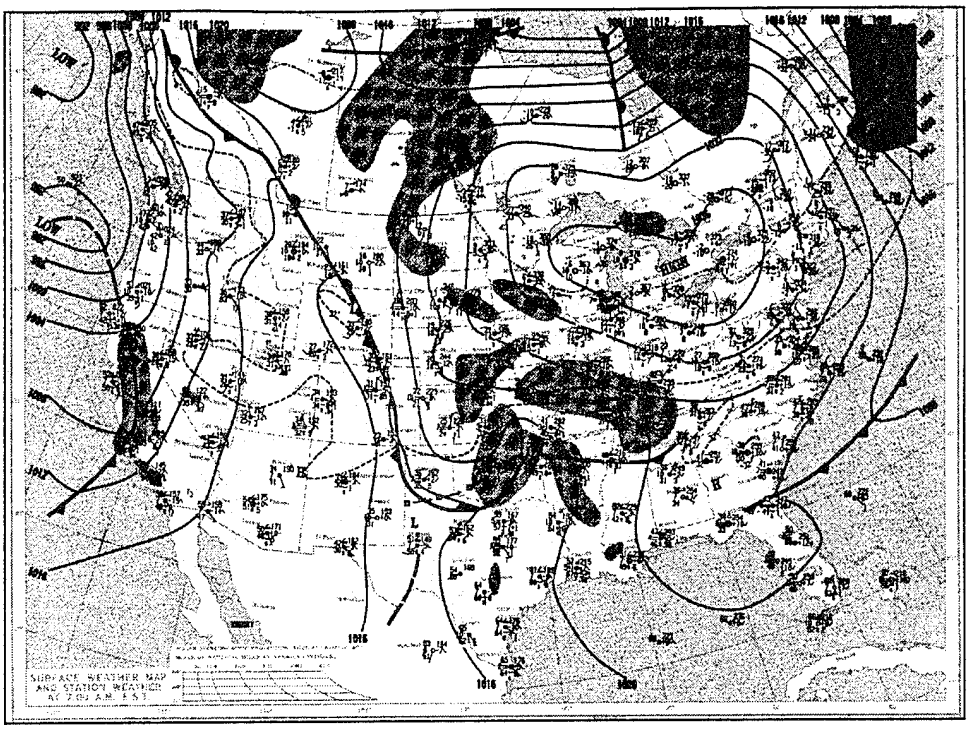

***Figure 3.15a**. Surface map for 12 Feb 1992.*

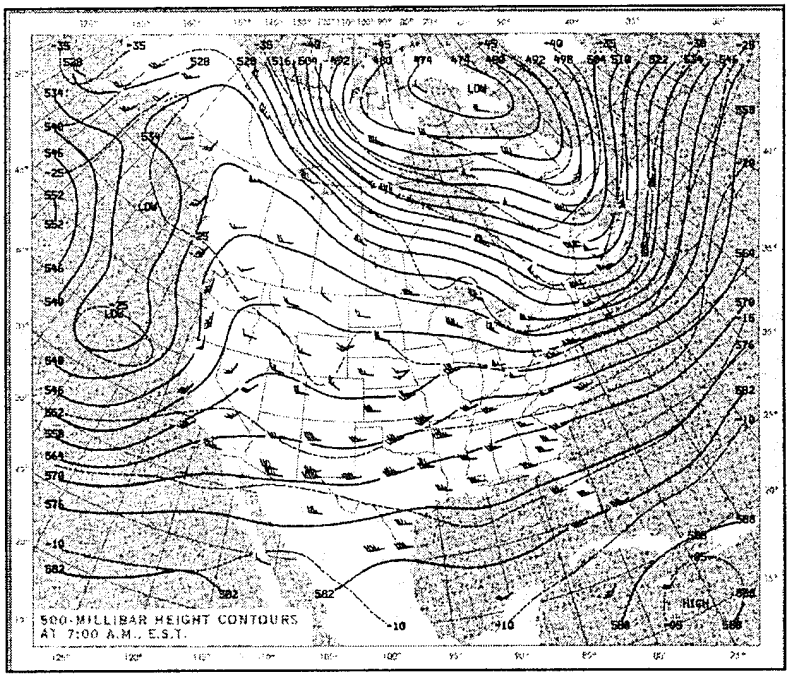

***Figure 3.15b**. 500mb Heights for 12 Feb 1992.*

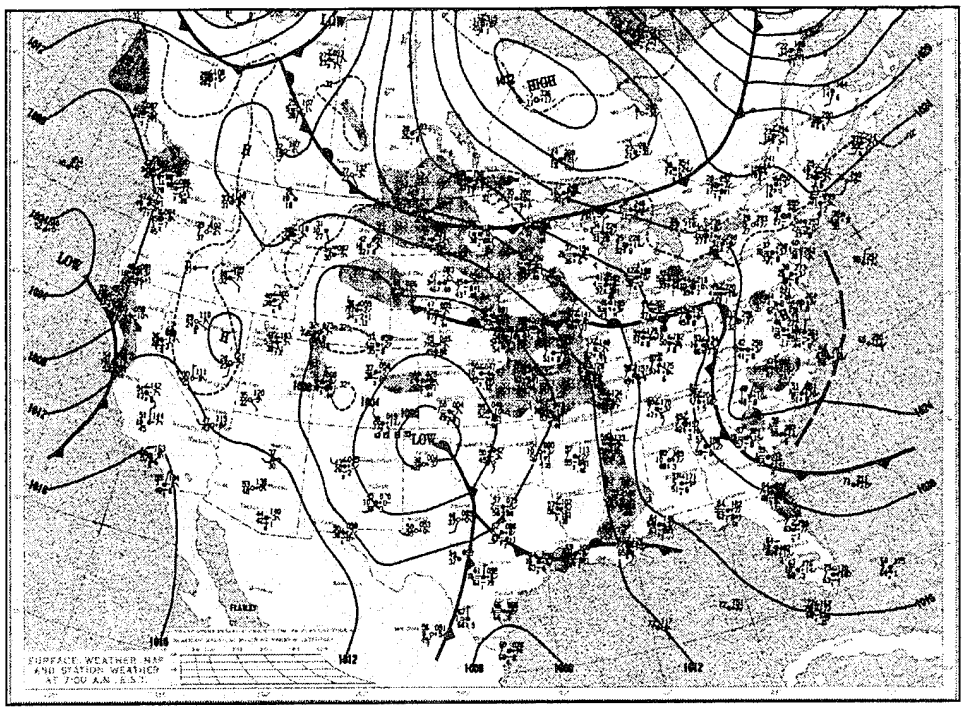

***Figure 3.16a**. Surface map for 12Z 5 Mar 1992.*

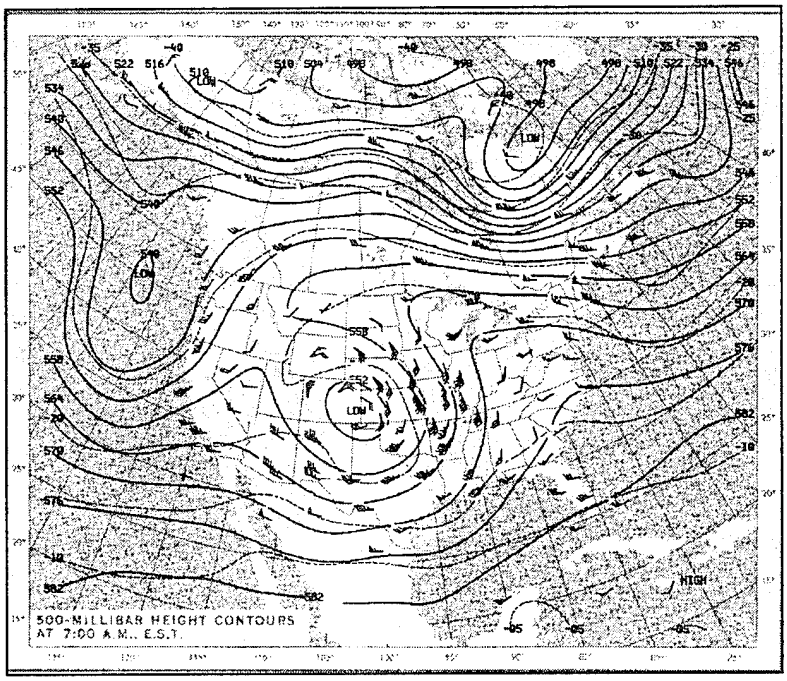

***Figure 3.16b**. 500 mb heights for 12Z 5 Mar 1992.*

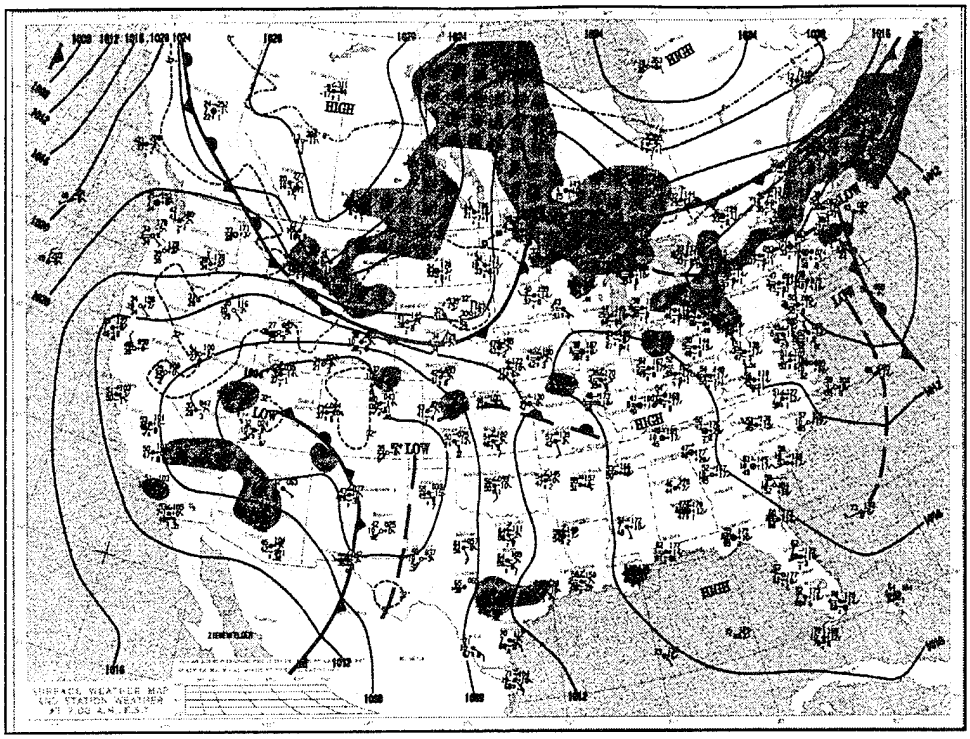

***Figure 3.17a**. Surface map for 12Z 8 Mar 1992.*

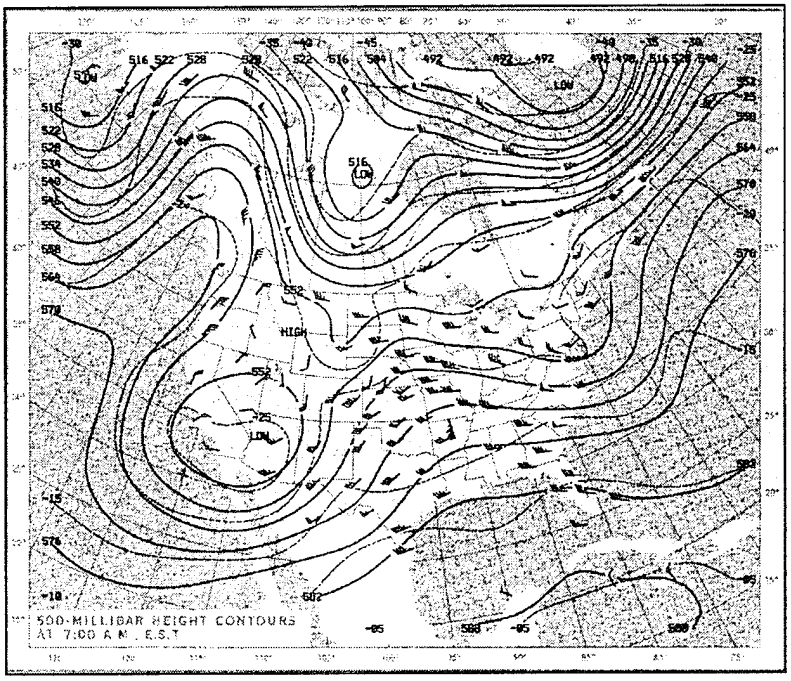

***Figure 3.17b**. 500mb Heights for 12Z 8 Mar 1992.*

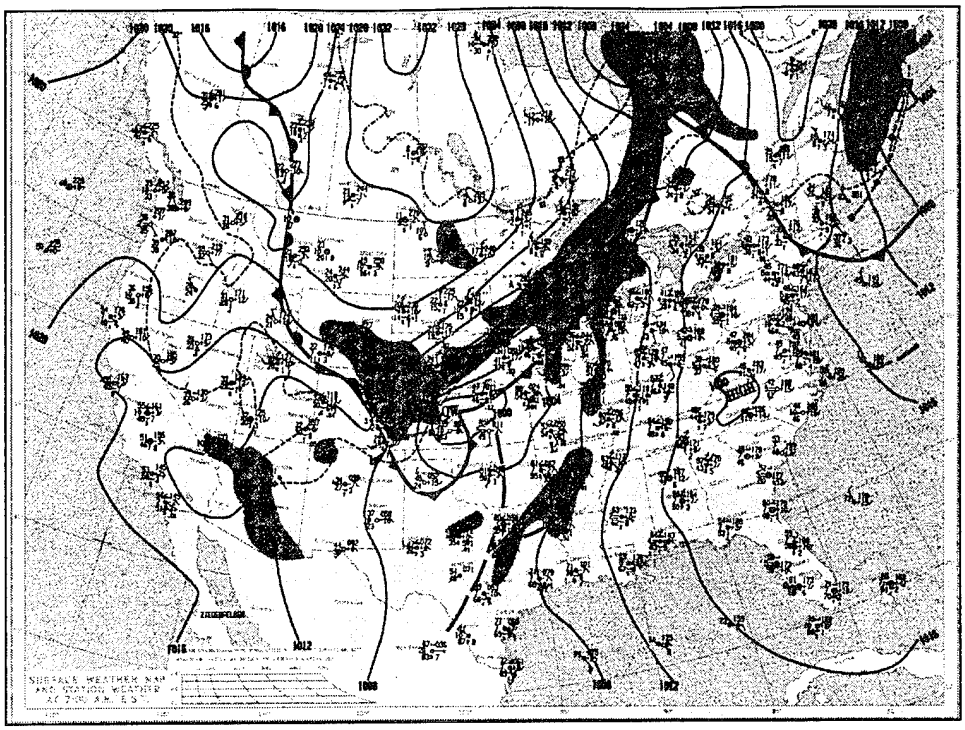

***Figure 3.18a**. Surface Map for 12Z 9 Mar 1992.*

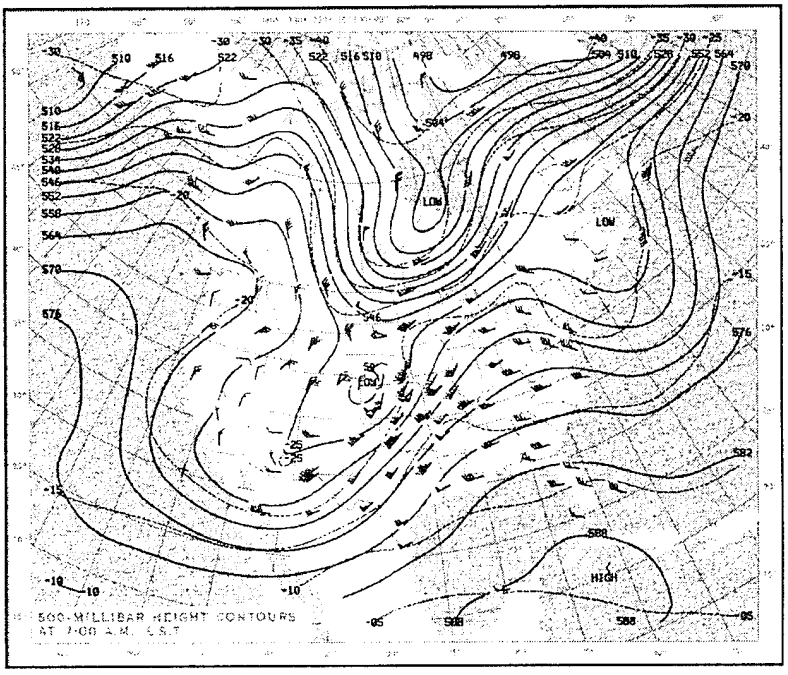

***Figure 3.18b**. 500mb Heights for 12Z 9 Mar 1992.*

4 Icing Index

4.1 General Description

The icing index proposed in this study is an empirically-derived index based on various meteorological parameters derived from satellite and ground-based measurements with a spatial resolution of 13 km. PIREPS will be used to "fine-tune" the Index. In this study, four basic meteorological parameters are assumed to be the major ingredients in determining the potential for aircraft icing. In a real world situation, however, there are many other factors which may indeed play a role in accurately predicting where and when icing will occur (e.g. drop size distribution, embedded convective elements, etc.). This Index is therefore in the initial stages of development and should not be considered otherwise. However, we feel fairly confident that realistic results can be obtained from this exploratory study.

The Index is used to classify different types of icing and is a function of four meteorological parameters as described by the following expression:

$$\textbf{Icing Index} = f\textbf{(CLW, CTT, CD, CT)} \qquad (4.1)$$

CLW (cloud liquid water) is the primary ingredient for determining the index with the expected relationship that increasing supercooled CLW (SCLW) increases the potential for icing. CTTs (cloud top temperatures) and CD (cloud depth) are the next most important components to the index (which are used to determine the CLW) which provide a vertical limit to the icing potential. Finally, CT (cloud texture or more

appropriately intensity) provides further information for determing icing potential. Cloud texture in this context is simply the spatial varation of the intensity (in this case, brightness temperature). The more spatial variation of the intensity, the more likelihood of texture(i.e. cumuliform type of cloud). The following sections of Chapter 4 provide details of the four components of the icing index.

4.2 Measurement of Surface Emittance

The estimation of surface emittance is essential in the determination of surface boundary conditions used in the computation of total upwelling radiance for the retrieval of CLW over land. The characteristics of the underlying surface can significantly alter the microwave radiation measured by the SSM/I sensors. This is due to the fact that the surface emittance in the microwave wavelengths can vary depending on the electromagnetic properties of the surface. Over land, the emittance can vary significantly depending on soil moisture content. For example, wet soils often have surface emittance values in the microwave region of approximately 0.6 while dry soils can have values near 1.0. Surface roughness effects such as vegetation and topography also have an affect on radiation measured by the satellite which in turn affects the measurement of emissivity. Jones and Vonder Haar (1990) measured surface emittance in a summer situation over the western high plains with absolute accuracies from 0.008 to 0.012.

4.2.1 Surface Emittance Retrieval Method

The surface emittance retrieval method used in this study is that of Jones and Vonder Haar (1990). This method employs collocated GOES VISSR IR data with SSM/I microwave data. The IR data are used to retrieve the surface skin temperature which is used in the radiative transfer equation (along with the microwave brightness temperature) to determine the surface emittance. It is important to note that the surface emittance is calculated for clear-sky conditions only.

The first step for this procedure is to remap the GOES IR and VIS satellite data into the SSM/I projection space using PORTAL as described earlier in section 3.3. After remapping the data, our next step is to determine the surface skin temperature. These temperatures are computed in clear-sky regions using the IR data. Since the surface emittance is calculated only for clear-sky conditions, a subjective cloud/no-cloud thresholding technique was applied to the IR GOES VISSR data for cloud discrimination. In addition, during daylight hours, the visible GOES VISSR data were used in conjunction with the IR data to help discern clouds from clear sky.

The surface skin temperature is calculated using equation 2.1 which can be written more compactly as,

$$L_m = L_{sfc} \qquad (4.1)$$

where L_m is the measured radiance from the IR surface channel and L_{sfc} is the surface contribution to the total upwelling radiance (for purposes of this study, we have neglected the direct and reflected atmospheric contributions to the upwelling radiance since their

contribution is small compared to the surface effects). The surface contribution is found by

$$L_{sfc} = B_{IR}(T_{BIR})\tau_{IR}(p_s,0) \qquad (4.2)$$

Equation 4.2 is then solved for the skin temperature, where the subscript IR refers to the infrared GOES channel 8 and for purposes of this study, τ_{IR} is assumed to be 1.0, then

$$\overline{T}_{BIR} = B_{IR}^{-1} L_{sfc} \qquad (4.3)$$

where B_{IR}^{-1} is the inverse Planck function. $\overline{T}_{BIR}$, the mean infrared brightness temperature for the microwave field of view (FOV) is given by a weighted average of the retrieval skin temperature within the SSM/I FOV,

$$\overline{T}_{BIR} = B_{IR}^{-1} \frac{\sum_{ij} W_{ij} B_{IR}(T_{BIR_{ij}})}{\sum_{ij} W_{ij}} \qquad (4.4)$$

where W_{ij} is the microwave sensor's response or weighting function. Once the mean surface skin temperatures are calculated, the integrated microwave radiative equation is solved for ε_v (neglecting atmospheric effects) and equation 2.2 becomes,

$$\varepsilon_{sfc} = \frac{T_{Bmw}}{\overline{T}_{BIR}} \qquad (4.5)$$

where T_{Bmw} is the measured brightness temperature from the SSM/I instrument.

4.2.2 Results

Surface emittance values could not be retrieved in regions of cloud since clouds in the IR region obscure the surface. As a result of this limitation, surface emittance values were composited in this study by averaging the retrieved surface emittance data over a period of several days to ensure a better spatial coverage of the final product. Note, PORTAL was used during the calculation of surface emittance which kept the results in JDF format. This procedure will allow for more accurate computation of CLW (described later in section 4.3).

Surface emittance results from 5-12 February 1992 were composited for the first case period in this study. Table 4.1 shows a statistical analysis of the composited surface emittance. Values range from near 0.6 (0.608) to nearly 0.95 (0.951). Standard deviations for the horizontally polarized channel (Channel 7) have consistently larger variability than the vertically polarized channel (Channel 6). This could possibly be due to surface roughness effects such as vegetation and topography as well as soil moisture, which is consistent with the surface measurement results of Choudbury et al. (1979).

Table 4.1. *Composite surface emittance statistics for 5-12 Feb 1992. N is the number of surface emittance values.*

	Mean	Std Deviation	Max	Min	N
Channel 6	0.951	0.047	1.011	0.674	60,681
Channel 7	0.931	0.061	1.006	0.608	60,681

Figures 4.1 and 4.2 are composite surface emittance images of the region of interest. Also note the spatial variability of the clear sky surface emittance for Channel 7 (Figure 4.2), the horizontal polarized 85.5 GHz channel which was indicated in Table 4.1. The dark areas in the image indicate that clouds persisted over the entire period of time, thus no values were calculated. In Figure 4.1 (Channel 6) relatively high emittance values(>.90) occurred over much of the area which is mainly free of snow cover. However, notice the lower values over eastern Colorado, northeast Wyoming, and northern South Dakota into Minnesota and northern Iowa. These are areas where snow is covering the ground resulting in lower surface emittance values.

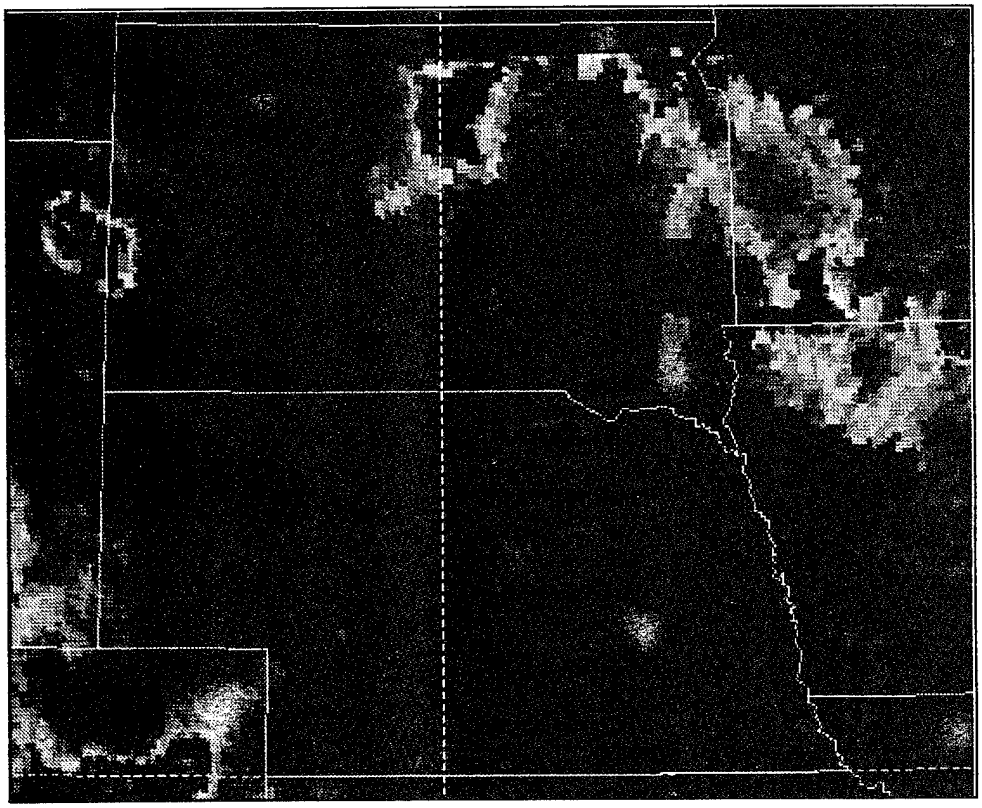

Figure 4.1. *Channel 6 composite surface emittance for 5-12 Feb 1992.*

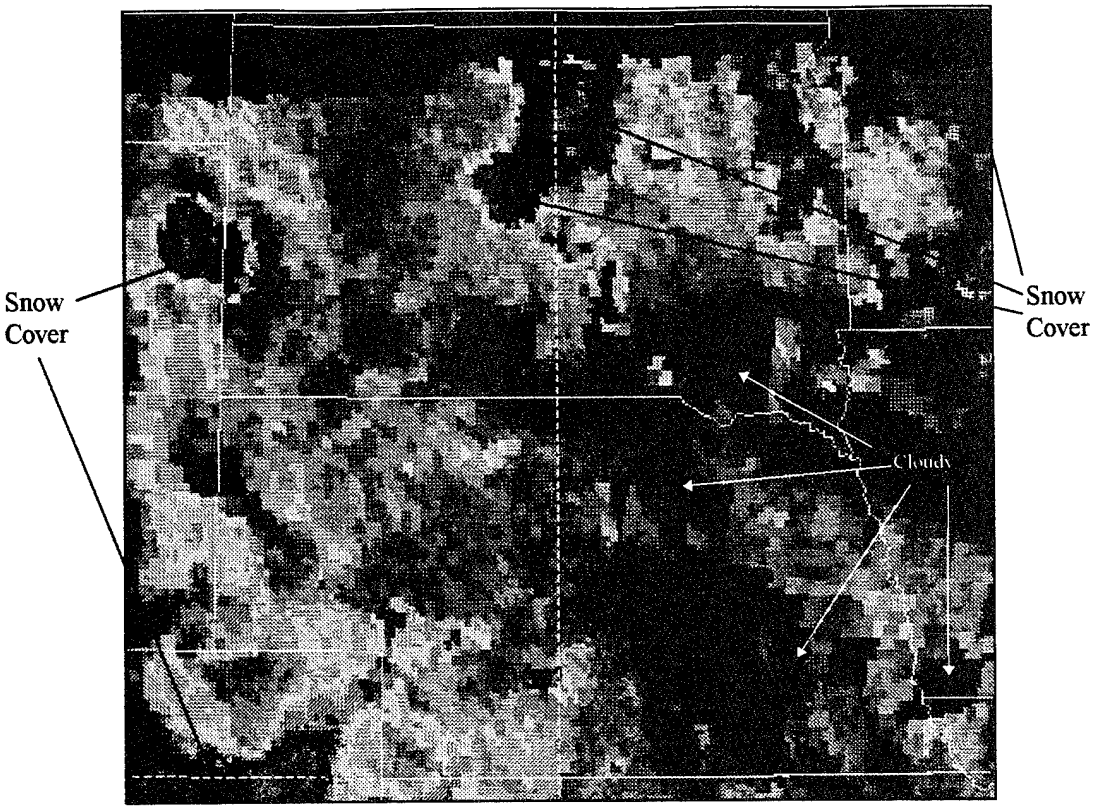

Figure 4.2. *Channel 7 composite surface emittance for 5-12 Feb 1992.*

Land surface emittance composites were also computed for the second case study from 5-9 March 1992. A statistical analysis was derived from these calculations and the results are shown in Table 4.2. Notice once again, that Channel 7 shows more variability (0.038) than Channel 6 (0.024). In this case, fewer emittances were calculated than in February with values averaging slightly higher for both channels. Figures 4.3 and 4.4 show the spatial distribution of surface emittance. There were several more periods of

cloudiness than in the first case so more areas appear black on the images. The one major difference between the two cases is the lack of areas of low emittance values in Figures 4.3 and 4.4. This can be attributed to the lack of major snow cover as reported by surface observations in the March case. A prime example of this is the absence of lower emittance values in the Black Hills of South Dakota (Figure 4.3). Most, if not all of the snow has melted from the area resulting in higher surface emittance values. Another area of interest is the high values in South Dakota, most likely attributed to the relatively dry, unforested surface. Much of the rest of the area has values near 0.90. These slightly lower values are primarily due to precipitation infiltrating the top layer of soil. Figure 4.5 shows the precipitation reports for 5 March from various observation stations across the region. As is evidenced by the reports, most of area received measurable precipitation in the past 24 hours.

Table 4.2. *Composite surface emittance statistics for 5-9 Mar 1992.*

	Mean	Std Deviation	Max	Min	N
Channel 6	0.972	0.024	1.019	0.671	38,562
Channel 7	0.955	0.038	1.008	0.671	38,562

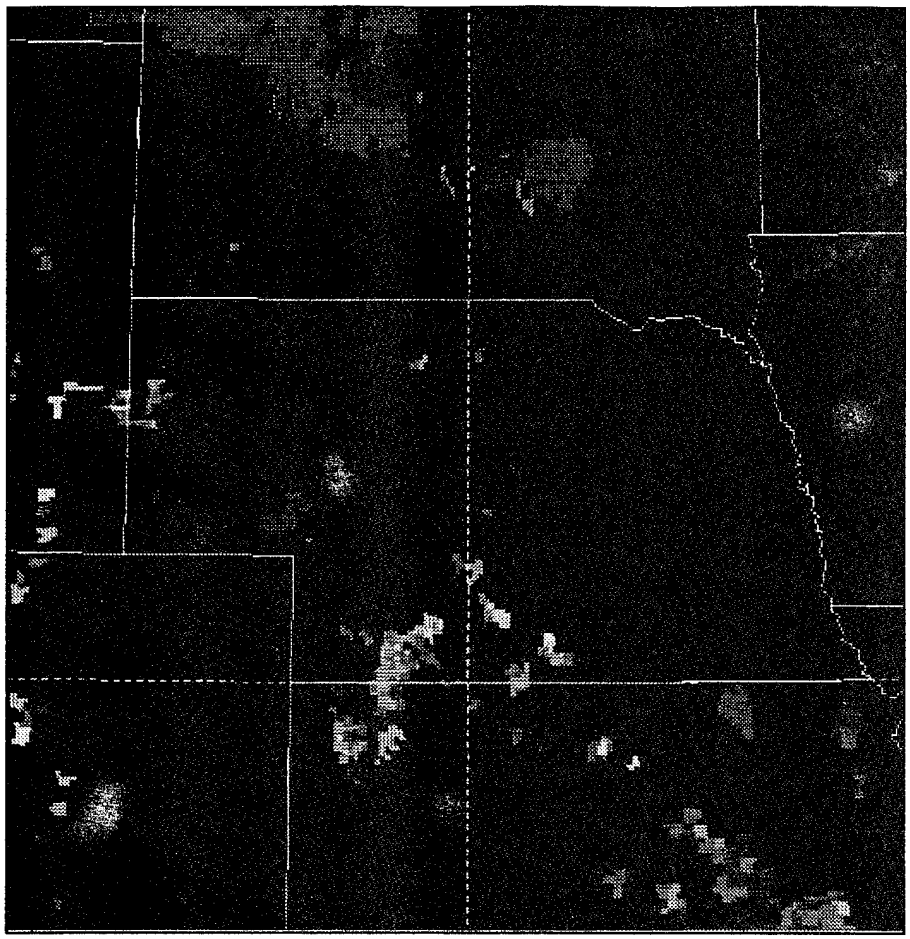

Figure 4.3. Channel 6 composite surface emittance for 5-9 Mar 1992. Black areas on the image indicate that clouds were present for the entire period and no surface emittance was calculated.

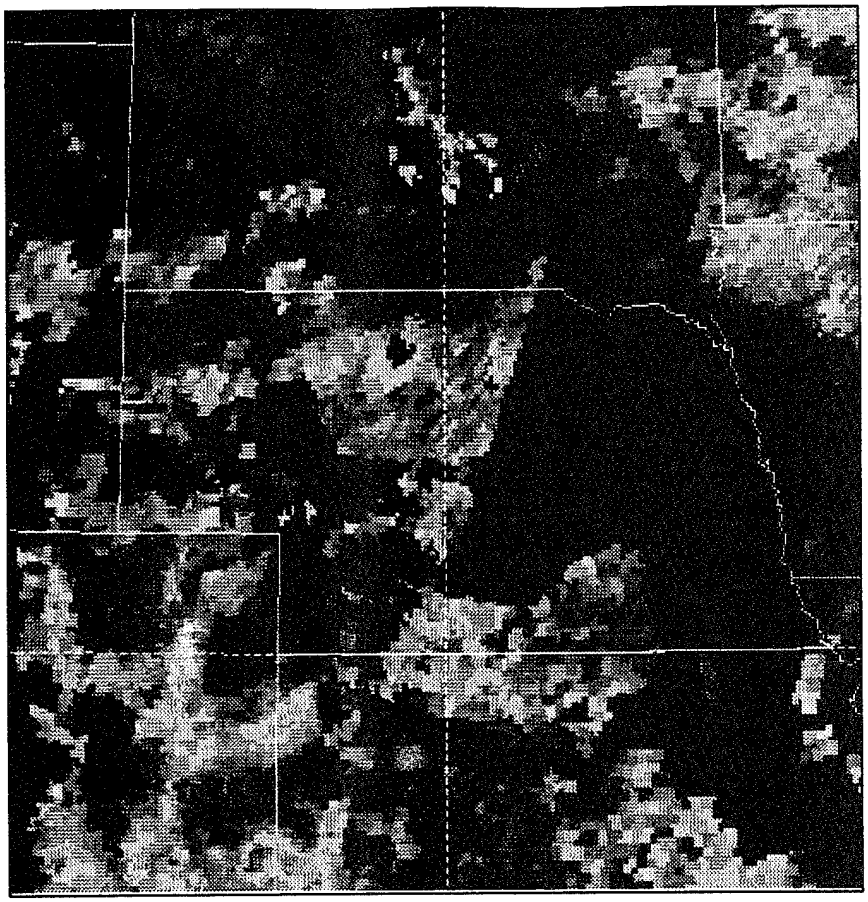

Figure 4.4 *Channel 7 composite surface emittance for 5-9 Mar 1992*

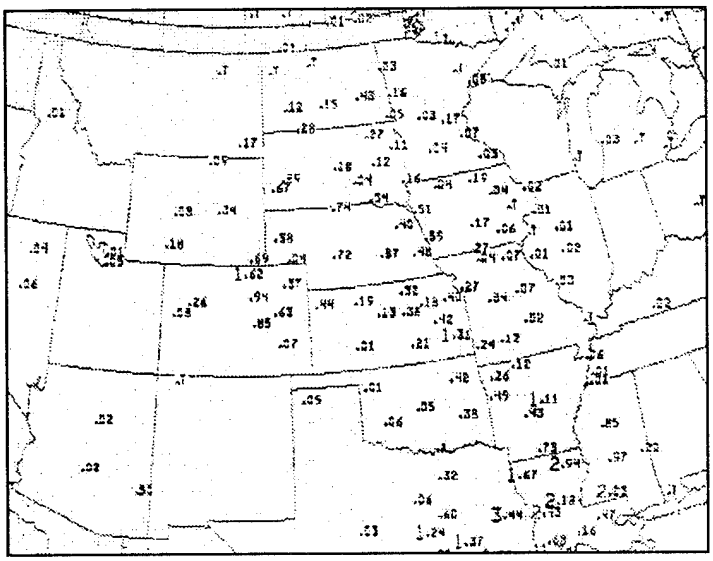

Figure 4.5. *24hr observed precipitation ending 12Z 5 Mar 1992.*

4.3 Cloud Liquid Water Retrieval

The cloud liquid water (CLW) retrieval method used in this study is the method developed by Jones and Vonder Haar (1990). This method retrieves CLW by calculating theoretical brightness temperatures and comparing them to observed brightness temperatures measured by the DMSP SSM/I for the 85.5 GHz channels (Channel 6 and 7, see Table 3.1). The 85.5 GHz channels were selected because this frequency is nearly twice as sensitive to liquid water than at lower frequencies (19 and 37 GHz). CLW attenuates the microwave radiation emitted from the surface and therefore emits at cooler brightness temperatures since the ambient temperature is colder at a higher altitude. The colder temperatures associated with higher cloud tops depress the brightness temperatures more which makes the brightness temperature more sensitive to CLW at high levels (See Figure 4.1).

4.3.1 Theoretical Brightness Temperature Calculations

The composite surface emittance results in section 4.2.2 are used to calculate brightness temperatures from the integrated microwave radiative transfer equation,

$$L_\nu(0) = \varepsilon_\nu B_\nu(T_s)\tau_\nu(p_s,0) + \int_{p_s}^{0} B_\nu[T(p)]\frac{\partial \tau_\nu(p,0)}{\partial p}dp$$

$$+(1-\varepsilon_\nu)[\tau_\nu(p_s,0)]^2 \int_{p_s}^{0} \frac{B_\nu[T(p)]}{[\tau_\nu(p,0)]^2}\frac{\partial \tau_\nu(p,0)}{\partial p}dp \qquad (4.6)$$

Here, the deep space cosmic radiation reflection term yields a very small number and is therefore neglected and not shown. The Liebe Millimeter-wave Propagation Model (MPM), which uses a time and space representative NWS or CLASS sounding, is used to

calculate the atmospheric transmittance. By using only one representative sounding, we assume that the spatial variations of water vapor are small compared to the spatial variations of CLW. T_s, the surface skin temperature, is taken from the surface observed temperature of the selected sounding.

The Liebe MPM was developed by Dr. Hans J. Liebe at the Institute for Telecommunication Sciences in Boulder, Colorado. This is a limited line model which uses an 80 line data base and is valid for a frequency range of 1 to 1000 GHz. Allen and Liebe (1983) provide a concise description of the model and the line paramaterizations used. The meteorological variables used in the model are, pressure, temperature, water vapor mixing ratio, and liquid water. Oxygen and water vapor absorption are calculated along with the cloud liquid water attenuation.. The verification of the MPM is within 4 percent of the experimental uncertainties of the observations.

4.3.2 Cloud Top and Base Determination

Cloud top pressure is determined using the infrared temperature from the corresponding GOES image and this pressure is related to the pressure contained within the temperature profile of the sounding. The cloud base is set as the Lifting Condensation Level (LCL) calculated from the in-situ sounding. This measurement of the cloud base provides a realistic observation of the cloud base. It should be noted that the LCL method often overestimates the cloud base during the winter months. This is mainly due to the fact that the lifting required to reach the condensation level rarely occurs in winter (especially at mid-latitudes). Quite often, cloud bases reported by surface observations (ceilometers) may be some 200-300 m lower than that measured

from a sounding. However for purposes of this study, the LCL cloud base will be used. The cloud top and base provide the vertical limits on the location of CLW which is summed during the retrieval process. The cloud generated in the retrieval process is assumed to have a uniform vertical distribution of liquid water. This is obviously an over simplification of the true vertical structure. Additional microwave sounding channels which are more opaque are necessary in order to provide a more detailed vertical resolution.

4.3.3 Precipitation Threshold

The Raleigh approximation used in the calculation of CLW attenuation is valid only for non-precipitating clouds at millimeter wavelengths. This method is therefore not applicable for retrieval of liquid water from precipitating clouds and a method must be derived for detecting precipitating clouds. This study uses a modified version of the threshold method developed by Spencer et al. (1989) for retrieving rain rates over both land and ocean. Specifically, this method involves adjusting the particular SSM/I brightness temperature threshold to the winter atmosphere. This threshold value is derived from theoretical absorption-only calculations of microwave radiation and represents the value when the microwave radiation with respect to the particular channel is completely saturated (i.e., 100 percent absorption). Therefore, regions with SSM/I brightness temperatures less than this threshold value (i.e., precipitating clouds) will be insensitive to change in CLW and excluded from the CLW retrieval calculation. A threshold value of 249K was used for this study based on the same theoretical radiation calculation with winter sounding conditions.

4.3.4 Procedure for Determining Cloud Liquid Water

Initially, the liquid water content is set to zero and the theoretical brightness temperature is calculated using equation 4.6. The difference between the observed brightness temperature $\tilde{T}_B$ and the theoretical brightness temperature T_B

$$\Delta T_B = \tilde{T}_B - T_B \qquad (4.7)$$

is used to increment the liquid water content until ΔT_B is within the SSM/I instrument noise level(0.5°K). The CLW content is calculated using Newton's method (Conte and de Boor, 1980) for a model cloud, such that

$$CLW_{i+1} = CLW_i - \frac{\Delta T_{Bi}(CLW_i - CLW_{i-1})}{(\Delta T_{B_i} - \Delta T_{B_{i-1}})} \qquad (4.8)$$

where the subscripts identify the iteration number. Initially, CLW_i is assumed to be on the order of 0.005 kg m^{-2}. Approximately 2-4 iterations occur before the method converges.

The integrated CLW is determined using the retrieved CLW content along with the pressure of cloud top and base, which are converted to height using hydrostatic equilibrium. The retrieved CLW content is integrated over the cloud depth resulting in vertically integrated CLW in units of kg m^{-2} (equivalent to mm of depth).

4.2.5 Results

Cloud liquid water was first calculated for non-precipitating clouds (SSM/I brightness temperatures > 249K) over the upper midwest for the 11-12 Feb 92 case. Minimal CLW was calculated on 11 Feb and is therefore not shown. However, a large

area of CLW was present on 12 Feb across portions of South Dakota and Nebraska at approximately 03Z (See Figures 4.7 and 4.8). Figure 4.6 shows the Huron, South Dakota sounding at 03Z on the 12th. This sounding was chosen as a representative sounding for the area of interest and was used in the Liebe MPM for calculating atmospheric transmittance as well as determining a representative cloud base. A deep moist layer was present from 900 mb to nearly 500mb with temperatures remaining below freezing through the entire atmosphere. This indicates that any liquid water present would be supercooled at least to near 400 mb where temperatures approached -40°C. Pure supercooled water droplets can exist to temperatures of -36°C before freezing by homogeneous nucleation (Wallace and Hobbs 1975; DeMott and Rogers 1990). Therefore it is assumed that liquid cannot exist below this temperature. For purposes of icing on aircraft, -20°C has been found to be the threshold temperature below which icing does not constitute a major hazard. Table 4.3 provides a statistical analysis of the vertically integrated CLW and cloud depth for 03Z on the 12th.

Average values of CLW were near 0.6 kgm^{-2} (liquid water content (LWC) of 0.15 gm^{-3}) for Channel 6 and 0.7 kgm^{-2} (LWC of 0.2 gm^{-3}) for Channel 7 with the highest average CLW measured by the horizontal polarized 85.5 GHz SSM/I channel. This is consistent with the surface emittance results from Section 4.2. Channel 7 emittance (Figure 4.2 and Table 4.1) indicated lower and more variable emittance values which would lead to higher and more variable CLW values (Table 4.2). These values of CLW were very consistent with LWC values obtained by research aircraft in wintertime clouds over the Great Plains and the Sierra Nevada during the late 1970's and mid 1980's.

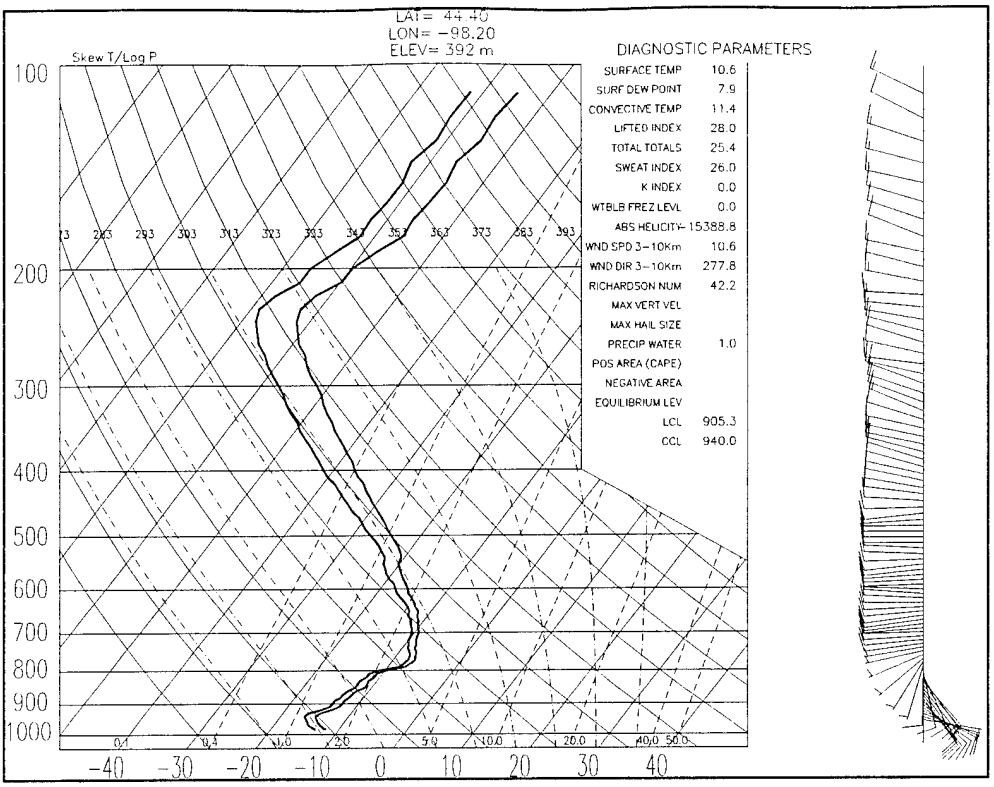

Figure 4.6. *Skewt plot of Huron(HON), SD sounding for 03Z 12 Feb 1992.*

Table 4.3. *CLW Statistics of South Dakota region for 03Z 12 Feb 1992. Channel 6 is the 85.5 GHz vertical polarized channel and Channel 7 is the 85.5 GHz horizontal polarized Channel.*

LCL=905, Height=1087m, Temp=-13.5°C				
	Mean	**Std Deviation**	**Max**	**Min**
Channel 6(Kgm^{-2})	0.57	0.39	2.64	0.19
Channel 7(Kgm^{-2})	0.77	0.28	1.44	0.3
Cloud Depth(m)	3951	317	4319	3240
Cloud Top(m,est.))	5039	317	5406	4327
Cloud Top Temperature(°C)	-21.6	2.1	-16.7	-25.2

(Politovich 1989; Sand et al. 1984). Aircraft measurements of liquid water contents averaged near 0.2 gm^{-3} with temperatures averaging around -7°C. These liquid water values were obviously taken from a different time period, however cloud temperatures and structures were very similar to this study. Also of importance to note here is the difference between Channel 6 and 7 CLW values. The CLW on average is higher for Channel 7 than Channel 6 because of the sensitivity of Channel 7 to the variance of surface emittance. Note, however, that the standard deviation for Channel 6 is greater than Channel 7. This can be explained by the fact that a few outlier values > 1.0 kgm^{-2} were computed which would tend to skew the standard deviation toward a high value. The majority of the CLW values, however, were < 1.0 kgm^{-2}. Earlier in this chapter (Section 4.1) I assumed the atmospheric effects were negligible in calculating the surface emittance. By including the atmospheric effects in the calculation of surface emittance, the horizontally polarized energy measured by the satellite would tend to be less variable, thus bringing the integrated CLW values more in line with the vertically polarized energy. Figure 4.7 (Channel 6) generally indicates higher CLW values in the areas of lower surface emittance especially over northern South Dakota.

Cloud thicknesses averaged just over 3900m over the area with the thickest clouds producing the highest CLW amounts. These thicker clouds were located in the brighter areas of the CLW image (Figure 4.7) where CLW approached 1.0 kgm^{-2} with a few values >1.0 kgm^{-2} (LWC > 0.25 gm^{-3}). These values seem a bit high for wintertime clouds and may be a result of lower surface emissivity values (snow cover) resulting in higher CLW values. On the average, however, CLW remained below 0.6 kgm^{-2} for channel 6 and

approximately 0.8 kgm^{-2} for channel 7 over South Dakota and Nebraska. This area of CLW would then be a prime area for potential icing from roughly 1100m (cloud base from sounding) to approximately 5000m AGL with temperatures ranging from -8°C(within the inversion) to -22°C near cloud top. These values are typical of areas where icing reports are common as analyzed by Politovich (1992), Curry and Liu (1992) and AWS (1980). In these studies, hazardous icing conditions were found to occur mainly in the temperature range from -2°C to -20°C. Figure 4.9 is a schematic diagram of the likely cloud situation measured across South Dakota. The entire depth of the cloud is supercooled with ice and liquid likely coexisting throughout the cloud and the hatched area in the diagram represents the area conducive to aircraft icing. However, this situation is likely a metastable situation that may not last long, therefore the icing threat may only persist for a short period of time. There is little additional information about the cloud microphysics such as droplet size and distribution for non-precipitating clouds that can be deduced from these CLW and CTT measurements.

As indicated by the IR image in Figure 4.10, central South Dakota and extreme northern Nebraska did indeed have considerable cloud cover as indicated by the brighter shading of gray. However, there are also bright clouds over Nebraska, but CLW was not indicated here (See Figures 4.7 & 4.8). This is due to the fact that the clouds were mostly likely thick cirrus and CLW was not likely present or was unable to be detected due to scattering effects in the 85.5 GHz channel.

For the second case study (5-9 Mar 1992), CLW was calculated for the 5th, 8th, 9th, and 10th. On the 5th, the 03Z Rapid City, South Dakota sounding was used in the

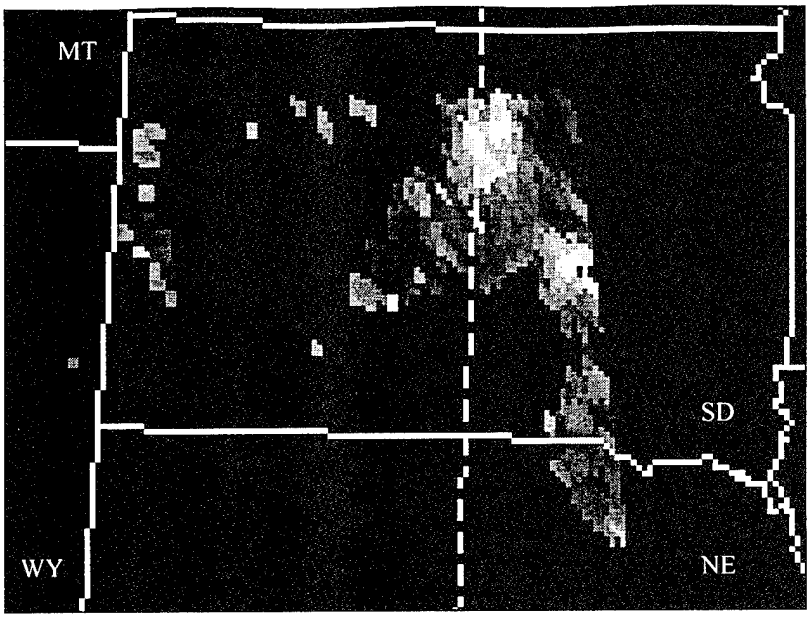

Figure 4.7. *Channel 6(85.5GHz vertical polarization) CLW for 12 Feb 1992 03Z. CLW values ranged from 0.19 kgm^{-2} to 2.64 kgm^{-2} with lighter colors indicating higher CLW.*

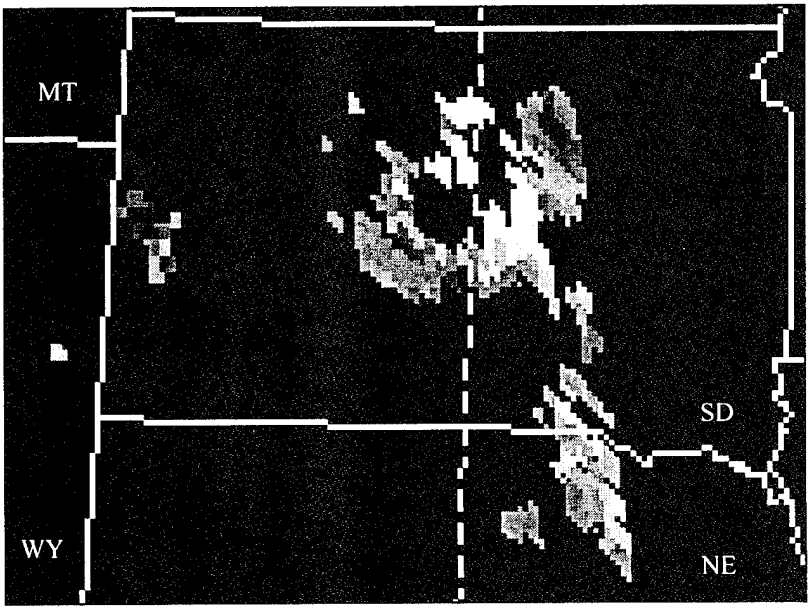

Figure 4.8. *Same as Figure 4.5 except Channel 7 (85.5GHz horizontal polarization). CLW ranged from 0.3 kgm^{-2} to 1.44 kg m^{-2}.*

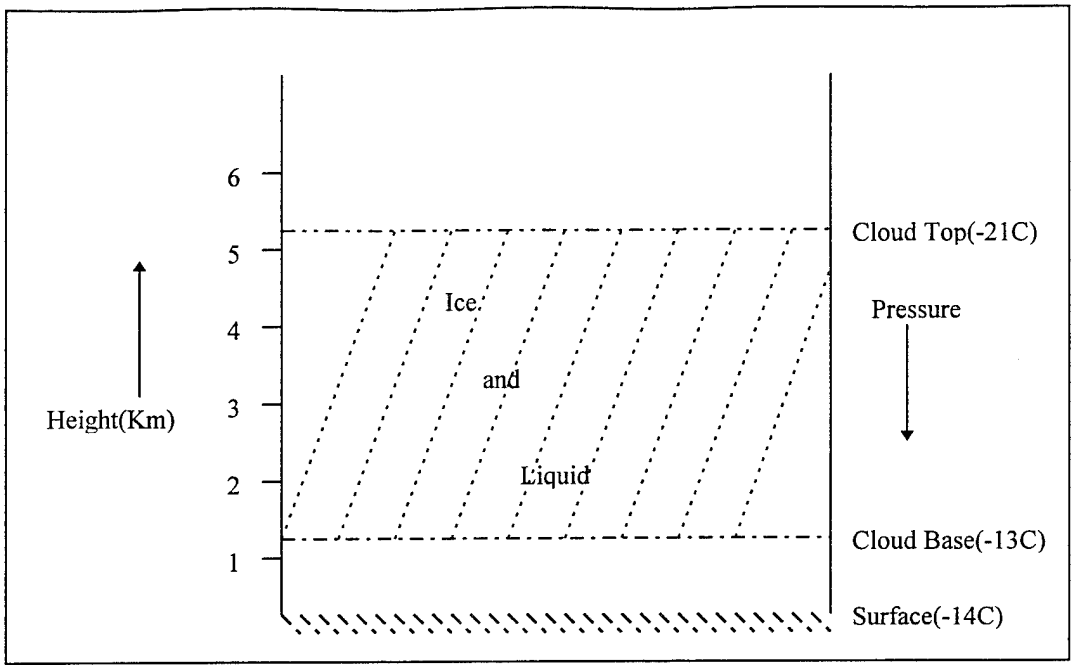

Figure 4.9. *Schematic depiction of a likely cloud situation over South Dakota for 03Z 12 Feb 1992. The hatched area is the region of icing potential based on sounding, Cloud liquid water and cloud top temperature information.*

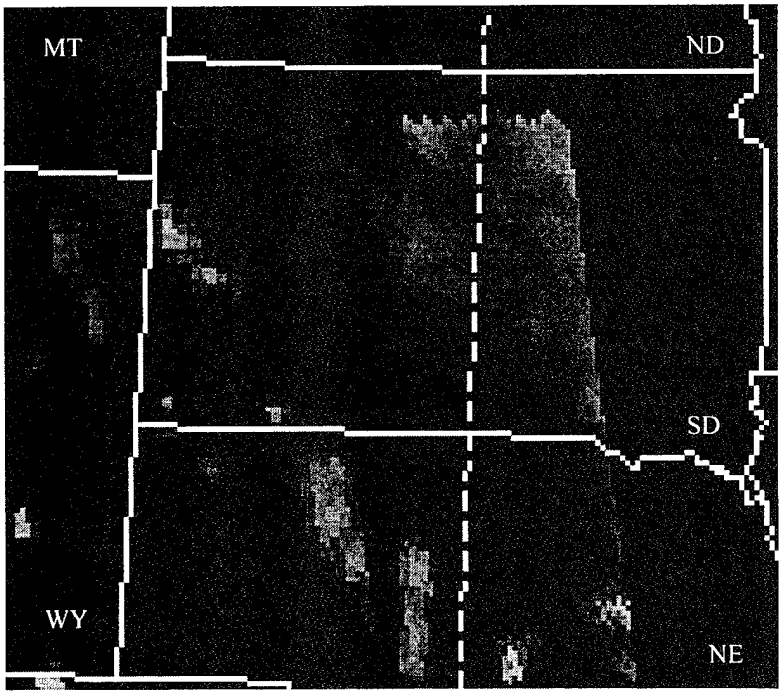

Figure 4.10. *Remapped GOES IR image for 03Z 12 Feb 1992.*

calculations (See Figure 4.11). Again as in the previous case, moisture was rather deep, but the temperatures were above freezing below 700 mb. The cloud base was estimated to be 840 mb with a temperature of 3°C. Also notice that the inversion in this sounding is much shallower and less distinct than in the 12 Feb case (See Figure 4.6). The lapse rate is more unstable in the lower levels and easterly winds prevail throughout the entire troposphere which agrees well with the 500mb and surface maps for 12Z (Figure 3.16a - b). Figures 4.12 and 4.13 show the Channel 6 and 7 integrated CLW values (note that CLW values are not scaled to the same shade of gray for each image, but are scaled to show various features of each channel, thus no direct comparison should be made between gray shades of the images) over the area of interest and Table 4.4 provides a brief statistical analysis for 03Z on the 5th of March. Once again Channel 7 is showing slightly higher CLW values and more variability although not nearly as much as in the 12 February case. Again, these values were consistent with the results of Politovich (1989) and Sand et al. (1984).

Overall, cloud depths are greater on 5 March even though the cloud base is about 400m higher. However, cloud top temperatures were much colder and lower CLW amounts were measured. A schematic vertical cross-section diagram is shown in Figure 4.14. This cloud structure is a bit more complicated due to range of temperatures in the cloud along with the apparent depth of the cloud. There appears to be three distinct regions within the cloud with ice near the top, a potential ice/liquid mixture near the middle, and liquid droplets near the base. The greatest icing potential would normally be

located from 4-6 km, however CLW amounts for this cloud are quite small. This would tend to indicate that there is probably a large amount of ice in this cloud compared to liquid amounts as calculated from the CLW retrieval. However, just minutes prior to the SSM/I pass, the cloud could have consisted entirely of supercooled water. The SSM/I observed brightness temperatures are similar to the theoretical brightness temperatures therefore CLW amounts are quite low. This can be explained from the fact that ice within the cloud is causing very cold SSM/I brightness temperatures (more scattering) and the theoretical brightness temperatures are cold as well, therefore CLW values are near the noise levels of the instrument and therefore undetectable.

Comparing the IR image (Figure 4.15) to CLW, there is generally good agreement especially over eastern Wyoming. Since the temperatures within the clouds are very cold(<-20°C), the amount of cloud liquid is likely to be small as indicated in Table 4.3. The lowest 150 mb of the cloud is above freezing and in fact could contribute a fair amount to the total integrated CLW. This would make it difficult to determine the icing potential. In addition, as mentioned earlier, CLW amounts were quite small (<0.1 kgm^{-2}). This finding is consistent with results obtained from the Cooperative Pilot Project in California discussed in Reynolds(1988). The researchers from this experiment found that values of CLW >0.2 kgm^{-2} were critical for cloud seeding purposes. Additionally, Lee et al, (1994) used a 0.2 kgm^{-2} threshold for icing potential over the North Pacific. This threshold agreed well with the work of Schultz and Politovich (1992) who incorporated model relative humidities into a forecast of icing potential over the same region.

The results of CLW calculations for 8 Mar are shown in Figures 4.17 and 4.18

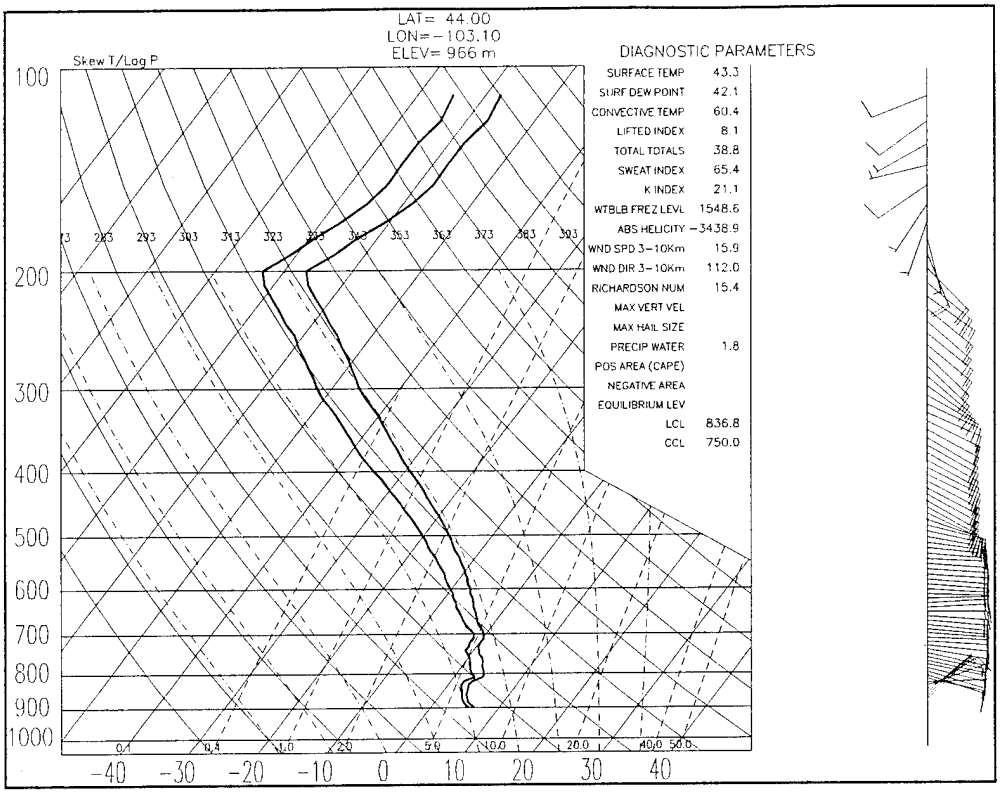

Figure 4.11. *Skewt of Rapid City, SD for 03Z 5 Mar 1992*

Table 4.4. *CLW Statistics for 03Z 5 Mar 1992.*

LCL=840mb, Height=1514m, Temp=3.3°C				
	Mean	Std Deviation	Max	Min
Ch 6 Cloud liquid Water (Kgm^{-2})	0.07	0.023	0.14	0.04
Ch 7 Cloud liquid Water (Kgm^{-2})	0.09	0.033	0.2	0.04
Cloud Depth(m)	6605	740	8168	5205
Cloud Top(m,(est.))	8119	740	9682	6719
Cloud Top Temperature(°C)	-36.4	6.16	-25.2	-49.4

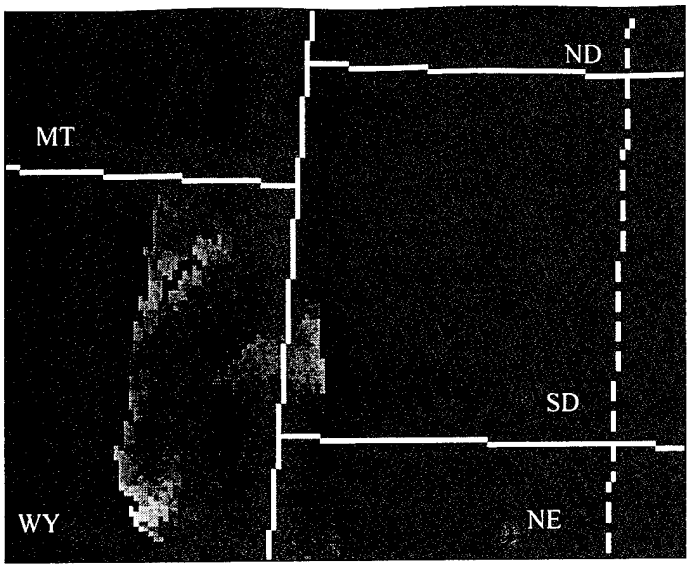

***Figure 4.12**. Channel 6 CLW for 03Z 5 Mar 1992. CLW values range from 0.04 kgm^{-2} (dark gray) to 0.14 kgm^{-2} (light gray).*

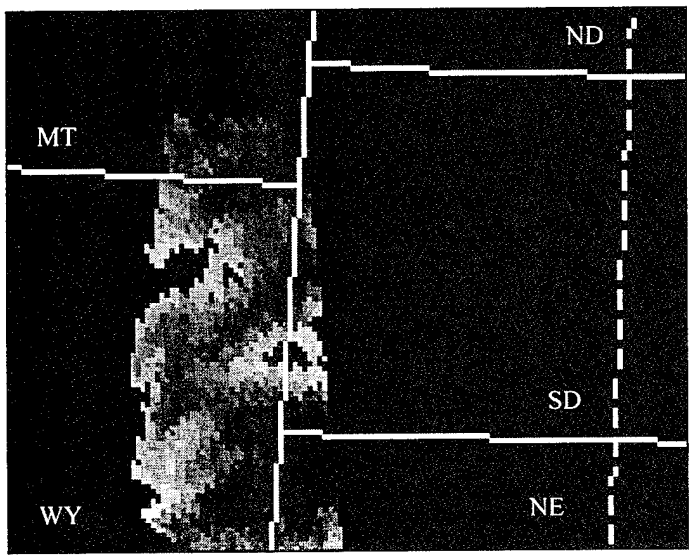

***Figure 4.13**. Channel 7 CLW for 03Z 5 Mar 1992. CLW values range from 0.04 kgm^{-2} to 0.20 kgm^{-2}.*

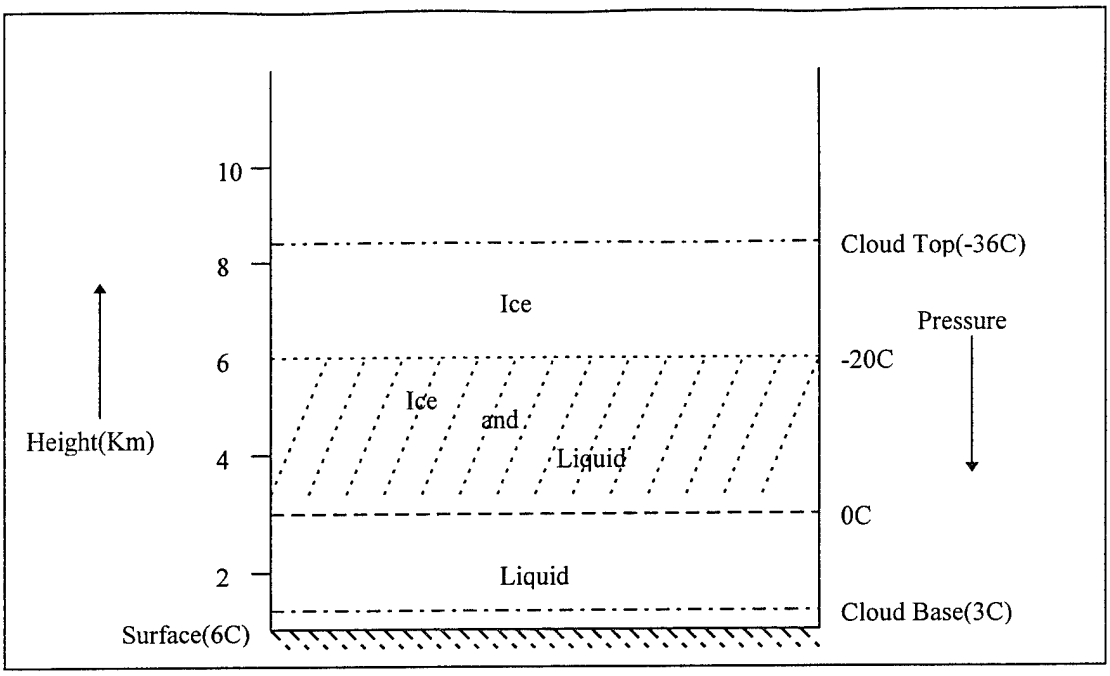

Figure 4.14. *Schematic depiction of a likely cloud situation over Wyoming for 03Z 5 Mar 1992. Hatched area indicates region of icing potential.*

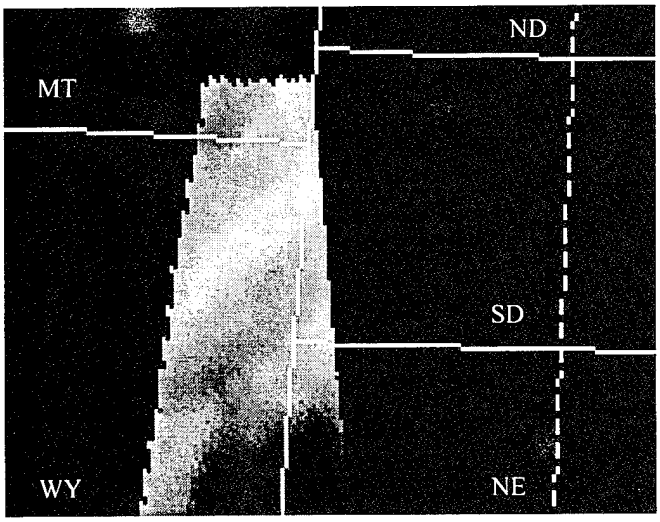

Figure 4.15. *Remapped GOES IR image for 03Z 5 Mar 1992. Note, the image is restricted to the SSM/I pass (right-hand side) and is also restricted by the GOES data received at the CIRA groundstation (left-hand side).*

with a brief statistical analysis in Table 4.5. Figure 4.16 shows the Skewt plot for Rapid City, SD at 00Z on 8 March as no soundings were available in the area at 03Z. The GOES IR image for the 8th at 03Z is shown in Figure 4.20. The remapped GOES IR shows very little data because of two reasons. First, the SSM/I pass only extended into eastern Wyoming therefore no data was available to the east. Secondly, the GOES data collected by the NESDIS RAMM branch at CIRA did not extend to the west of eastern Wyoming. Therefore, only a small section of the GOES and SSM/I data were available for CLW retrieval.

Deep moisture was present on 8 Mar with subfreezing temperatures throughout the troposphere. CLW amounts were comparable with the 12 Feb case, but the clouds were much shallower and warmer with average temperatures ranging from -6.5°C at cloud base to only -10.5°C at the top (See Figure 4.19). This particular case had the warmest conditions of all the cases, but covered only a small area. The clouds in this small area of Wyoming only extended from about 1850m to 3380m. Since the sounding used in this CLW case was several kilometers away from the cloudy area it may not be very representative. However, there does appear to be an icing potential in eastern Wyoming with temperatures below freezing and CLW amounts exceeding 0.2 kgm^{-2} (with the greatest risk occurring in the lighter shaded areas of the CLW images).

CLW was calculated for the 9th of March with nearly all of the CLW in an area over South Dakota. Table 4.6 provides a brief statistical analysis of the CLW data and Figures 4.22 and 4.23 provide images of the CLW for both channel 6 and 7 respectively. Rapid City, SD 00Z sounding was the most recent and representative sounding available

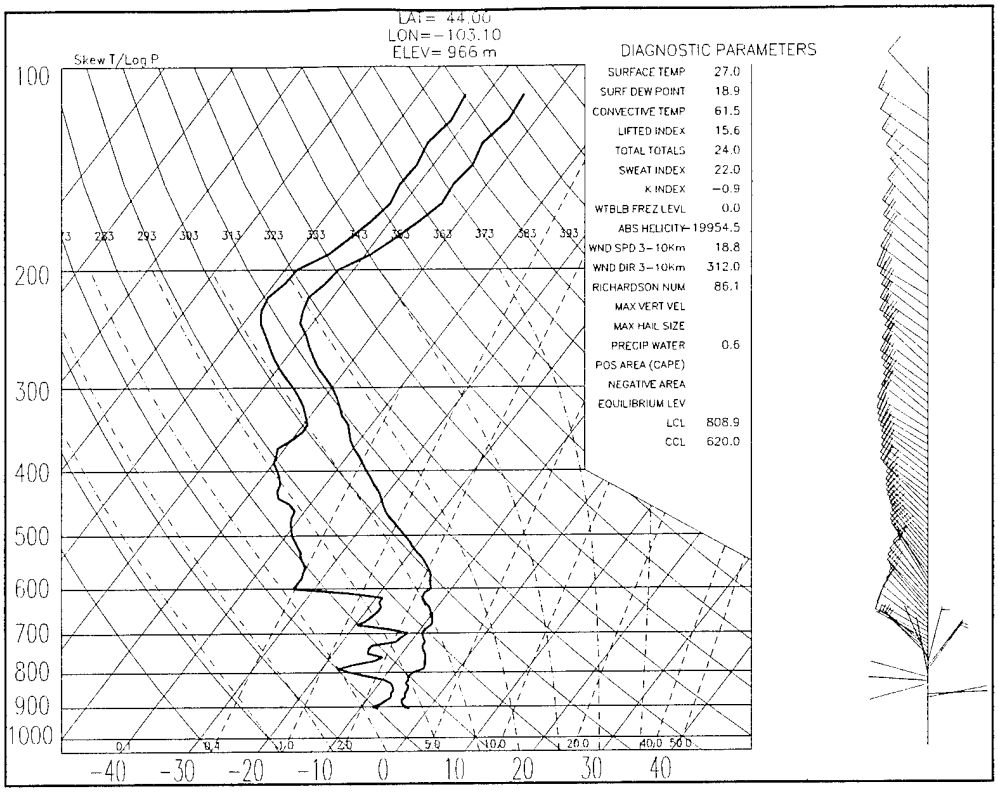

***Figure 4.16**. Skewt of Rapid City, SD for 00Z 8 Mar 1992.*

***Table 4.5**. CLW Statistics for 03Z 8 Mar 1992.*

LCL=809mb, Height=1850m, Temp=-6.5°C				
	Mean	Std Deviation	Max	Min
Ch 6 Cloud liquid Water (Kgm^{-2})	0.78	0.428	1.68	0.21
Ch 7 Cloud liquid Water (Kgm^{-2})	1.61	0.86	2.89	0.31
Cloud Depth(m)	1531	663	2781	602
Cloud Top(m,(est.))	3380	663	4631	2452
Cloud Top Temperature(°C)	-10.3	2.95	-6.9	-16.3

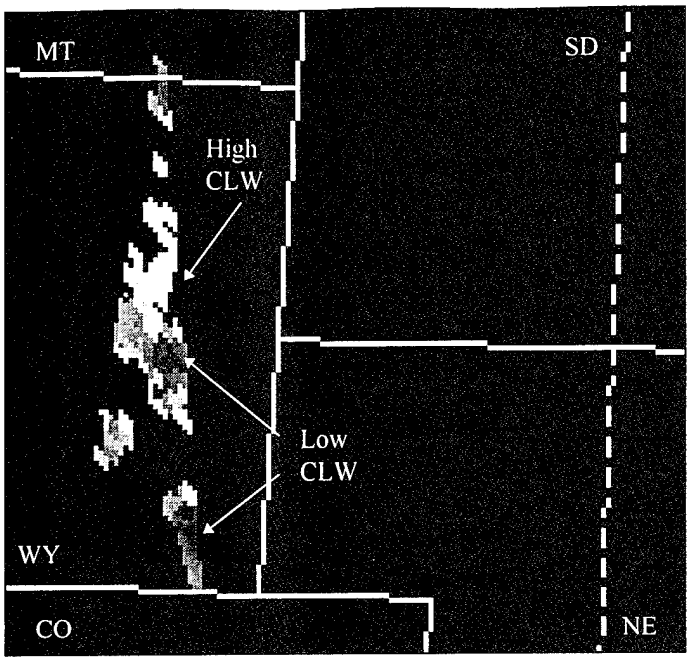

***Figure 4.17**. Channel 6 CLW for 03Z 8 Mar 1992. CLW values ranged from 0.21 kgm^{-2} to 1.68 kgm^{-2} with values increasing from dark gray to light gray.*

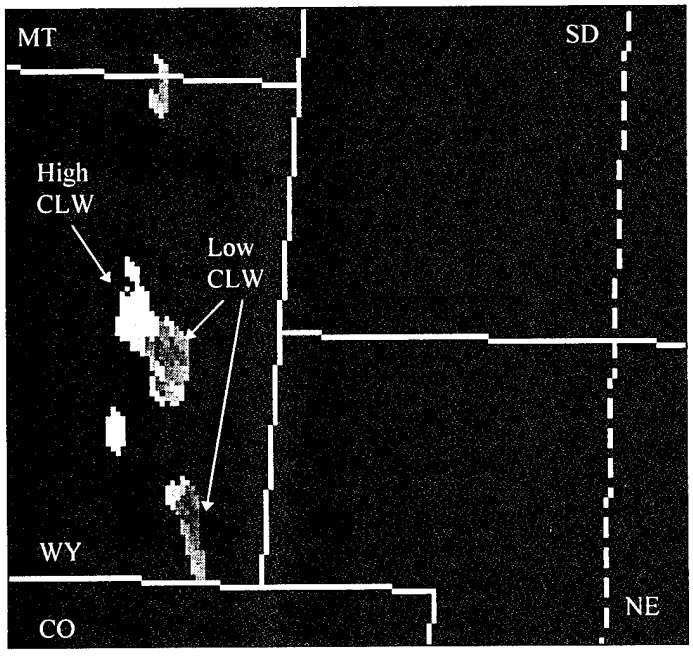

***Figure 4.18**. Channel 7 CLW for 03Z 8 Mar 1992. CLW values ranged from 0.31 kgm^{-2} to 2.89 kgm^{-2}.*

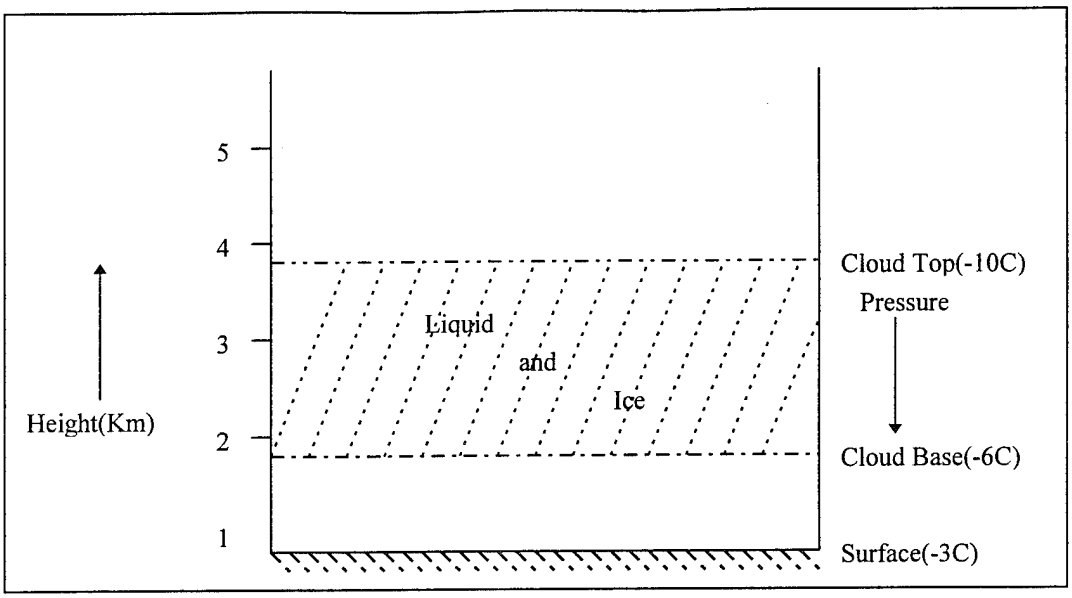

***Figure 4.19**. Schematic depiction of a likely cloud situation over eastern Wyoming for 03Z 8 Mar 1992. Hatched area represents region of icing potential.*

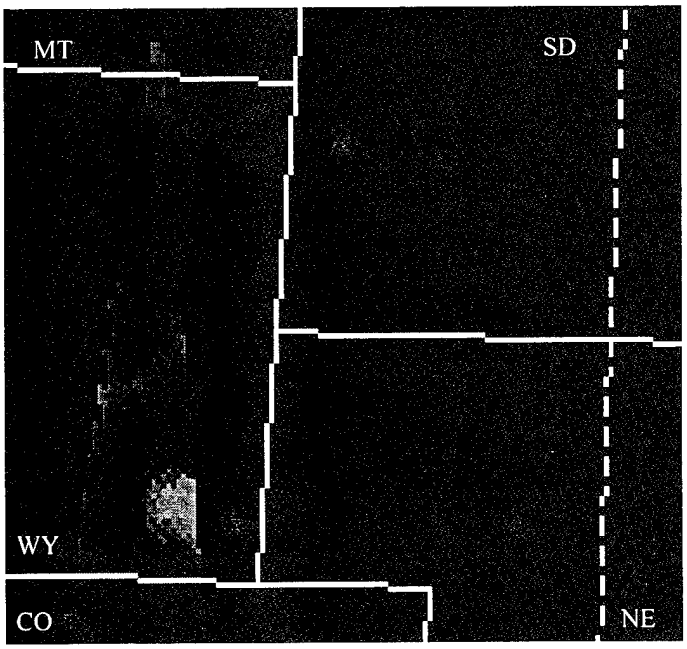

***Figure 4.20.** Remapped GOES IR image for 03Z 8 Mar 1992. The image was limited to both the SSM/I pass and the GOES data gathered by the CIRA groundstation.*

for the CLW retrieval and is shown in Figure 4.21. Deep moisture is present (as was the case on the 12th of Feb) with temperatures remaining below freezing through the entire troposphere. The corresponding IR image is shown in Figure 4.25. Very bright clouds on the image agree well with the CLW retrieval, but no CLW was measured below the swath in the image because the clouds in northeast Nebraska were precipitating (SSM/I brightness temperature < 249K) and cirrus clouds were found over the rest of the area. The cloud base was approximately 1550m while estimated cloud tops averaged over 7100m producing cloud thicknesses over 5500m. Once again, clouds were very deep and cold, but CLW was low, <0.1 kgm^{-2}. A schematic vertical cross-section of the likely cloud situation over South Dakota is shown in Figure 4.24. Much of the middle to lower portion of the cloud most likely consisted of an ice and liquid mixture with the top 1500 km consisting mainly of ice. Even though this cloud was deep, it most likely contained a great deal of ice, as identified by scattered radiation detected by the SSM/I. There is also the distinct possibility that there may have been more than one layer of clouds, one consisting entirely of ice and the other ice and minimal liquid. This would verify the small amounts of cloud liquid retrieved over the area.

The dark swath in the center of the image is a result of the PORTAL remapping technique briefly described earlier. When the GOES image is remapped to the SSM/I projection space, PORTAL checks for missing data. In this case, the SSM/I data was missing so PORTAL assigned missing values to the corresponding GOES image to alleviate any possible miscalculations of surface emittance and CLW later on. This is one of many advantages of using PORTAL.

The final CLW retrieval was computed for the evening of the 9th (00Z 10 Mar)

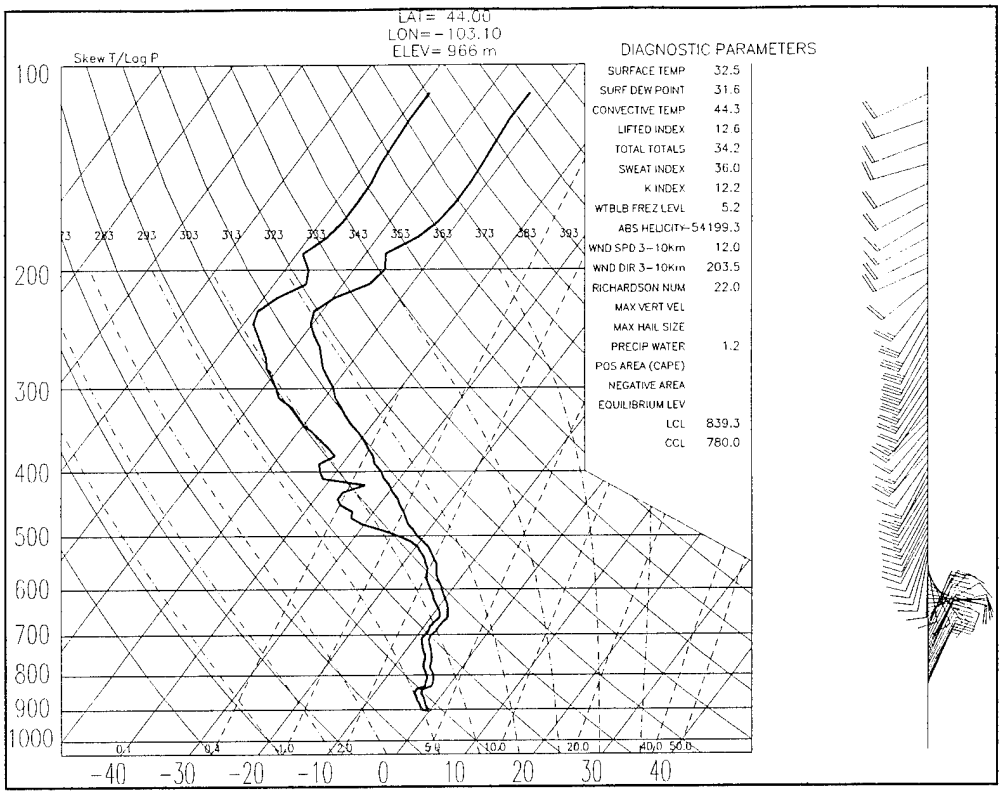

***Figure 4.21**. Skewt of Rapid City, SD for 00Z 9 Mar 1992.*

***Table 4.6**. CLW Statistics for 03Z 9 Mar 1992.*

LCL=840mb, Height=1554, Temp=-3.3°C				
	Mean	Std Deviation	Max	Min
Ch 6 Cloud liquid Water (Kgm^{-2})	0.07	0.011	0.1	0.05
Ch 7 Cloud liquid Water (Kgm^{-2})	0.09	0.022	0.14	0.07
Cloud Depth(m)	6180	510	6931	5100
Cloud Top(m,(est.))	7735	510	8485	6654
Cloud Top Temperature(°C)	-38.1	4.14	-29.4	-44.6

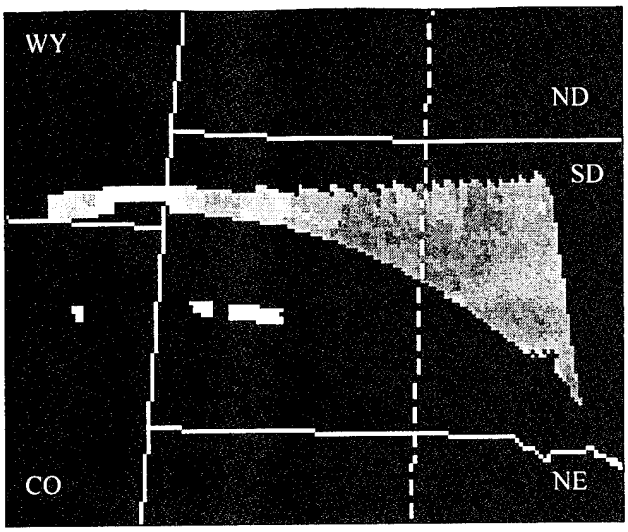

***Figure 4.22**. Channel 6 CLW for 03Z 9 Mar 1992*

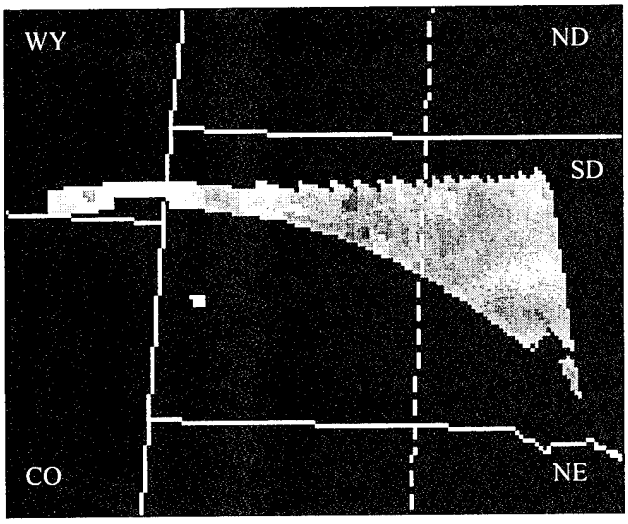

***Figure 4.23**. Channel 7 CLW for 03Z 9 Mar 1992.*

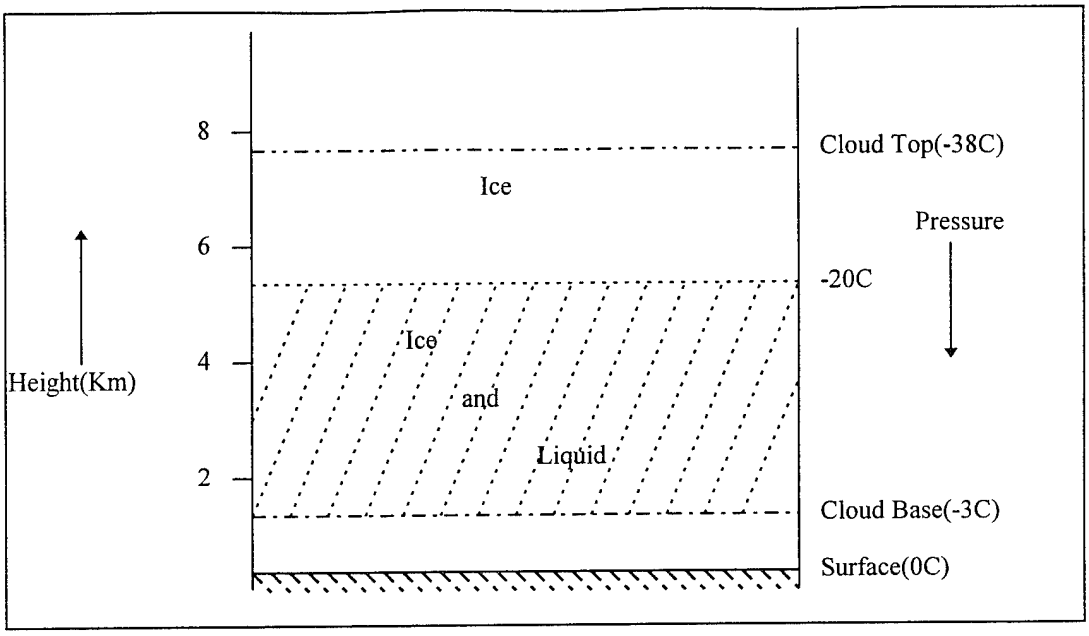

***Figure 4.24**. Schematic depiction of a likely cloud situation over South Dakota for 03Z 9 Mar 1992. Hatched area indicates region of icing potential.*

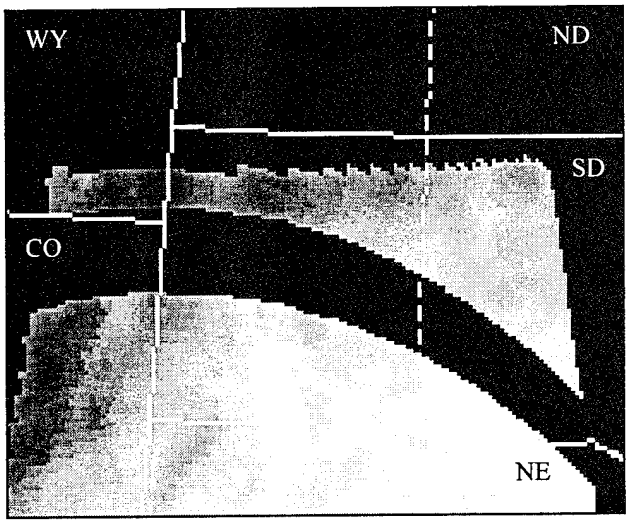

***Figure 4.25**. GOES IR image for 03Z 9 Mar 1992. The dark swath in the center of the image is a result of missing SSM/I data.*

with the results for Channel 6 and 7 shown in Figures 4.27 and 4.28 and the Rapid City, SD 21Z sounding used in the CLW retrieval shown in Figure 4.26. Moisture was quite variable and rather limited throughout much of the troposphere with the cloud base fairly high AGL ($\approx$ 2150m). The CLW statistics are shown in Table 4.7. Cloud depths averaged over 1300m with CLW values averaging from 0.6 kgm^{-2} for Channel 6 to 1.2 kgm^{-2} for Channel 7. Cloud top temperatures averaged near -15°C with the cloud base temperature at -10°C. Thus, clouds were not thick or cold, but CLW values were quite high. Figure 4.29 shows a schematic diagram of the vertical cross-section of the average cloud over South Dakota. These were relatively thin clouds (about 1 km thick) probably consisting of a mixture of ice and liquid throughout the cloud. Icing potential therefore would exist anywhere within the cloud. The high CLW values noted in Table 4.7 are not very realistic and are not consistent with CLW results obtained by Jones and Vonder Haar (1990). These values are likely a result of the low surface emittances in the area. Even eliminating the large values of CLW area, the area would still be a prime area for icing potential based on temperature within the clouds (-10°C to -15°C) and CLW amounts greater than 0.2 kgm^{-2}.

Figure 4.30 shows the GOES IR image used in the CLW retrieval and does indicate similar characteristics to the retrieved CLW field. The dark area within the CLW field (Figures 4.27 and 4.28) is assigned missing values due to the fact that no surface emittance values were available for the theoretical brightness temperature calculation used in the CLW retrieval.

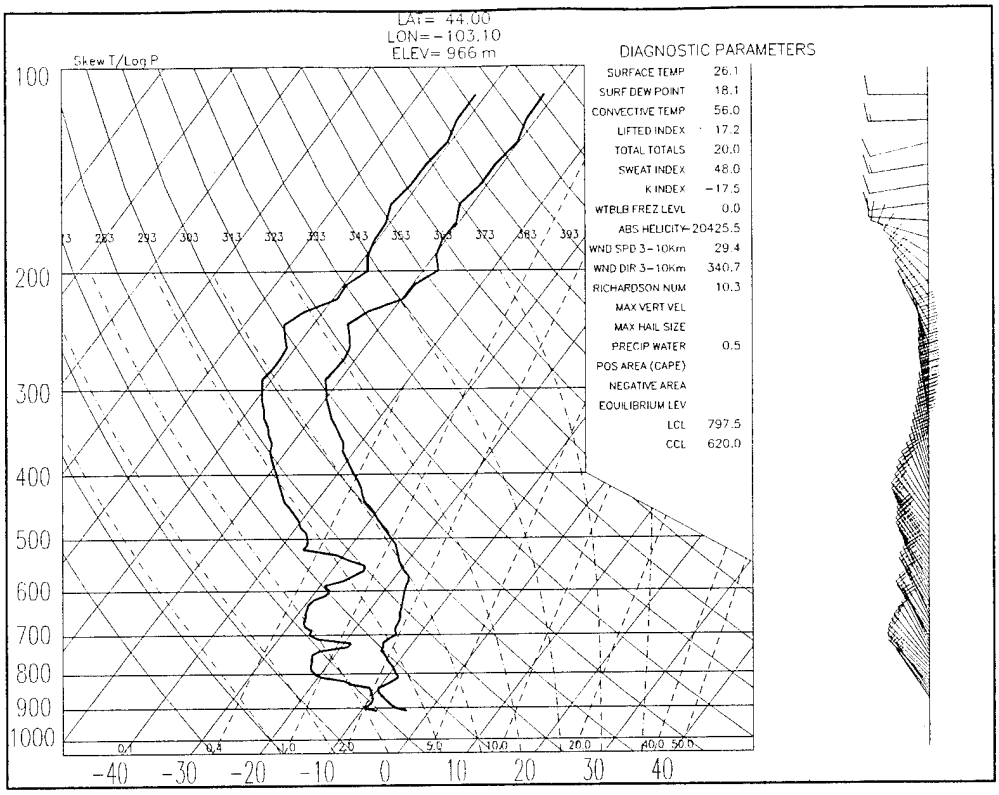

***Figure 4.26**. Skewt of Rapid City, SD for 21 Z 9 Mar 1992*

***Table 4.7** CLW Statistics for 00Z 10 Mar 1992.*

LCL = 780mb, Height=2156m, Temp=-10.4°C				
	Mean	Std Deviation	Max	Min
Ch 6 Cloud liquid Water (Kgm^{-2})	0.58	0.73	2.97	0.06
Ch 7 Cloud liquid Water (Kgm^{-2})	1.17	1.27	4.83	0.17
Cloud Depth(m)	1312	663	2373	99
Cloud Top(m,(est.))	3468	663	4529	2255
Cloud Top Temperature(°C)	-15.1	1.76	-11.2	-18.1

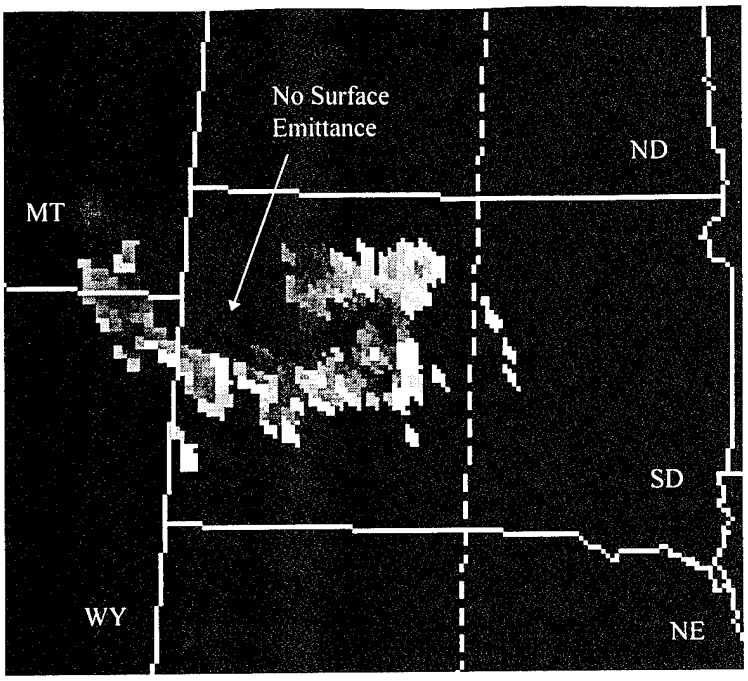

***Figure 4.27**. Channel 6 CLW for 00Z 10 Mar 1992.*

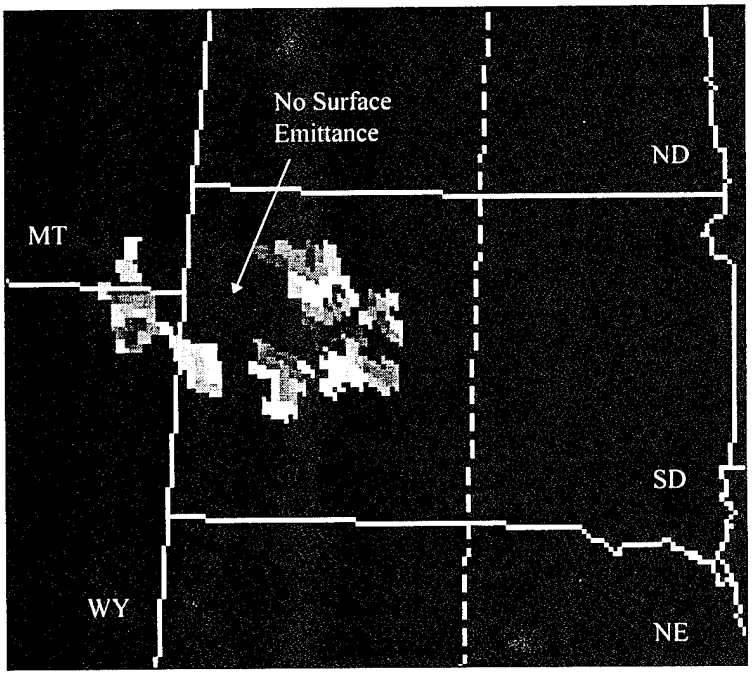

***Figure 4.28**. Channel 7 CLW for 00Z 10 Mar 1992.*

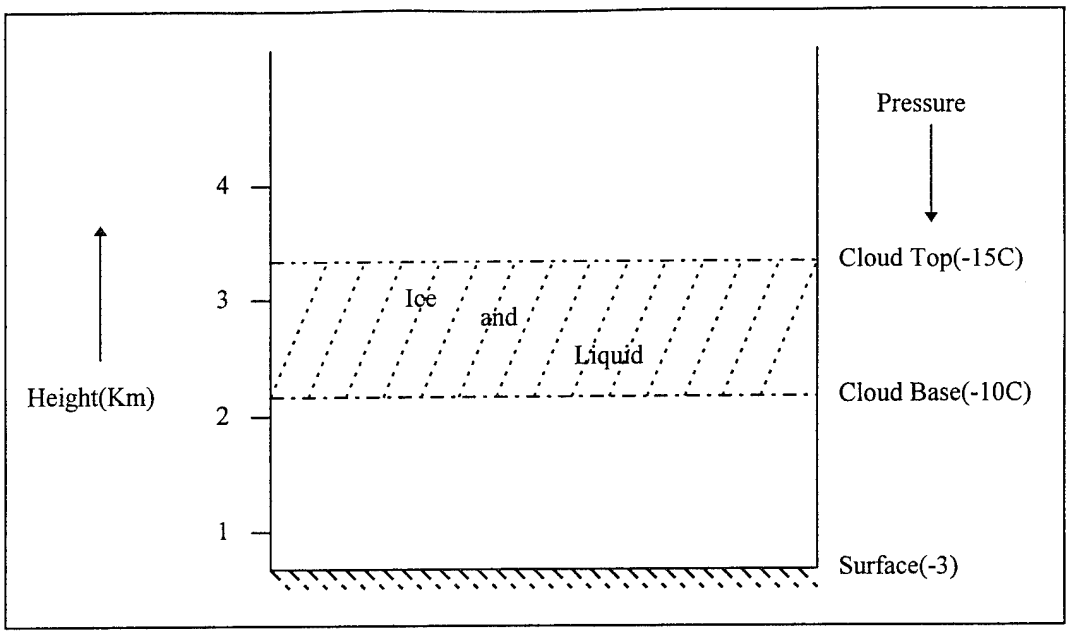

Figure 4.29. *Schematic depiction of a likely cloud situation over South Dakota for 00Z 10 Mar 1992. Hatched area indicates area of icing potential.*

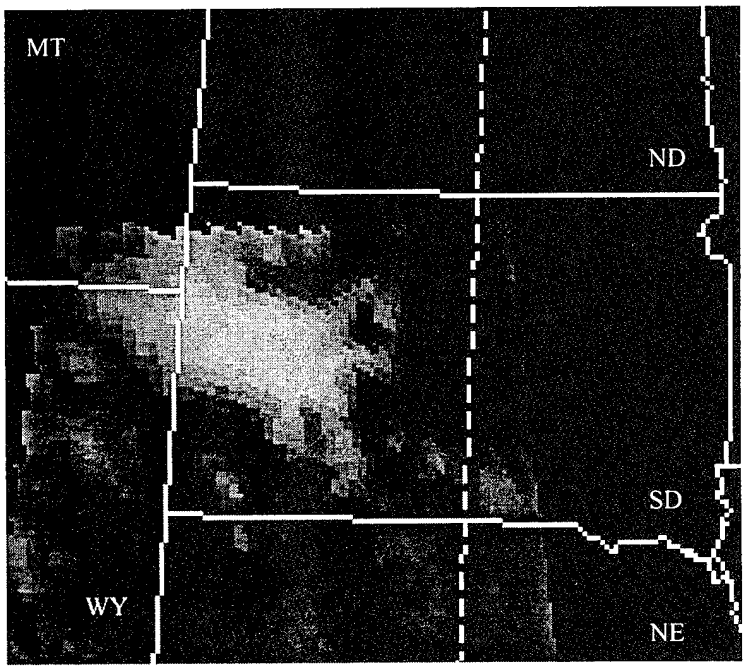

Figure 4.30. *Remapped GOES IR image for 00Z 10 Mar 1992. GOES image is limited to both the SSM/I pass and data received at CIRA groundstation.*

4.4 Infrared Cloud-Top Temperature Measurement

The GOES-7 satellite measures radiation in several frequencies as mentioned in section 3.2. The infrared window (weak atmospheric absorption) wavelength in the electromagnetic spectrum is located at approximately 11μm and Channel 8 on the VISSR instrument measures radiation in the 10.5 - 12.5μm band. If no clouds are present, this channel measures skin temperatures on the earth's surface. However, if clouds are present, no infrared radiation can penetrate the clouds. Therefore, radiation measured by the satellite is absorbed, scattered and re-emitted by the tops of the clouds. It is the re-emitted energy from the tops of clouds which provides important temperature information and therefore height information about the clouds when used in conjunction with representative surface-based upper air soundings.

4.4.1 Cloud Top Temperature Procedure

In this study, 8 bit images were produced from JDF files created from the raw data using PORTAL. Each image is composed of pixels containing discrete digital values ranging from 0 to 255 which corresponds directly to an equivalent blackbody temperature. Because these data are in 8 bit count values, a calibration table is used to covert from counts to effective infrared temperature. The calibration table used to determine CTTs is shown in Table 4.8.

Table 4.8. *GOES 7 channel 8 calibration table.*

Count	T_B(K)	Count	T_B(K)	Count	T_B(K)	Count	T_B(K)
0	330.0989	65	297.741	130	265.299	195	223.084
1	329.7574	66	297.2388	131	264.7127	196	222.0324
2	329.244	67	296.7345	132	264.2213	197	220.9614
3	328.7862	68	296.2281	133	263.727	198	219.8702
4	328.2695	69	295.7195	134	263.2302	199	218.945
5	327.7512	70	295.2089	135	262.7304	200	218.0033
6	327.2891	71	294.7694	136	262.2279	201	217.0465
7	326.7675	72	296.2546	137	261.7224	202	216.0717
8	326.2442	73	293.7376	138	261.2141	203	215.0802
9	325.7776	74	293.2927	139	260.8054	204	214.0688
10	325.2509	75	292.7714	140	260.2915	205	213.0392
11	324.7225	76	292.2478	141	259.7748	206	211.9876
12	324.2512	77	291.6206	142	259.2548	207	210.9158
13	323.7785	78	291.2691	143	258.7318	208	210.0413
14	323.2449	79	290.7388	144	258.311	209	209.1515
15	322.7095	80	290.2822	145	257.782	210	208.0157
16	322.2319	81	289.7471	146	257.2498	211	206.8551
17	321.7529	82	289.2097	147	256.8216	212	205.9056
18	321.2723	83	288.7469	148	256.2831	213	204.9372
19	320.7902	84	288.2822	149	255.7413	214	203.9487
20	320.2458	85	287.7376	150	255.3052	215	202.9391
21	319.6996	86	287.1905	151	254.7567	216	201.9072
22	319.2123	87	286.7193	152	254.2047	217	200.8517
23	318.7234	88	286.2462	153	253.7604	218	200.0446
24	318.2329	89	285.7709	154	253.3136	219	199.221
25	317.7407	90	285.2937	155	252.7515	220	198.0999
26	317.2468	91	284.8143	156	252.1856	221	196.9496
27	316.7513	92	284.2523	157	251.73	222	196.0674
28	316.2539	93	283.6875	158	251.2717	223	195.1646
29	315.7549	94	283.201	159	250.8107	224	193.9317
30	315.2542	95	282.7123	160	250.3471	225	192.9838
31	314.7517	96	282.2213	161	249.7635	226	192.0113
32	314.2474	97	281.7281	162	249.1758	227	191.0176
33	313.7413	98	281.2325	163	248.7023	228	189.9961
34	313.2333	99	280.7346	164	248.2258	229	188.9507
35	312.7235	100	280.2344	165	247.7464	230	187.8735
36	312.2119	101	279.7318	166	247.264	231	186.769
37	311.6983	102	279.2267	167	246.7785	232	186.0134
38	311.2474	103	278.7191	168	246.2898	233	185.2424
39	310.795	104	278.209	169	245.798	234	184.0532
40	310.2761	105	277.6964	170	245.3029	235	182.8289
41	309.7552	106	277.1813	171	244.8046	236	181.9877
42	309.2323	107	276.75	172	244.3028	237	181.1263
43	308.7075	108	276.3168	173	243.7976	238	180.2436
44	308.2465	109	275.7945	174	243.2889	239	179.3381
45	307.7839	110	275.2695	175	242.7767	240	178.4084
46	307.2533	111	274.7417	176	242.001	241	177.4528
47	306.7206	112	274.2112	177	240.9542	242	176.4695
48	306.2527	113	273.7669	178	240.0258	243	175.4563
49	305.7831	114	273.3205	179	239.0844	244	174.4111
50	305.2444	115	272.7821	180	237.9931	245	173.3311
51	304.7035	116	272.2409	181	237.0242	246	172.2135
52	304.2283	117	271.6965	182	236.0407	247	171.0549
53	303.7513	118	271.2407	183	235.0434	248	169.8514
54	303.2727	119	270.7825	184	234.0304	249	168.5985
55	302.7922	120	270.2298	185	233.0023	250	167.9448
56	302.2408	121	269.7669	186	231.9571	251	167.2991
57	301.7565	122	269.3015	187	230.8956	252	165.9231
58	301.2702	123	268.7402	188	229.9712	253	165.2051
59	300.7122	124	268.2698	189	229.0332	254	164.4871
60	300.2219	125	267.797	190	228.0809	255	164.3747
61	299.7297	126	267.2265	191	227.1138		
62	299.2356	127	266.7485	192	226.1312		
63	298.7393	128	266.2678	193	225.1326		
64	298.2412	129	265.7848	194	224.1171		

4.4.2 Results

CTTs were determined from the JDF Infrared data and stored by latitude and longitude pixel locations corresponding to the CLW pixel locations. A question to ask at this point is if the CTTs and CLW amounts are known, can one infer aircraft icing potential? Curry and Liu (1992) found that there was no simple increase in averaged CLW with average CTTs for supercooled low and mid-level clouds. However, they found that the largest values of CLW did occur at high temperatures, but small values of CLW occurred at nearly any temperature.

Figures 4.31 and 4.32 are scatterplots of CLW vs CTT for Channel 6 and Channel 7 respectively for 03Z 12 Feb 1992. CTTs in the area of CLW retrieval ranged from approximately -16°C to -24°C. There is no linear relationship, as expected, and CLW amounts are not large for warm CTTs or small for cold CTTs. There does appear to be clusters of points on both figures, especially Figure 4.31. Disregarding the four points near the top of the graph, there are approximately three clusters in the figure. One from -22°C to -24°C with CLW values from 0.3 kgm^{-2} to 0.6 kgm^{-2}, another from -19°C to -22°C with CLW of 0.4 kgm^{-2} to 0.9 kgm^{-2} and the last from -16°C to -19°C with CLW of 0.3 kgm^{-2} to 0.7 kgm^{-2}. These clustering of points may be an indication of multiple layers of clouds in which an overestimation of the true cloud top could have been made. Cloud top temperatures may in fact be warmer than measured by the satellite which would tend to pull these values on the graph towards the right.

Scatterplots of CLW versus cloud depth for the same time are shown in Figures 4.33 and 4.34. Cloud depths ranged from 3300m to approximately 4300m for

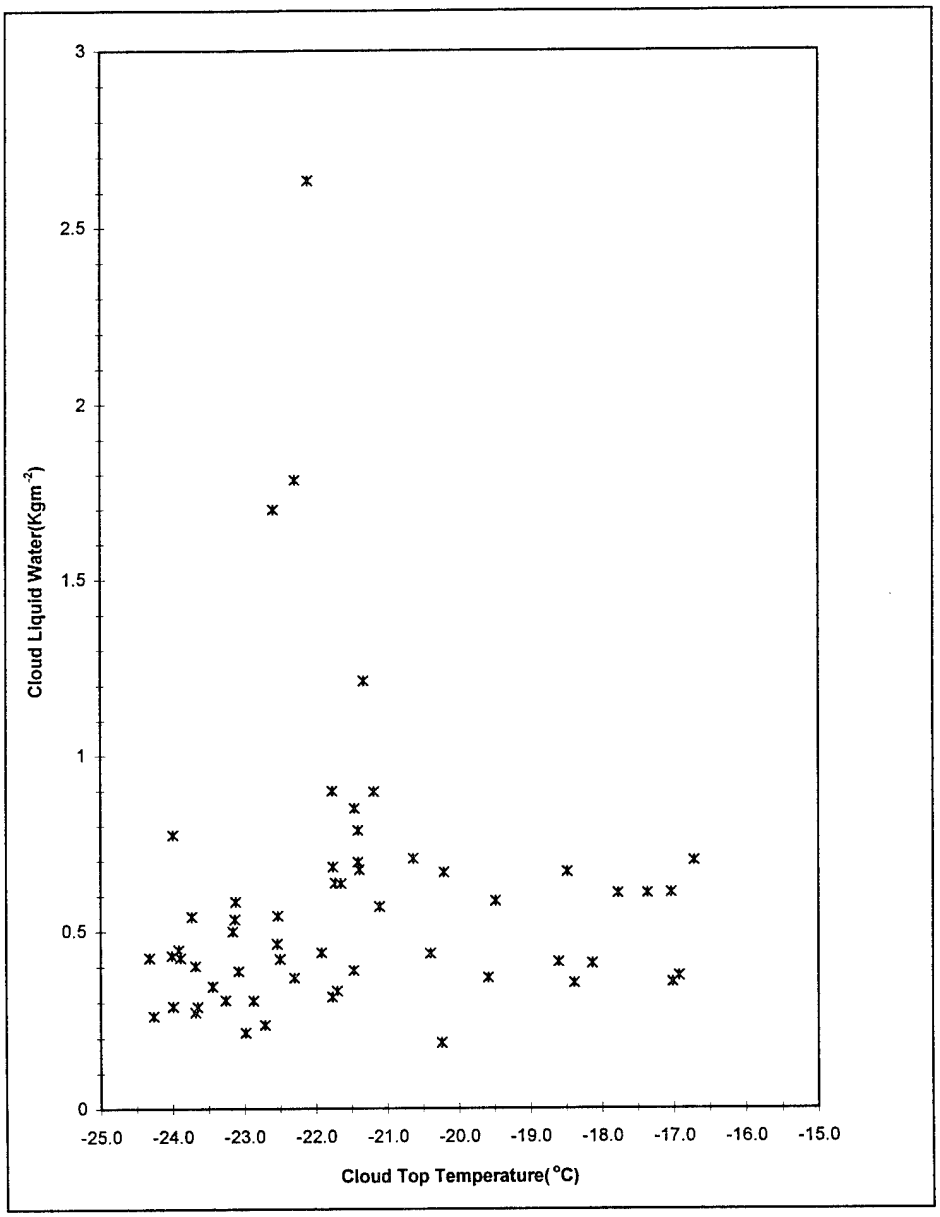

Figure 4.31. *Scatterplot of Channel 6 cloud liquid water versus cloud top temperature for 03Z 12 Feb 1992.*

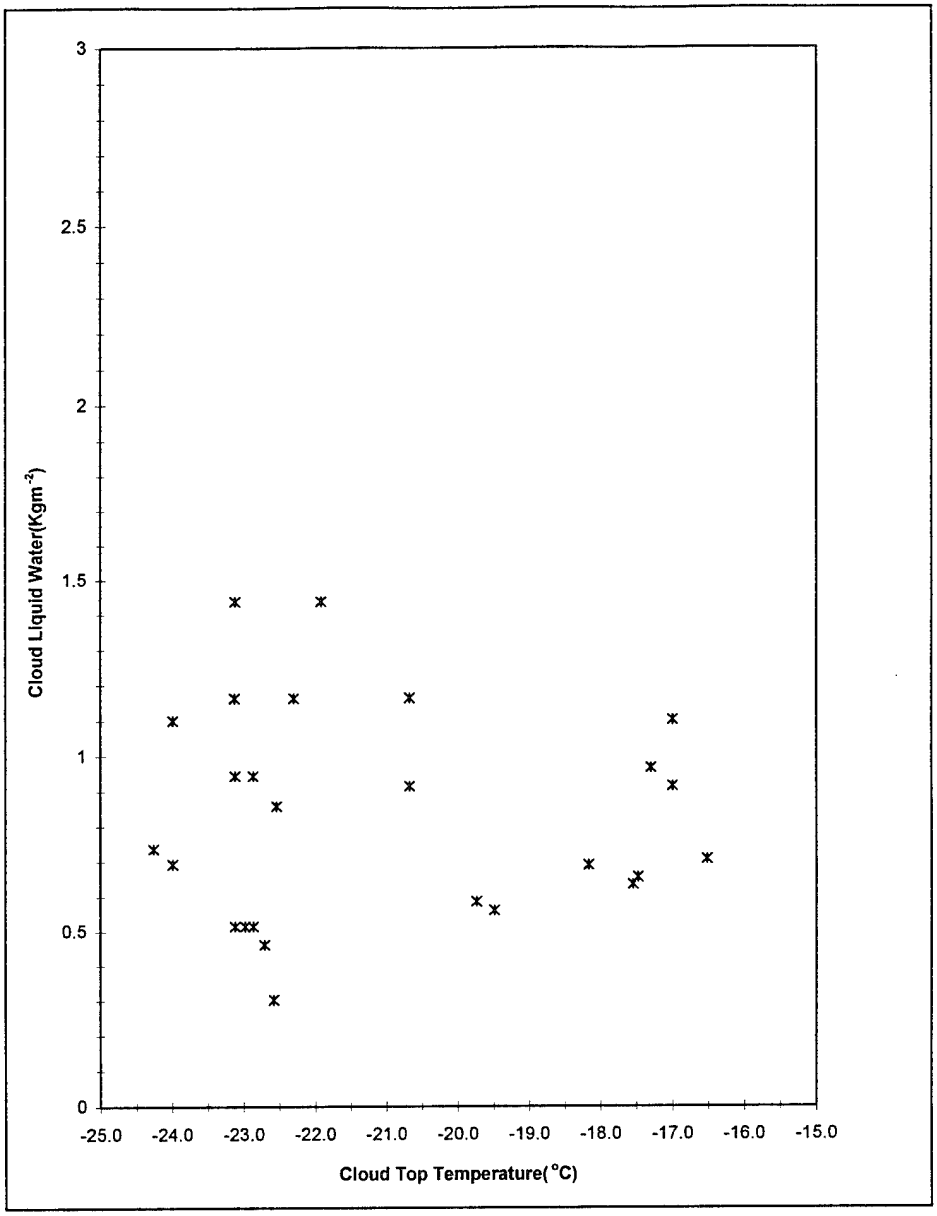

Figure 4.32. *Scatterplot of Channel 7 cloud liquid water versus cloud top temperature for 03Z 12 Feb 1992.*

both channels with CLW values mainly in the range from 0.2 kgm^{-2} to 1 kgm^{-2} for Channel 6 and from 0.5 kgm^{-2} to 1.5 kgm^{-2} for Channel 7 (these higher values of CLW can be attributed to lower surface emissivities). There appears to be no clear-cut relationship between CLW and cloud depth for this case. However, some microphysics can be interpreted from these graphs. Thick clouds (> 4000m) containing large amounts of CLW (> 0.5 kgm^{-2}) would probably have small ice populations while thick clouds containing low CLW would likely have a large ice population(ice would deplete CLW). These conditions could certainly exist in a natural cloud but the microphysics could change rapidly resulting in a different cloud structure and hence aircraft icing potential.

The plots of Channel 6 and Channel 7 03Z 5 Mar 1992 CLW versus CTTs are shown in Figures 4.35 and 4.36 and CLW versus cloud depth are shown in Figures 4.37 and 4.38. Notice the temperatures are considerably colder (by 10 to 25°C), the CLW values are much lower (all less than 0.2 kgm^{-2}), and cloud depths are much deeper (4500 to 8300m deep) than the 12 February case. In this case, much more ice is present which would deplete the CLW available in the cloud. Even though CLW is quite low as are temperatures, icing would not likely be a threat near cloud top (as is often the case) but in a shallow layer in the lower portions of the cloud. Once again, clusters of points are noted mainly in two areas. One from -45 to -50°C and the other larger cluster from -25 to -40°C. This again as in the 12 February case could be a result of an underestimate of the cloud top by the satellite. As is evidenced in Figures 4.37 and 4.38, the top of the cloud is likely to be cirrus and in fact may be a very shallow. The more prevalent cloud may indeed be at mid-levels of the atmosphere where temperatures are warmer, thus the more

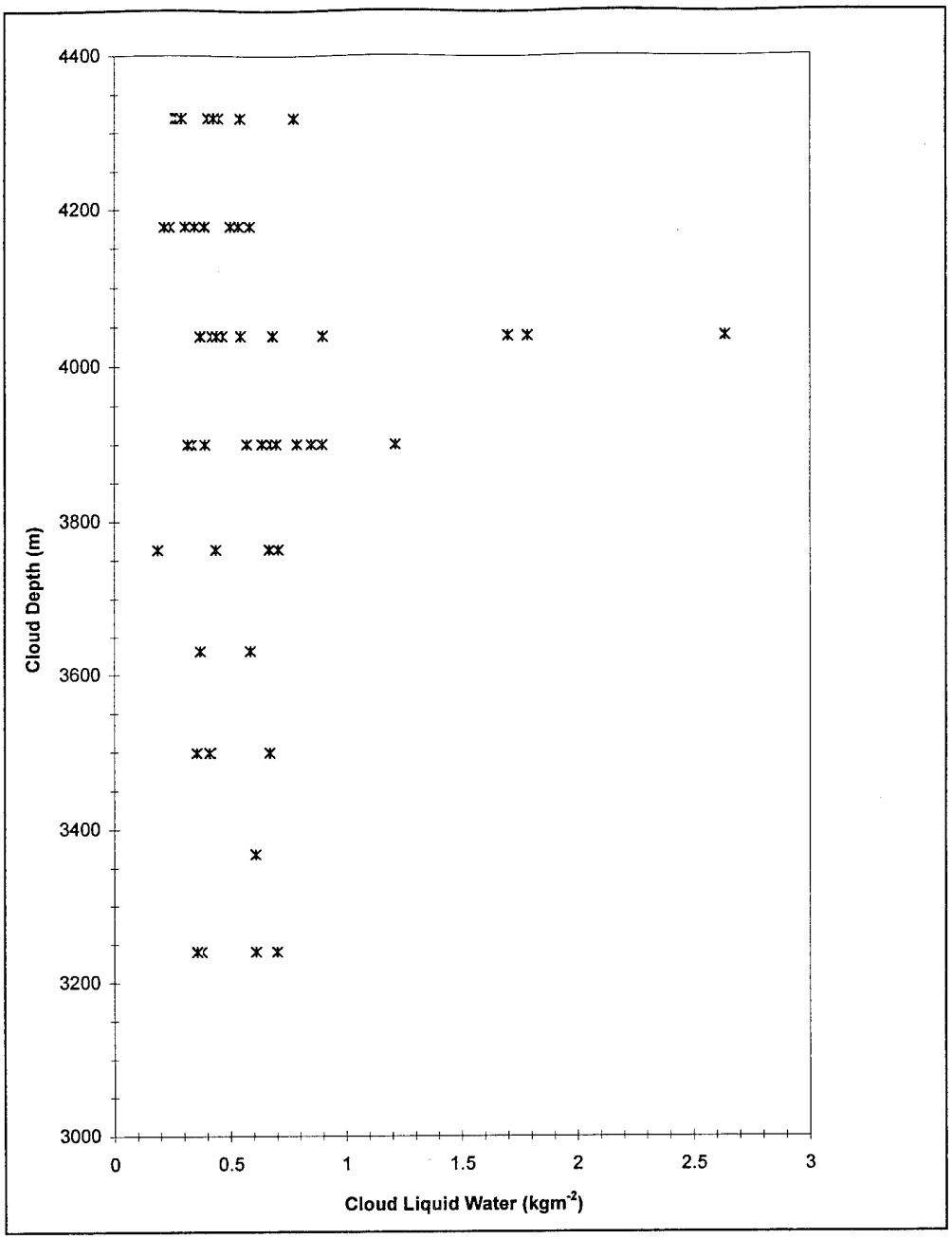

***Figure 4.33**. Scatterplot of Channel 6 cloud liquid water versus cloud depth for 03Z 12 Feb 1992..*

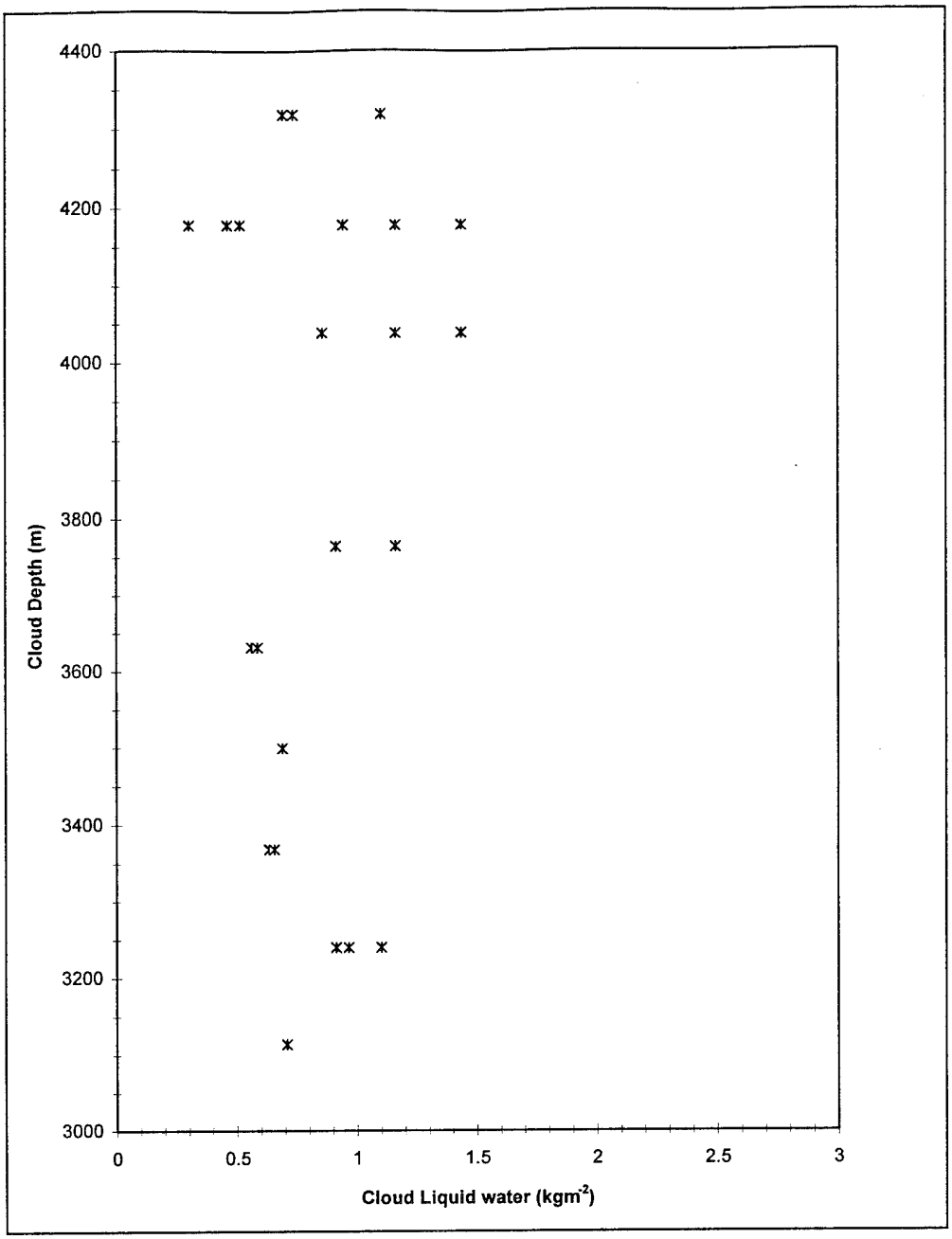

***Figure 4.34**. Scatterplot of Channel 7 cloud liquid water versus cloud depth for 03Z 12 Feb 1992.*

important cloud depths for icing potential in reality would be shallower.

The other cases in this study are not shown but exhibit similar characteristics as the two cases described above. An overall pattern exists for all of the cases with generally warmer CTTs coinciding with higher CLW values but small CLW values occurring at any CTT. In order to study the overall pattern of CLW, CTTs, and cloud depths, scatterplots were composited for all of the cases (Figure 4.39 and Figure 4.40). This pattern is in agreement with Curry and Liu (1990) with the highest CLW amounts occurring at relatively warm CTTs (> -25°C), however low CLW amounts can be found at any temperature. This bit of information could be extremely useful for forecasting of icing potential. If the CTTs are <-25°C, then only small amounts of CLW exist and icing potential is at a minimum. This situation is likely a result of the efficiency of ice nucleation within the cloud. The presence of ice reduces the amount of SCLW in the cloud through the process of riming. In addition, often times supercooled liquid water is present only near the top of a cold cloud and is suppressed at all other levels due to the effects of ice. However, a shallow layer of supercooled water near cloud top still presents the possibility of aircraft icing. But as mentioned earlier, the critical temperature regime for aircraft icing has been observed to be from 0 to -20°C (Shultz and Politovich, 1992) and Figures 4.39 and 4.40 do show large amounts of supercooled liquid water existing in this temperature range with cloud depths of between 1 and 4.5 km. Another more interesting feature of Figure 4.39 is the sudden drop in CLW when the CTT reaches about -25°C. Hobbs (1969) and Grant (1968) conducted research on ice multiplication and found that the ratio of ice particles to ice nuclei in clouds decreases with decreasing cloud

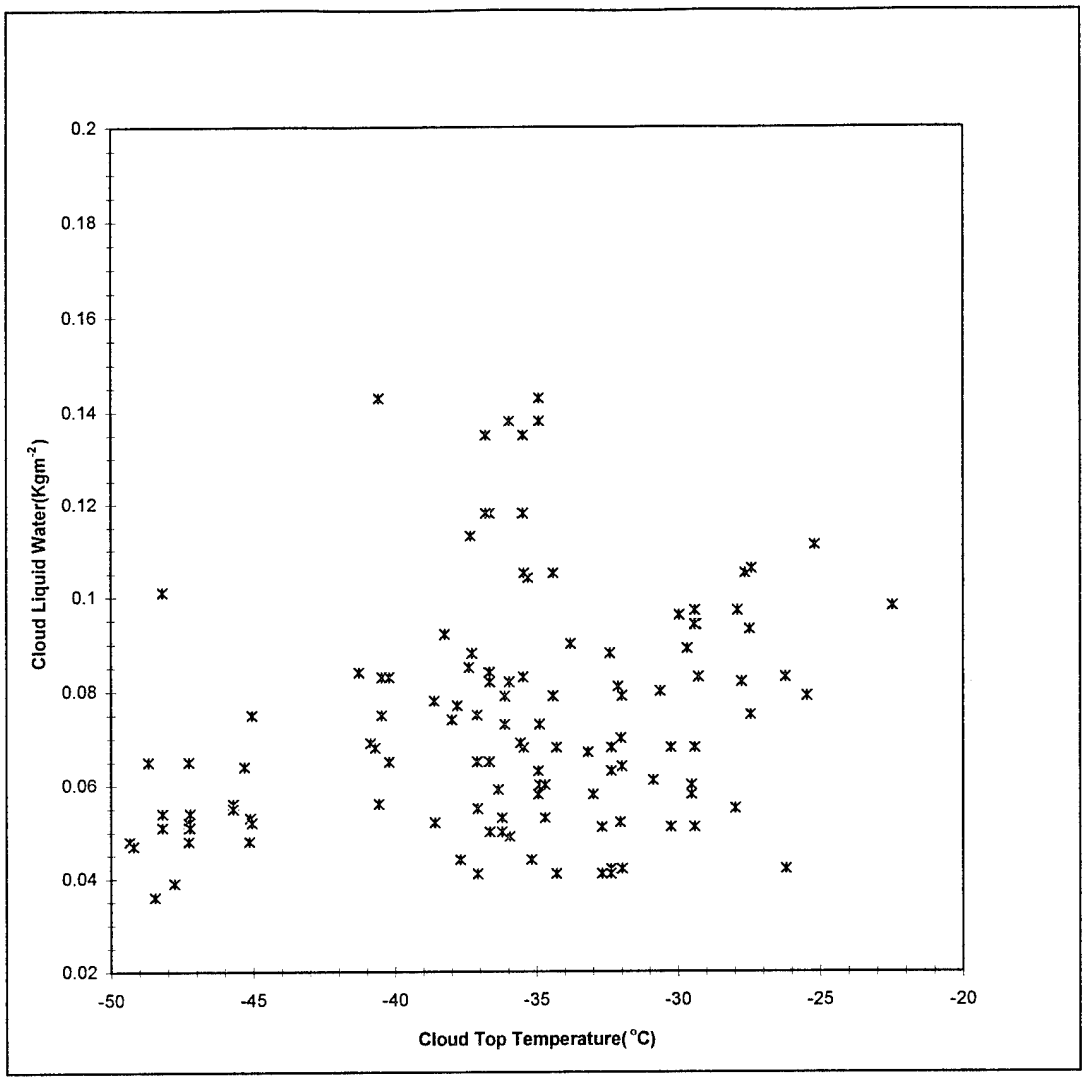

Figure 4.35. *Scatterplot of Channel 6 cloud liquid water versus cloud top temperature for 03Z 5 Mar 1992.*

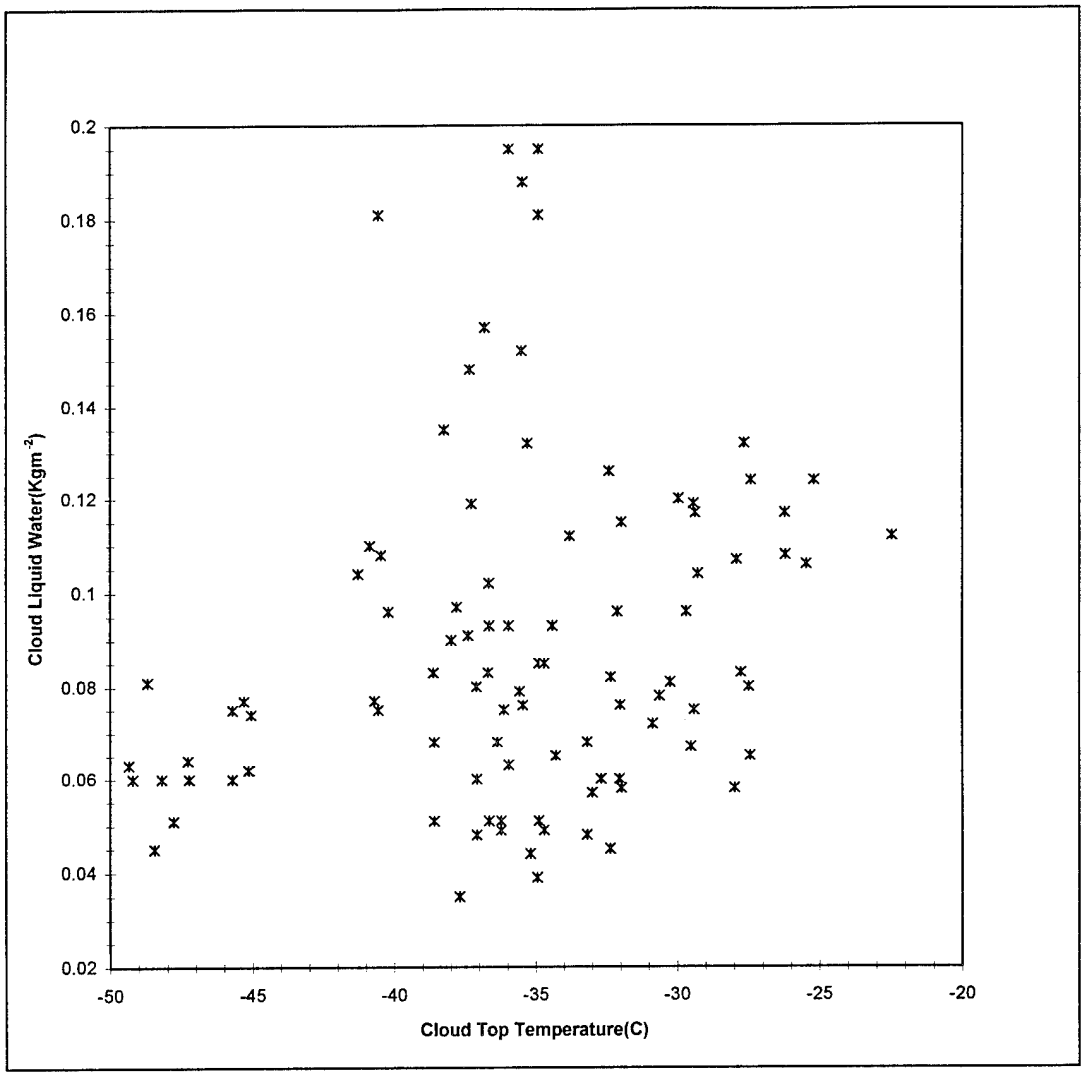

***Figure 4.36**. Scatterplot of Channel 7 cloud liquid water versus cloud top temperature for 03Z 5 Mar 1992.*

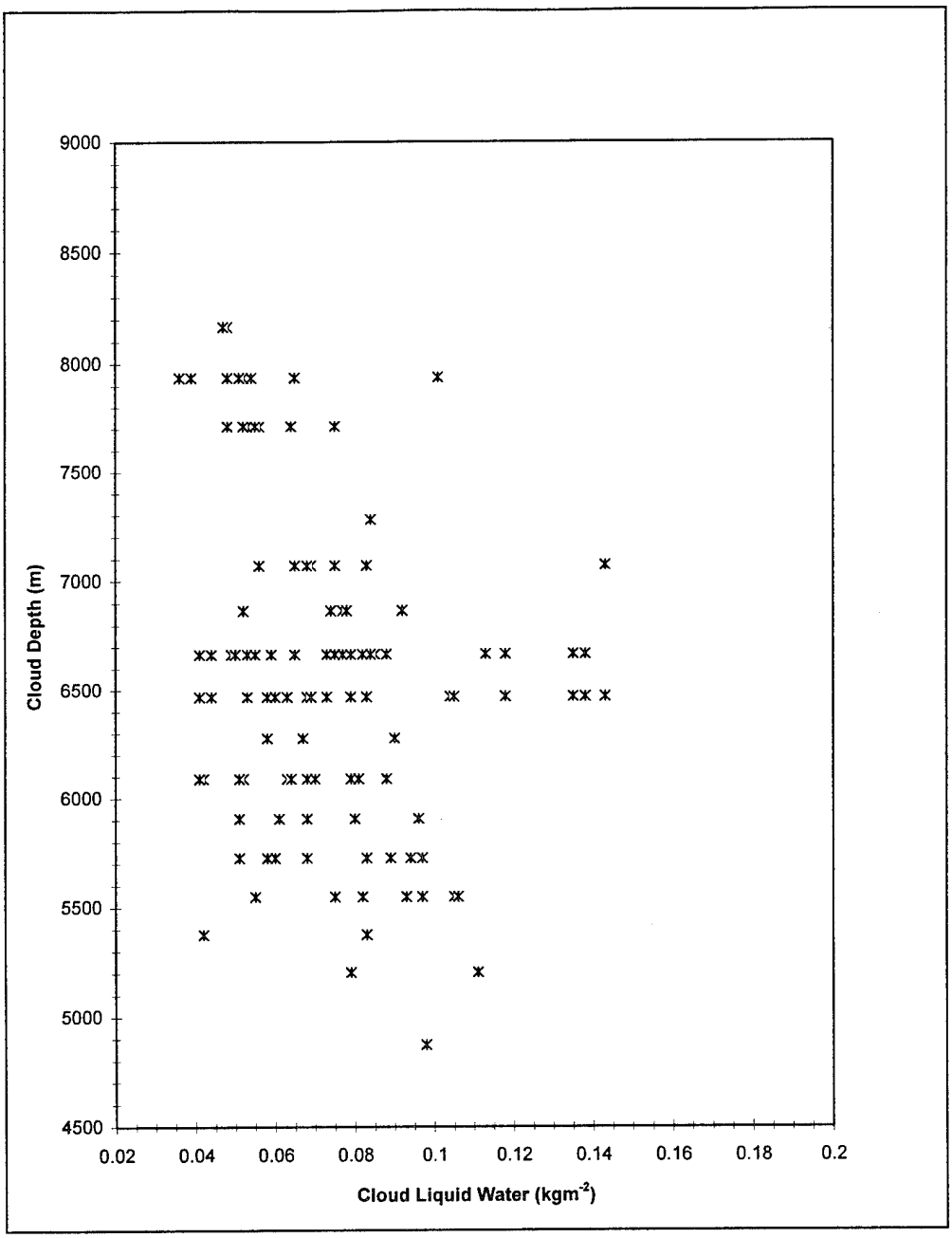

Figure 4.37*. Scatterplot of Channel 6 cloud liquid water versus cloud depth for 03Z 5 Mar 1992.*

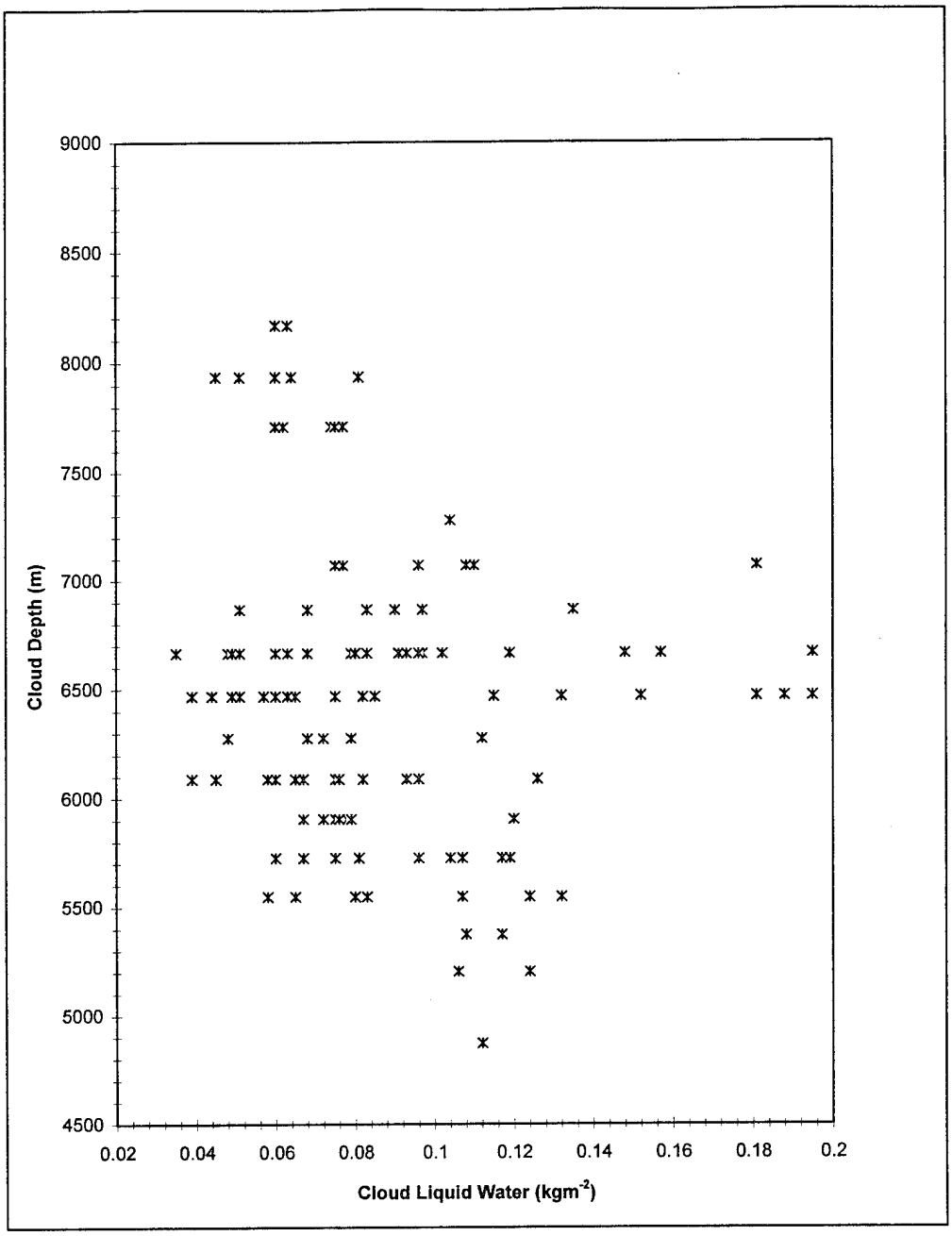

***Figure 4.38**. Scatterplot of Channel 7 cloud liquid water versus cloud depth for 03Z 5 Mar 1992.*

top temperature. Moreover, for cloud top temperatures in the range from -20 to -26°C, the ratio of ice particles to ice nuclei was generally in the range from 1 to 10 with the ratio reaching unity at -26°C. These results were explained by the fact that the freezing of supercooled cloud droplets in a cloud were responsible for the higher ratios (>1) of ice particles to ice nuclei. With decreasing CTTs, the growth of ice crystals from the vapor phase becomes increasingly important compared to the nucleation of supercooled droplets. Further more, the lower the temperature, the less important will be the nucleation of droplets by riming. Therefore, the ratio of ice particles to ice nuclei should approach one as the temperature of the cloud decreases. Interestingly, these results could in fact explain the results as shown in Figure 4.39. At about -25°C, the amount of cloud liquid water decreases to less than 0.2 kgm^{-2}. This is in close agreement with Grant and Hobbs. If the ratio of ice particles to ice nuclei is unity, then it is likely that SCLW amounts would be quite small therefore ice crystals would dominate and could continue to grow through deposition rather than by riming of the supercooled cloud droplets (which would not be abundant within the cloud).

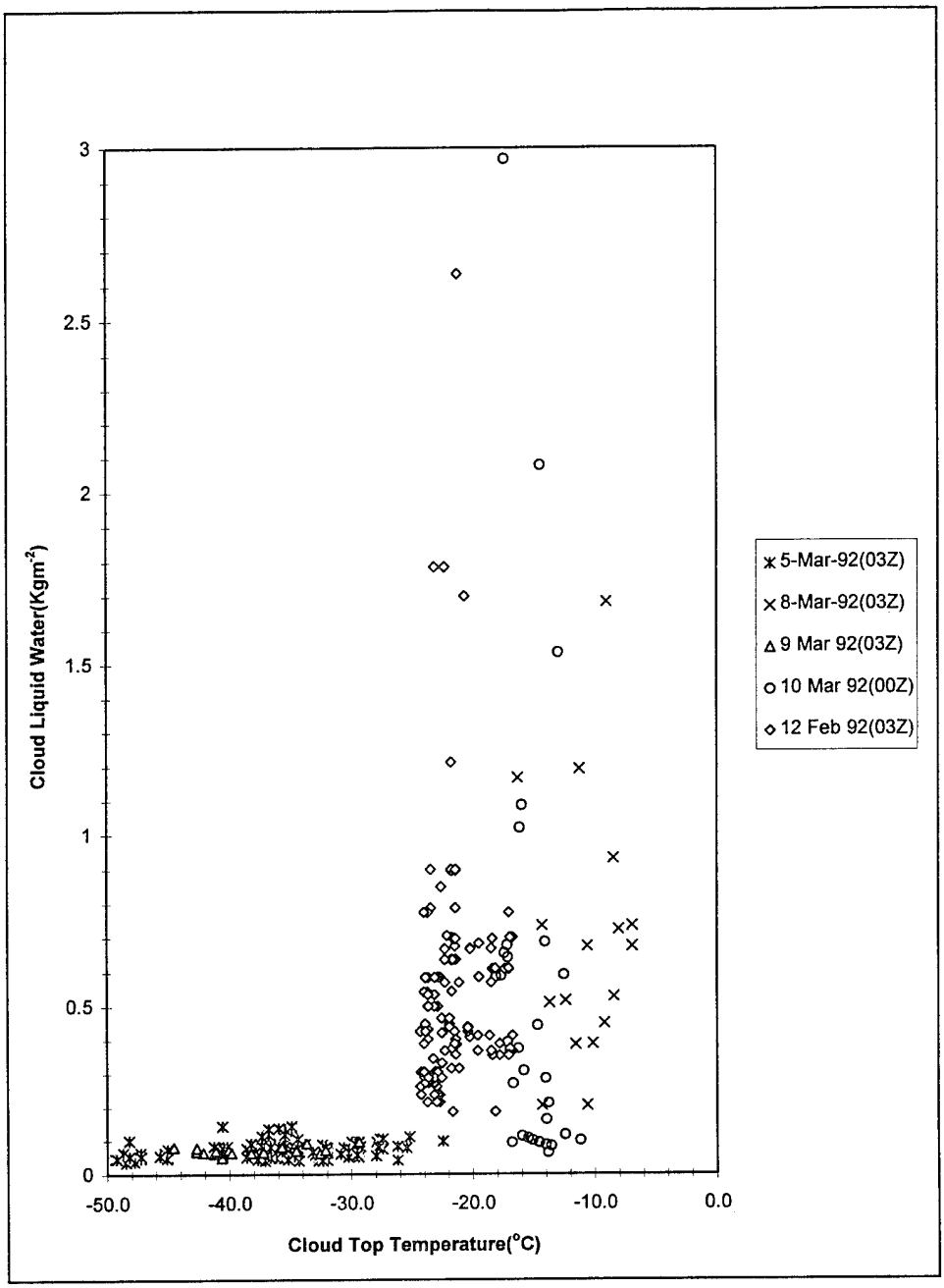

***Figure 4.39**. Combined Scatterplot of Channel 6 cloud liquid water versus cloud top temperature for 12 Feb, 5, 8, 9, and 10 Mar 1992.*

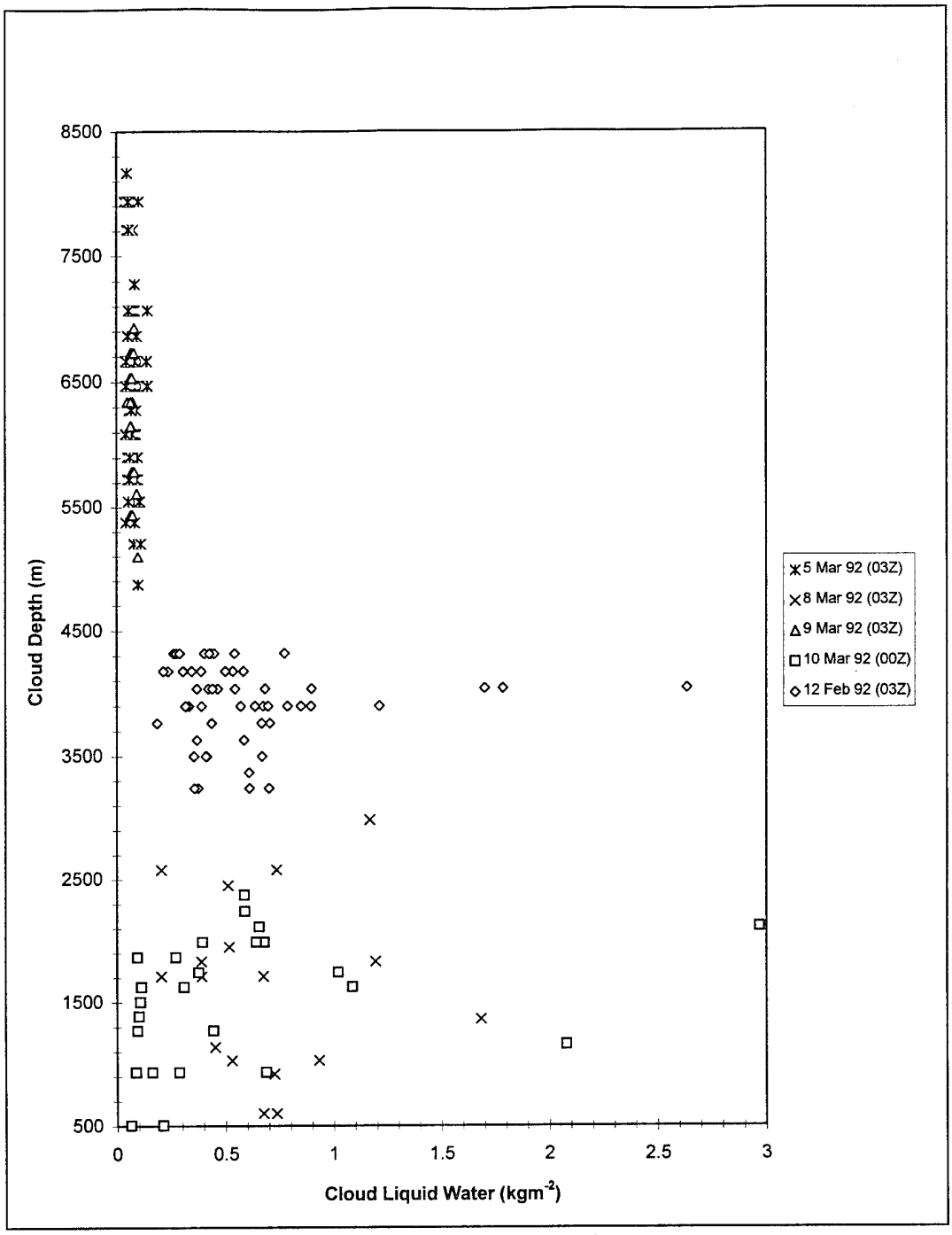

***Figure 4.40**. Composite scatterplot of Channel 6 cloud liquid water versus cloud depth for 12 Feb, 5, 8, 9, and 10 Mar 1992.*

4.5 Cloud Texture Method From Visible and Infrared Imagery

Digital satellite visible and infrared imagery not only contains information about radiance and thus temperature from the top of the cloud, but "texture" information as well. From this "texture", clouds can be classified into separate categories such as stratiform, cumuliform, and cirriform. This particular piece of texture information can then be used to infer vertical motion. For example, if little texture is noted in a specific portion of a cloudy area of an image, then one can infer minimal vertical motion near the cloud top, thus the cloud is likely to be stratiform. However, if some texture is present, then vertical motion is likely near the cloud top so the cloud would be classified as cumuliform. The next two sections (4.5.1 and 4.5.2) will briefly describe two specific techniques for determining cloud texture and section 4.5.3 will describe the texture technique employed in this study.

4.5.1 Gray Level Co-Occurrent Matrix (GLCM)

The Gray Level Co-occurrence Matrix (GLCM) technique is a statistically-based texture analysis method used to classify clouds into different categories. Welch et al. (1988) was able to correctly classify clouds with accuracies of 85-95% and standard deviations from 2-7% using this technique.

Basically, this method is a way of counting the number of occurrences when two pixels at two brightness levels are a certain distance apart. Since an image consists of pixels, the distance is measured in pixels. Given a line and element location of a pixel,

one can define the neighboring pixels in terms of distances and angles. Angles of 0, 45, 90, and 135 are used in the GLCM technique. This spatial information can be combined with the pixel gray level at one distance and angle. The results of counting can be described in matrix form for each angle and distance and this matrix is called the GLCM. Once all possible GLCM's are computed, the textural parameters need to be calculated. Haralick et al. (1973) proposed a set of 28 textural measures to be used as cloud classifiers, however, Welch et al. (1988) found that only 6 to 8 parameters would suffice for correctly classifying cloud images. Which of theses measures to use would certainly depend on both the image and the purpose of the cloud classification. Welch et al. (1988) found the following textural features to be most useful:

1. **Contrast -** A measure of the local variation between pixels or more specifically a measure of the difference second moment of the co-occurrence matrices.

2. **Angular Second Moment** - A measure of homogeneity in the scene. A small value indicates that there are few dominant gray tones. Conversely, a large value indicates some gray levels are dominant because of larger probability.

3. **Local Homogeneity** - The inverse difference moment of the co-occurrence matrices and represents a measure of the amount of local similarity of the scene.

4. **Entropy** - A measure of disorder in the scene. It is largest if the probabilities of gray levels are equal, and small when the probabilities of gray levels are unequal.

4.5.2 Neural Network Based Texture Method

Because of the massive amounts of satellite data available day and the need to process the data rapidly, it is virtually impossible to process and interpret satellite imagery without the aid of automation. The emergence of neural network technology has provided a means by which image processing and pattern recognition tasks can be performed. Neural networks are ideally suited because of there inherent high parallelism and their capability to learn from examples and generalize on new data. The neural network structure, learning algorithm, network architecture, input representation, and training data set are vitally important for accurate and consistent performance.

Liou et al. (1994) used Singular Value Decomposition (SVD) to extract textural features from visible and IR GOES imagery. This information was then presented to an unsupervised self-organizing feature map (Kohonen neural network) for automatic detection and classification of clouds. Over 20 days of IR and visible imagery were collected of which 15 of those days were selected for training. The remaining days were used to test the trained set. Results indicated that some misdetections and false alarms were created for both the IR and visible. The misdetections were caused by improper selection of the training data set. All possible cases should be included in the training set to obtain sound generalization capability, thereby eliminating this misdetection problem. The false alarms were caused by background variations which did not obey the simple

decision rule during the map monitoring task and visualization. However, the authors classification scheme could identify a significant portion of cirrus clouds which are often difficult, if not impossible to detect by a simple threshold.

3.5.1 Subjective Cloud Texture Analysis

For this study, a simple spatial variation technique (personal conversation with Don Reinke of STC METSAT Inc.) was used to determine cloud texture. A representative pixel was chosen near the center of a cloud mass whose area was generally < 100 km^2 in the vicinity of an icing report and CLW calculation. Pixels were subjectively compared a distance of 2-3 pixels in any direction of the center pixel using an interactive display system. If there was any significant variation in the pixel intensity over this distance, the cloud was classified as cumuliform. Conversely, if no significant variation in pixel intensities were noted, the cloud was classified as stratiform. For the cases chosen in this study, there were no visible images available for texture analysis, only IR images.

Results from the texture analysis indicated all of the cases exhibited stratiform characteristics with little variation in pixel intensity. Cloud texture is used in the icing index algorithm to further categorize icing potential. Since texture is not a major component of the index, this simple, subjective technique should provide enough useful information for further classification of icing potential. If texture is present, then the icing potential increases. This can be explained by the fact that large droplets are more common in cumuliform clouds due to increased vertical motion which increases the potential for clear icing. These large droplets tend to spread out over the airframe or rotor

when impacted, and subsequently freeze, thereby affecting the aircraft's flying performance. If no texture is detected, then no increased icing threat exists for the aircraft.

4.6 Operational Icing Index Nomogram

The icing index which is being developed and proposed in this study can easily be represented as a Nomogram for ease of use to operational forecasters. The Nomogram consists of two major components, cloud liquid water and cloud top temperature along with a third important factor, cloud depth. The cloud texture(intensity) information is used as a supplement to the main Nomogram and as explained in the previous section would increase the icing threat by one category if texture is present and would not change the threat if no texture is indicated. Figure 4.41 shows the prototype nomogram developed from results described earlier in this chapter. Representative CTT intervals are along the x axis, corresponding CLW values along the y-axis, and cloud depth are diagonals on the inner portion of the diagram. The inner portions of the nomogram are defined according to icing intensity ranging from light to severe. Table 4.9 defines the icing intensities from the nomogram as an icing index ranging from 1 (Trace) to 8 (Severe).

To reiterate the physical basis for Figure 4.41, we note that with warmer CTTs there would likely be thinner clouds containing less CLW, but with thicker clouds and warmer CTTs, large amounts of CLW may be present posing a serious threat for aircraft icing (Clear icing, which is extremely hazardous to aircraft, is normally found in the

temperature range from 0 to -10°C, AWS (1980)). If CTTs are in this temperature range, then we know CLW and an icing threat exists based on findings in this study. Most supercooled water is generally found in a 800 to 1000 m thick layer within the cloud (AWS 1980; Politovich, 1989) and often times near the cloud top. On the other hand, when CTTs are very cold, the clouds are normally thick and CLW amounts could vary range from low to high. However, due to the fact that the cloud top is quite cold, the threat of icing is diminished since much of the cloud top may be glaciated thereby reducing SCLW and hence the threat for icing. We also emphasize that the estimated parameters of CTT, CLW and CD are some of the key parameters to aircraft icing but are certainly not the exclusive list. Such factors as size distribution of cloud droplets, vertical embedded convective elements, and stability also play important roles in icing. If some of the parameters we cannot estimate are dominant in a given situation, then the icing index will fail. However, this means that the new index would be a good "positive" indicator of an icing threat, but not a failsafe "negative" indicator.

A total of nine PIREPS were chosen from all available PIREPS from all of the cases, and the intensities and altitudes are shown geographically in Figures 4.42 and 4.43. The PIREPS were chosen within ± 2 hours and a 100 km radius (similar to Brown et al. 1993) of the CLW retrieval and the intensities are plotted in the nomogram (Figure 4.41) Since the PIREPS were the only means of icing verification, they were used to "fine-tune" the icing nomogram. Only 33 % of the reports did not fit in the icing scheme (the PIREPS in the Nomogram which are not bold face). CLW and CTT values were in agreement with these PIREPS, however the depths of the clouds were much less than

Table 4.9. *Icing Index classification.*

Icing Index	Icing Intensity
1	Trace
2	Trace - Light
3	Light
4	Light - Mod
5	Moderate
6	Mod - Severe
7	Mod - Severe
8	Severe

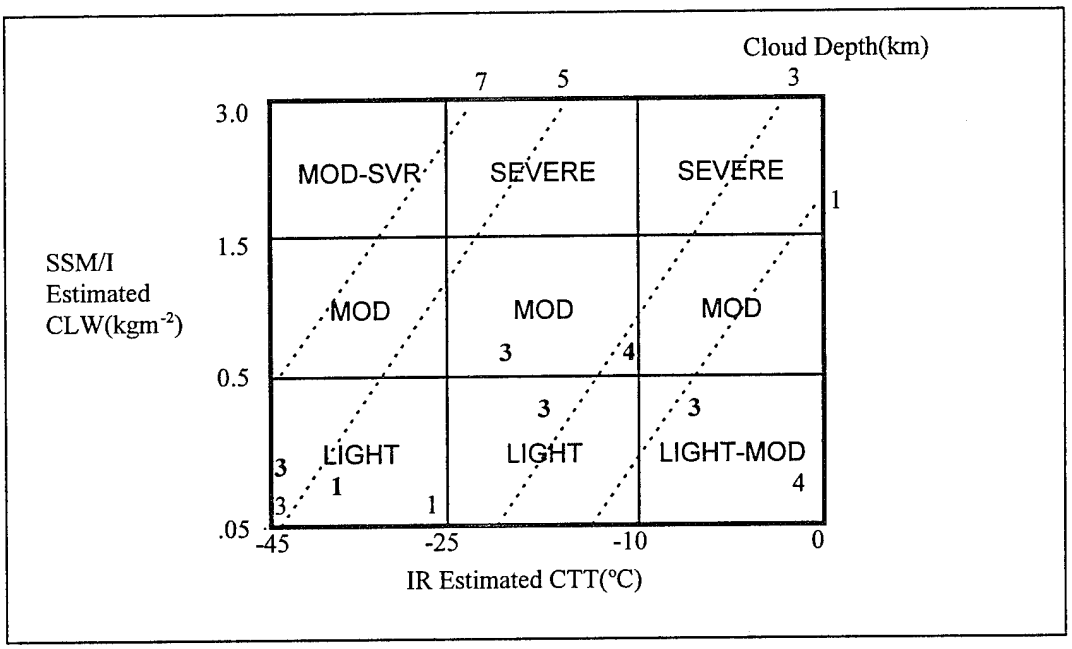

Figure 4.41*. Mid-latitude prototype icing nomogram. Categories of estimated CTT are located along the x axis, SSM/I estimated CLW categories are along the y axis, and the dashed diagonal lines are isolines of cloud depth. The* ***bold*** *numbers inside the chart are observed PIREP intensities which fell within the Nomogram guidelines.*

would be expected by the nomogram. This could be a result of miscalculation of cloud tops from the cloud thresholding technique. Unfortunately, there were no visible images available for the theses times to further discriminate cloud from no cloud. A note of caution should be stressed at this point. Even though the PIREPS were used as a means of verification for the nomogram, they are by no means considered exact (Brown et al. 1993). Pilot experience in icing conditions and the type of aircraft make PIREPS very subjective and often unreliable. However, from the results obtained in Section 4.2.5, the PIREPS used in the nomogram verification were consistent with the cloud analysis derived in each case. This, in itself is a verification of the PIREP icing altitudes, but the intensities still remain questionable.

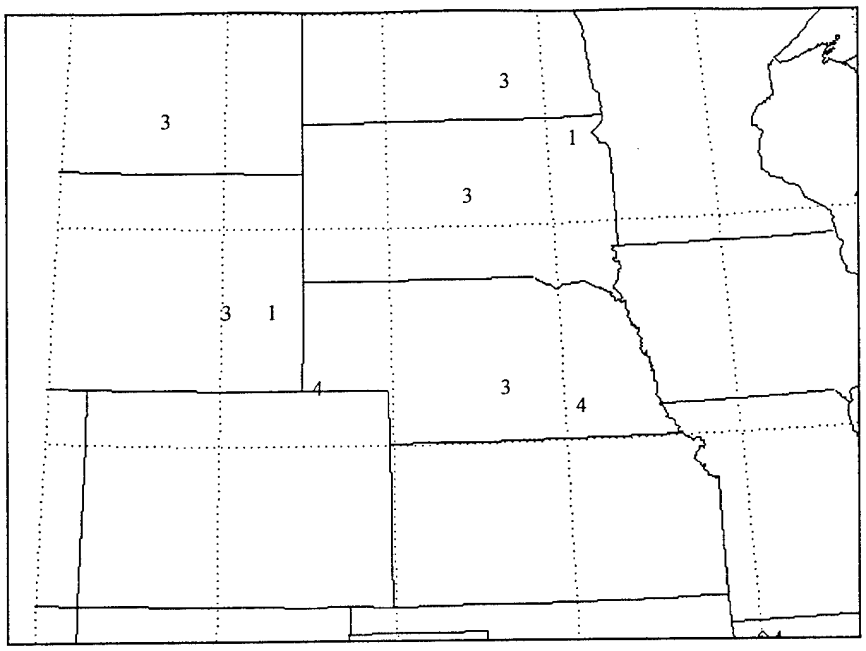

***Figure 4.42**. PIREP icing intensities from 12 Feb, 5 Mar, 8 Mar and 9 Mar used for "fine-tuning" of icing nomogram.*

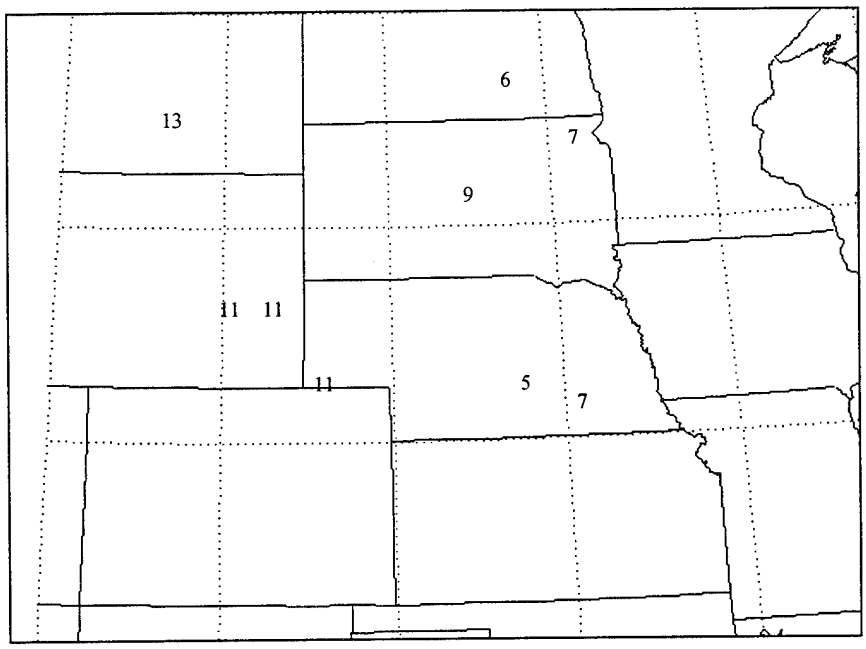

***Figure 4.43**. PIREP icing altitudes in thousands of feet from 12 Feb 5 Mar, 8 Mar, 9 Mar used for "fine-tuning" of icing nomogram.*

5 Summary and Conclusions

Unlike other remote sensing applications to aircraft icing over the oceans, this study focused on applications of icing potential from satellite retrieved CLW over land. Winter time situations were chosen in which icing conditions were known to exist. The CLW retrieval scheme required several ingredients for measurement of CLW. Surface emissivity is the most important component of the retrieval method and it was found that the 85.5 GHz horizontal polarized channel (Channel 7) showed more variability than in the vertical which agrees with other research conducted recently (Jones and Vonder Haar, 1990). Values ranged from 0.6 to 1 across portions of the upper midwest with the lowest values in snow covered areas.

The physically-based integrated CLW retrieval method of Jones and Vonder Haar (1990) was used to compute CLW from non-precipitating clouds. CLW values were found to vary from 0.07 kgm^{-2} to 3 kgm^{-2} for Channel 6 (vertical polarized channel) and from 0.09 kgm^{-2} to 5 kgm^{-2} for Channel 7 (horizontal polarized channel). These CLW values were consistent with measurements taken from research aircraft flown over the Great Plains and Sierra Nevada in the late 1970's to mid 1980's (Politovich 1989) in most cases. These findings are certainly a step in the right direction in using retrieved CLW over land for determination of the potential for aircraft icing.

It was found that very little CLW existed when CTTs were less than -25°C indicating the presence of a good ice nuclei population therefore reducing the amount of SCLW. However, CLW amounts were much more variable at CTTs greater than -25°C which would reflect the metastable nature of supercooled water which in turn may give

an indication of the cloud's lifecycle (i.e., young, mature, old). Microphysical results concluded from this study were in close agreement with Hobbs (1969) and Grant (1968) in regards to low CLW amounts at CTTs < -25◦C. The ratio of ice particles to ice nuclei were near one indicating that CLW amounts would be low in order for ice particles and ice nuclei to be nearly the same. In addition, some of the CLW values do appear to be a bit high for wintertime clouds which may be a result of the effects of low surface emittance used to retrieve CLW (i.e., lower surface emittance, higher CLW values). Four of the five cases yielded CLW and clouds below freezing which meant any liquid was supercooled. Areas within each cloud mass for each case were determined to be conducive to aircraft icing with the most probable areas occurring from 0◦C to -20◦C. These potential icing areas were verified by available PIREPS, however, no conclusions could be drawn about the PIREP intensities.

A prototype icing index nomogram was developed from CLW, CTTs and cloud depth with available PIREPS serving to "fine-tune" the possible categories of icing. 66% of the PIREPS agreed with the mid-latitude icing nomogram. Light to moderate icing occurred in the areas of CLW >0.5 kgm^{-2} and CTTs from -10 ◦C to -25◦C. When CTTs and CLW were low, the PIREPS indicated trace to light icing even though the clouds were thick (6-7 km). This was a good indication that much of the cloud must have contained ice which is not hazardous to the aircraft. However, a few minutes prior to the satellite pass, this particular area of cloud may have posed a severe threat to aircraft icing.

5.1 Plan for a Forecasting Test of the Icing Index

In order to provide the most useful forecasting tool, further verification of the satellite derived icing index is needed. This would likely include planning a project or exercise in which research aircraft would provide a realistic, non subjective verification of icing. The Winter Icing and Storms Project (WISP) has recently concluded a 6 year program specifically designed to study aircraft icing as well as winter storms in Colorado. This past season (Jan-Mar 1994) would provide a particularly good data base to further test the icing index proposed in this study. If, upon further investigation, the index proves beneficial, then the index should be tested for forecast potential. This plan would include obtaining CLW from some source (satellite-based, ground-based radiometers, or model-based) along with IR CTTs and IR and Visible texture information and cloud base data. This collection of data could then be used in the icing index nomogram to come up with a forecast of icing potential primarily over a region much smaller than icing forecasts produced today. It would be extremely beneficial to plan this test in or near an ongoing or future project in a climatologically known icing prone area of the country.

5.2 Future Work and Applications of the Satellite Derived Icing Index

While microwave CLW retrieval over land is still in its infancy, the results from this study indicate that this type of retrieval is certainly applicable to aircraft icing. One major drawback for forecasting of icing potential is the coarse temporal resolution. The polar orbiting satellite normally passes over the same area twice a day, sometimes four times if two satellites are in orbit. This poses a problem for forecasting, or more appropriately, "nowcasting". One solution to this problem would be to place a

microwave radiometer aboard a geostationary satellite platform as suggested by Vonder Haar et al. (1986). This would allow researchers to study the high frequency microphysics through improved observations.

Further work needs to be done to verify the CLW retrieved from satellite. "Ground truth" information from ground-based radiometers would offer this opportunity. One of the keys to CLW retrieval over land is the measurement of surface emissivity. Clouds in the field of view of the satellite impair this measurement from satellite. Surface temperature might provide the missing link for emissivity calculations during cloudy situations. In addition, this study did not include atmospheric effects in the measurement of surface emittance. It has been found (Jones and Vonder Haar 1990) that the atmosphere does have some effect on the satellite's measurement of surface emissivity therefore future work should include atmospheric effects. Another possible area of improvement is in the area of cloud/ no cloud thresholding. This technique needs to become more objective for ease of computation especially in areas where cloud and ground temperature are similar. In the CLW algorithm, additional soundings would provide greater vertical and horizontal detail for CLW retrieval. These suggestions would likely improve the microwave CLW retrieval over land. It is also appropriate to note a non-microwave method of using new GOES-8 data should be developed to augment methods in the present study. Its principle is to use time varying, multi-spectral data for ice/supercooled water discrimination capability for the top of cloud layers. If it develops, it would augment the icing index proposed in this study.

As expected, the proposed icing index will need further improvement. Aircraft and satellite-based radar would provide such an improvement in producing considerably more detail on the cloud structure, including cloud base and top as well as detecting multilayered cloud systems. This type of information is critical in determining icing potential within a cloud. Another avenue to pursue in the future would be to combine the synoptic scale forecast methods of both NAWAU and AFGWC with the new satellite-based index. This would provide a more regionalized product which would be much more useful than forecasts issued today. Additional cases from different icing prone regions of the country need to be studied in order to provide a more detailed data base for further refinement of the icing index proposed in this study.

REFERENCES

Allen, K.C., and H.J. Liebe, 1983: Tropospheric absorption and dispersion of millimeter and submillimeter waves. *IEEE Trans. Antennas Propag.*, **AP-31**, 221-223.

AWS, 1980: *Forecaster's Guide on Aircraft Icing.* Air Weather Service ANS/TR-80/001.

Bain, M., and J.F. Gayet, 1982: Aircraft measurements of icing in supercooled and water droplet/ice crystal clouds. *J. Applied. Meteor.*, 21, 631-641.

Brown, B.G., T. Fowler, B.B. Derstein, and G.G. Forbes, 1993: Use of pilot reports for verification of aircraft icing diagnoses and forecasts. Preprints, *Fifth Int'l Conf. of Aviation Weather Systems*, Vienna, VA., Amer. Meteor. Soc., 2-6 Aug 1993.

Brown, J.M., J.A. Mcginley, and D. Rodgers, 1994: Forecasting for a large field program: STORM-FEST. *Weather and Forecasting*, **9**, 593-605.

Cagle, M.W. and C.G. Halpine, 1970: *A Pilot's Meteorology.* Van Nostrand Reinhold, New York, N.Y., 407 pp.

Choudhury, B.J., T.J. Schmugge, R.W. Newton, and A. Chang, 1979: Effect of surface roughness on the microwave emission from soils. *J. Geophys. Res.*, **84**, 5699-5706.

Cole, J. and W.R. Sand, 1991: Statistical study of aircraft icing accidents. *Proc. 29th Aerospace Sciences Meeting*, Reno, NV, Amer. Inst. Aero. and Astro., AIAA 91-0558.

Conte, S.D. and C. de Boor, 1980: *Elementary Numerical Analysis.* Mcgraw-Hill, Inc., New York, 432 pp.

Cooper, W.A., W.R. Sand, M.K. Politovich, and D.L. Veal, 1984: Effects of icing on the performance of a research aircraft. *Journal. of Aircraft*, **21**, 708-715.

Cotton, W.R., G. Thompson, and P.W. Mielke Jr., 1994: Real-time mesoscale prediction on workstations. *Bull. Amer. Meteor. Soc.*, **75**, *349-362.*

Curry, J.A., and G. Liu, 1992: Assessment of aircraft icing potential using satellite data. *J. Applied. Meteor.*, **31**, 605-621.

DeMott, P.J. and D.C. Rogers, 1990: Freezing nucleation rates of dilute solution droplets between -30 and -40C in laboratory simulations of natural clouds. *J. Atmos. Sci.*, **47**, 1056-1064.

Federal Coordinator for Meteorological Services and Supporting Research, 1986a: National Aircraft Icing Technology Plan. FCM-P20-1986, Washington, D.C., 47 pp.

Federal Coordinator for Meteorological Services and Supporting Research, 1986b: National Plan to Improve Aircraft Icing Forecasts. FCM-P21-1986, Washington, D.C., 24 pp.

Forbes, G.S., Y. Hu, B.G. Brown, B.C. Berstein, M.K. Politovich, 1993: Examination of conditions in the proximity of pilot reports of aircraft icing during STORM-FEST. Preprints, *Fifth Int'l Conf. on Aviation Weather Systems*, Vienna, VA., Amer. Meteor. Soc., 2-6 Aug 1993.

Grant, L.O., 1968: The role of ice nuclei in the formation of precipitation. *Proc. Intern. Conf. Cloud Physics*, Toronto, 305 pp.

Greenwald, T.J., G.L. Stephens, T.H. Vonder Haar, and D.L. Jackson, 1993: A physical retrieval of cloud liquid water over the global oceans using SSM/I observations. *J. of Geophys. Res.*, **98**, 18,471-18,488.

Haralick, R.M., K. Shanmugam, and I.H. Dinstein, 1973: Textural features for image classification. *IEEE Trans. on Systems, Man, and Cybernetics*, **SMC-3**, 610-621.

Hobbs, P.V., 1969: Ice multiplication in clouds. *J. Atmos. Sci.*, **26**, 315-318.

Hogg, D.C., F.O. Guiraud, J.B. Snider, M.T. Decker, and E.R. Westwater, 1983: A steerable dual-channel microwave radiometer for measurement of water vapor and liquid in the troposphere. *J. Applied. Meteor*, **22**, 789-806.

Hogg, D.C., F.O. Guirard, and E.B. Burton, 1980: Simultaneous observation of cool cloud liquid by ground-based microwave radiometry and icing of aircraft. *J. Applied. Meteor.*, **19**, 893-895.

Hollinger, J.P., J.L. Pierce, and G.A. Poe, 1990: SSM/I instrument evaluation. *IEEE Trans. Geosci. Remote Sensing.*, **28**, 781-790.

Jones, A.S., K.E. Eis, and T.H. Vonder Haar, 1995: A method for multisensor-multispectral satellite data fusion. *J. Atmos. Oceanic. Tech.*, in press.

Jones, A.S. and T.H. Vonder Haar, 1990: Passive microwave radiometry of cloud liquid water over land regions. *J. Geophys. Res.*, **95**(D10), 16,673-16,683.

Kidder, S.Q. and T.H. Vonder Haar, 1995: *Satellite Meteorology: An Introduction.* Academic Press, San Diego, CA., in print.

Lee, T.F., J.R. Clarc, and S.D. Swadley, 1994: Potential applications of the SSM/I cloud liquid water parameter to the estimation of marine aircraft icing. *Weather and Forecasting*, **9**, 173-182.

Lewis, W., 1947: A flight investigation of the meteorological conditions conducive to the formation of ice on airplanes. NACA TN 1393, 50 pp.

Liebe, H.J., 1985: An updated model for millimeter wave propagation in moist air, *Radio Sci.*, 20, 1069-1089

Liou, K., 1980: *An Introduction to Atmospheric Radiation.* Academic Press, San Diego, CA., 392 pp.

Liou, R.J., M.R. Azimi, D.L. Reinke, T.H. Vonder Haar, and K.E. Eis, 1994: Detection and classification of cloud data from geostationary satellite using artificial neural networks. Proceedings, *The 1994 IEEE International Conference on Neural Networks*, 27-29 June, 1994, Orlando, Florida, 4327-4332.

Petty, G.W., and K.B. Katsaros, 1990: New geophysical algorithms for the Special Sensor Microwave Imager. Preprints, *Fifth Conf. on Satellite Meteorology and Oceanography*, London, England. Amer. Meteor. Soc., Boston, Mass., 247-251.

Politovich, M.K., 1989: Aircraft icing caused by large supercooled droplets. *J. of App. Meteor.*, **28**, 856-868.

Popa Fotino, I.A., J.A. Schroeder, and M.T. Decker, 1986: Ground-based detection of aircraft icing conditions using microwave radiometers. *IEEE Trans. Geosci. Remote Sensing*, **6**, 9750982.

Pruppacher, H.R., and Klett, 1980: *Microphysics of Clouds and Precipitation.* D. Reidel Publishing Co., Dordrecht, Holland, 714 pp.

Rasmussen, R., M. Politovich, J.Marwitz, W. Sand, J. McGinley, J. Smart, R. Pielke, S. Futledge, D. Wesley, G. Stossmeister, B. Bernstein, K. Elmore, N. Powell, E. Westwater, B.B. Stankov and D. Burrows, 1992: Winter icing and storms project(WISP). *Bull. Amer. Meteor. Soc.*, **73**, 951-974.

Rogers, R.R. and M.K. Yau, 1989: *A Short Course in Cloud Microphysics*. Pergamon Press, Oxford, England, 293 pp.

Sand, W.R., W.A. Cooper, M.K. Politovich, and D.L. Veal, 1984: Icing conditions encountered by a research aircraft. *J. Climate. and Applied. Meteor.*, **23**, 1427-1440.

Schultz, P. and M.K. Politovich, 1992: Toward the improvement of aircraft icing forecasts for the continental United States. *Weather and Forecasting*, **7**, 491-500.

Schmugge, T.J., 1985: Remote sensing of soil moisture, in *Hydrological Forecasting*, edited by M.G. Anderson and T.B. Burt, John Wiley, New York, NY.

Schmugge, T.J. and B.J. Choudhury, 1981: A comparison of radiative transfer models for predicting the microwave emission from soils. *Radio Sci.*, **16**, 927-938.

Spencer, R.W., H.M. Goodman, and R.E. Hood, 1989: Precipitation retrieval over land and ocean with the SSM/I: Identification and characteristics of the scattering signal. *J. Atmos. and Ocean. Tech.*, **6**, 254-273.

Stankov, B.B. and A.J. Bedard Jr., 1994: Remote sensing observations of winter aircraft icing conditions: A case study. *Journal of Aircraft*, **31**, 79-89.

Stankov, B.B., E.R. Westwater, J.B. Snider, and R.L. Weber, 1992: Remote measurements of supercooled integrated liquid water during WISP/FAA aircraft icing program. *Journal of Aircraft*, **29**, 604-611.

Telford, J.W., and S.K. Chai, 1980: A new aspect of condensation theory. *Pure Appl. Geophys.*, **119**, 720-742.

Telford, J.W., T.S. Keck and S.K. Chai, 1984: Entrainment at cloud tops and the droplet spectra. *J. Atmos. Sci.*, **41**, 3170-3179.

Ulaby, F.T., R.K. Moore, and A.K. Fung, 1986: *Microwave Remote Sensing Active and Passive, Vol III From Theory to Applications*. Addison-Wesley Publishing Co., Reading, Mass., 1097 pp.

Ulaby, F.T., R.K. Moore, and A.K. Fung, 1981: *Microwave Remote Sensing Active and Passive, Vol I Microwave Remote Sensing Fundamentals and Radiometry*. Addison-Wesley Publishing Co., Reading, Mass., 456 pp.

U.S. Air Force, 1982: Weather for Aircrews. *AF Manual 51-12*, **I**, 101 pp.

U.S. Air Force, 1992: Weather for Aircrews. *AF Manual 51-12*, **II**, 66 pp.

Vonder Haar, T.H., W.E. Shenk, and D.W. Gaul, 1986: Passive microwave radiometer experiment for GOES-NEXT. *Preprint Volume, Second Conference on Satellite Meteorology and Remote Sensing Applications*, 13-16 May, Williamsburg, VA., 514-518.

Wallace, J.M. and P.V. Hobbs, 1977: *Atmospheric Science an Introductory Survey.* Academic Press, New York, NY., 467 pp.

Welch, R.M., S.K. Sengupta, and D.W. Chen, 1988: Cloud field classification based upon high spatial resolution textural features. 1. Gray-level co-occurrance matrix approach. *J. Geophys. Res.*, **93**, 12663-12,681.

Yeh, H., and K. Liou, 1983: Remote sounding of cloud parameters from a combination of infrared and microwave channels. *J. Climate and Applied Meteor.*, **22**, 201-213.